INFORMATION TO USERS

The most advanced technology has been used to photograph and reproduce this manuscript from the microfilm master. UMI films the original text directly from the copy submitted. Thus, some dissertation copies are in typewriter face, while others may be from a computer printer.

In the unlikely event that the author did not send UMI a complete manuscript and there are missing pages, these will be noted. Also, if unauthorized copyrighted material had to be removed, a note will indicate the deletion.

Oversize materials (e.g., maps, drawings, charts) are reproduced by sectioning the original, beginning at the upper left-hand corner and continuing from left to right in equal sections with small overlaps. Each oversize page is available as one exposure on a standard 35 mm slide or as a 17″ × 23″ black and white photographic print for an additional charge.

Photographs included in the original manuscript have been reproduced xerographically in this copy. 35 mm slides or 6″ × 9″ black and white photographic prints are available for any photographs or illustrations appearing in this copy for an additional charge. Contact UMI directly to order.

Accessing the World's Information since 1938

300 North Zeeb Road, Ann Arbor, MI 48106-1346 USA

Order Number 8801691

Resonance excitation of linear and non-linear spiral density waves in a gaseous disk

Cheng, Ye, Ph.D.

City University of New York, 1987

U·M·I
300 N. Zeeb Rd.
Ann Arbor, MI 48106

RESONANCE EXCITATION OF LINEAR AND NON-LINEAR SPIRAL DENSITY WAVES IN A GASEOUS DISK

by

Ye Cheng

A dissertation submitted to the Graduate Faculty in Physics in partial fulfillment of the requirements for the degree of Doctor of Philosophy, The City University of New York.

1987

This manuscript has been read and accepted for the Graduate Faculty in Physics in satisfaction of the dissertation requirement for the degree of Doctor of Philosophy.

6-2-87
Date

C. Yuan
Chairman of Examining Committee

6/8/87
Date

Executive Officer

Timothy H. Boyer

Richard B. Mathews

C. Mr. Tchen
Supervisory Committee

The City University of New York

ABSTRACT

RESONANCE EXCITATION OF LINEAR AND NON-LINEAR SPIRAL DENSITY WAVES IN A GASEOUS DISK

by

Ye Cheng

Adviser: Professor Chi Yuan

This thesis develops the theory of linear and non-linear density and/or acoustic waves in a gaseous disk responding to a periodic perturbational force, such as that caused by a satellite in a ring system, or by a rotating mass distortion in the central region of a galaxy.

Based on the non-linear formulation devised by Shu, Yuan and Lissauer (1985), we rederive a fundamental integro-differential equation with the inclusion of all three factors: pressure, self-gravity and viscosity. To apply this equation, physical parameters used in various astrophysics problems are examined and approximations justified. The amplitude relation and the dispersion relation indicate the appropriate replacement for the integro-differential equation by a non-linear differential equation. These relations also describe the features of the excitation and propagation processes.

We work out a complete linear theory of density and/or acoustic waves with viscosity and self-gravity. We study the excitation mechanism by which the waves are generated in the gaseous disk. The asymptotic solutions to the linearized equation which are presented along with the numerical solutions help to clarify several important aspects concerning the nature of the waves in a disk system.

In an application to the 3-kpc arm problem in the Galaxy, we solve the non-linear differential equation numerically with the aid of the linear solutions. We find that an oval distortion of 5% of the mean gravitational field near the outer Lindblad resonance can generate a wave in a close resemblance to the observed 3-kpc arm.

The present theory has potential applications to astrophysical problems such as the proto-stellar disk of the solar nebula, the possible existence of the circumstellar disk of a binary, and the structure of barred galaxies.

ACKNOWLEDGMENT

It is a great pleasure to acknowledge my deep gratitude to Professor Chi Yuan for his continued support, encouragement, instruction, and patient guidance during the course of this research.

I wish to express my sincere thanks to the Physics Faculty of the Department of The City College for its instruction and help, especially to Professors J. F. Aschner, T. Boyer, V. Canuto, N. P. Chang, V. Chung and R. Stothers.

I am greatly indebted to Professor C. M. Tchen of the Engineering School and Professor R. Dickman of the University of Massachusetts for their guidance and help.

I am also grateful to Dr. P. Cassen of NASA-Ames Research Center for his interest in this research and for his arrangement of the financial support through a University Consortium (NCA2-186) which helps me to complete this thesis.

Special thanks also to my former advisors, Professor Wang Shouguan and Professor Hong Siyi, directors of the Beijing Astronomical Observatory.

TABLE OF CONTENTS

LIST OF FIGURES

CHAPTER I

INTRODUCTION

The theory of density waves has been used successfully in explaining the spiral structure of disk systems in astrophysics. The self-excited modes have been studied in great detail by Lin and his associates (Lin and Bertin 1985, Lin and Thurstans 1984, Bertin, Lin and Lowe 1984) in explaining the quasi-stationary spiral structure of disk galaxies. Spiral density waves driven by a satellite or an oval distortion are found to play an important role in shaping the structure of disk systems in general. Mimas is responsible for the Cassini division in Saturn's rings (Goldreich and Tremaine 1978); about fifty wave trains in Saturn's ring disk have been detected and identified as waves resonantly excited by external satellites (Lissauer and Cuzzi 1982). The Milky Way's 3-kpc arm is interpreted as a part of a spiral density wave driven by a minor oval distortion in the central regions of the Galaxy (Yuan 1984).

The theory of spiral density waves driven by a periodic disturbing field was first studied by Feldman and Lin (1973), and Lin and Lau (1975). Their emphasis was focused on the resonance effects at the co-rotation circle. A more complete linear theory has been developed by Goldreich and Tremaine (1978, 1979). Realizing that the random velocity of the particles in Saturn's rings is so small that the effects of pressure can be neglected, Cuzzi, Lissauer and Shu (1981) worked out a simplified theory. The same theory was used to interpret the bending waves in Saturn's rings (Shu, Cuzzi and Lissauer 1983). Another limiting version of the

theory was considered by Yuan (1984) to account for the large-scale motion of the interstellar gas in a galactic disk system in which the effect of self-gravity may be ignored. Yuan has used the theory to interpret the 3-kpc arm. All the theoretical works quoted above use linear WKBJ-type analysis, based on the hydrodynamic formulation. Viscous effects were estimated only through the WKBJ dispersion relation.

Spiral density waves excited at the Lindblad resonances are extremely sensitive to the perturbation field. Small disturbances from the satellites or a central oval distortion can produce waves of extremely high density contrast and long wavelength, much more than what the linear theory can provide. Viscosity also seems to have a strong effect in damping those waves in Saturn's rings as well as in galactic disks. A non-linear analysis, using a finite difference scheme, was carried out for the gaseous disk without self-gravitation (Yuan 1984). Although the calculations successfully demonstrate that a minor oval distortion at the center of the Galaxy can excite a wave at a galacto-centric distance of 3-kpc in close resemblance to the observed 3-kpc arm, the method, due to the adoption of a local approximation, cannot be used generally for applications to other similar problems in astrophysics. Furthermore, it is difficult to extend the theory to include viscosity and self-gravitation properly in the calculations. The difficulty is resolved by the formulation proposed by Shu, Yuan and Lissauer (1985, hereafter SYL) who also obtained the solution for the fully non-linear waves in the inviscid ring disk of Saturn. The viscous theory of the non-linear density waves was subsequently worked out by Shu, Dones, Lissauer, Yuan and Cuzzi (1985, hereafter Shu et al.), using the same formulation plus the results on viscosity studied by Shu and Ste-

ward (1985, hereafter SS). Borderies, Goldreich and Tremaine (1982, 1983, 1984) have taken an entirely different approach in treating non-linearity, in which they place their emphasis on the transport of angular momentum and its relation to the sharp edges of Saturn's ring gaps (Porco and Goldreich 1987). The non-linear theory for Saturn's rings developed so far does not, and indeed need not, include pressure effects in the analysis.

The purpose of our study is to develop a non-linear theory for a gaseous disk. The theory is still based on the formulation of SYL but all three factors – self-gravity, pressure and viscosity are being considered. The results of the non-linear theory are computed in general terms for disk problems in astrophysics, with the intention of applying this to the 3-kpc arm. The first part of our work is a thorough treatment of the linear theory. The accurate linear theory is necessary to provide the precise boundary conditions without which the non-linear equation formulated here can not be adequately integrated. We find that the linear theory can be represented elegantly by the Airy functions. Important physics which was obscured in the early treatments is now revealed in the present study. In the second part of our study, we shall present a non-linear analysis. The results, which may be regarded as an improvement over the early theory on the 3-kpc arm, have potential applications to other problems in astrophysics, including the proto-solar disk, the possible existence of a circumstellar disk surrounding a binary and the spiral structure of barred galaxies. Discussions on the advantages and the limitations of the present non-linear analysis are given in the concluding chapter.

CHAPTER II

MATHEMATICAL FORMULATION

We consider a self-gravitating gaseous disk. The mean rotational motions of the gas are in balance with the gravitational field provided by the central star (for the cases of the solar nebula, planetary rings and circumstellar disk of a binary) or by the background stars (for the case of the gas in disk galaxies). In the case of a barred galaxy, motions of the gas are completely supported by self-gravity. The random motions of the gas give rise to the pressure and viscosity (turbulent) in the system. The random speed of the gas is taken to be constant and the pressure p is assumed to take the simple isothermal relation to the density ρ,

$$p = a^2\rho \qquad or \qquad P = a^2\sigma, \tag{2.1}$$

where σ is the surface density and P is the pressure integrated over the scale height H. Furthermore, we use the classical stress-strain relations in representing the viscous forces. The collision time scale among gas particles therefore is assumed to be much shorter than the dynamical time scale. The coefficients of the shear and bulk viscosity, μ and μ', are treated as constants.

The disk is disturbed periodically by an external force field, which may be due to a circling satellite or an uneven distribution of mass rotating rapidly in the central regions. In any case, the perturbational field is regarded small as compared to the mean field. Its strength varies on the scale of the radius of the disk.

2. 1. The Lagrangian Dynamical Equations

It is shown that the non-linear wave motion in the disk is governed by an integro-differential equation (SYL and Shu et al.). For the sake of completeness, we rederive the equation here, adopting the same procedure and notation as in the two papers quoted above, with the inclusion of the classic viscous formulae. The gas motion is assumed to be two-dimensional. The equations of motion for a fluid particle located at (r, θ) at time t with angular momentum per unit mass J are

$$\frac{d^2 r}{dt^2} = \frac{J^2}{r^3} - \frac{\partial \tilde{V}}{\partial r} - \frac{T_r}{\sigma}, \tag{2.2a}$$

$$\frac{dJ}{dt} = -\frac{\partial \tilde{V}}{\partial \theta} - \frac{r}{\sigma} T_\theta, \tag{2.2b}$$

$$\frac{d\theta}{dt} = \frac{J}{r^2}, \tag{2.2c}$$

where σ is the surface density, and (T_r, T_θ) is the force due to pressure and viscosity averaged over the scale height in the z-direction defined as follows:

$$T_r = \frac{\partial P_{rr}}{\partial r} + \frac{1}{r}\frac{\partial P_{r\theta}}{\partial \theta} + \frac{1}{r}(P_{rr} - P_{\theta\theta}), \tag{2.3a}$$

$$T_\theta = \frac{1}{r^2}\frac{\partial}{\partial r}(r^2 P_{r\theta}) + \frac{1}{r}\frac{\partial P_{\theta\theta}}{\partial \theta}, \tag{2.3b}$$

where P_{rr}, $P_{r\theta}$ and $P_{\theta\theta}$ are the elements of the two-dimensional stress tensor (see SS). The total potential, $\tilde{V}$, consists of contributions from the central mass or the background stellar population in the disk, the perturbational mass, and the mass of the gas itself.

$$\tilde{V}(r,\theta,t) = \tilde{V}_0(r) + \tilde{V}_1(r,\theta,t) + \tilde{V}_D(r,\theta,t). \tag{2.4}$$

In the absence of any disturbance, the gas is in circular motion around the center. Its angular speed $\Omega(r)$ at $r = r_0$ may be calculated from

$$r_0\Omega^2(r_0) = \frac{d\tilde{V}}{dr}, \tag{2.5}$$

and the angular momentum is

$$J_0 = r_0^2\,\Omega(r_0). \tag{2.6}$$

The periodic potential due to the external perturbational mass may be expressed in terms of Fourier components,

$$\tilde{V}_1(r,\theta,t) = \Phi_1(r)\cos(\omega t - m\theta). \tag{2.7}$$

Therefore, in a frame of reference rotating at pattern speed $\Omega_P = \omega/m$, $\tilde{V}_1$ is time-independent and the flow pattern of the gas becomes steady state with respect to coordinates (r, ϕ) with

$$\phi = \theta - \Omega_P t. \tag{2.8}$$

Following SYL, we consider the perturbation quantities r_1 and ϕ_1 which are specified as

$$r = r_0 + r_1, \tag{2.9a}$$

$$\phi = \phi_0 + [\Omega(r_0) - \Omega_P]t + \phi_1, \tag{2.9b}$$

where (r_0, ϕ_0) is the unperturbed reference location of the particle. The equations of motion in terms of perturbation quantities are

$$\frac{d^2r_1}{dt^2} + \kappa^2(r_0)r_1 = 2\Omega(r_0)\frac{J_1}{r_0} - \frac{\partial\tilde{V}_1}{\partial r} - \frac{\partial\tilde{V}_D}{\partial r} - \frac{1}{\sigma}T_r, \tag{2.10a}$$

$$r_0^2 \frac{d\phi_1}{dt} = J_1 - 2r_0\Omega(r_0)r_1 , \tag{2.10b}$$

$$\frac{dJ_1}{dt} = -\frac{\partial \tilde{V}_1}{\partial \phi} - \frac{\partial \tilde{V}_D}{\partial \phi} - \frac{r}{\sigma} T_\theta , \tag{2.10c}$$

in which

$$\kappa^2 = 4\Omega(r_0)^2 \left[1 + \frac{r_0}{2\Omega(r_0)} \frac{d\,\Omega(r_0)}{dr_0} \right], \tag{2.11}$$

$$J_1 = J - J_0 . \tag{2.12}$$

It might be noted that these equations are not linear. The non-linear contributions enter the equations through the self-gravitating terms involving $\tilde{V}_D$ and the stress terms (T_r, T_θ). To understand the situation better, it is useful to distinguish between the functional dependence of $\tilde{V}_1$ and $\tilde{V}_D$ on r. $\tilde{V}_1$ represents the long range force ; it varies slowly with r. Thus, we may expand $\tilde{V}_1$ at r_0 as long as r_1 is small. $\tilde{V}_D$, however, is expected to vary rapidly with r such that the corresponding waves are tightly wound. Therefore, $\tilde{V}_D$ must be evaluated at $r_0 + r_1$, not at r_0. On the other hand, both $\tilde{V}_1$ and $\tilde{V}_D$ can be evaluated at $\phi = \phi_0 + [\Omega(r_0) - \Omega_P]\,t$. With this approximation, we may rewrite equation (2.10c) by ignoring $\partial \tilde{V}_D / \partial \phi$, since $|\partial \tilde{V}_D / \partial \phi| \ll |r\,\partial \tilde{V}_D / \partial r|$ and $|r\,\partial \tilde{V}_D / \partial r|$ is comparable with $|r\,\partial \tilde{V}_1 / \partial r|$ or $|\partial \tilde{V}_1 / \partial \phi|$:

$$-[\omega - m\,\Omega(r_0)]\frac{dJ_1}{d\psi_0} = m\,\Phi_1 \sin\psi_0 - \frac{1}{\sigma r}\frac{\partial}{\partial r}(r^2 P_{r\theta}) - \frac{1}{\sigma}\frac{\partial P_{\theta\theta}}{\partial \theta} , \tag{2.13}$$

where

$$\psi_0 \equiv m\,\phi_0 - [\omega - m\,\Omega(r_0)]\,t\ . \tag{2.14}$$

For the steady state response, the solutions of r_1 and ϕ_1 are periodic in ψ_0. With the help of the following (WKBJ) approximations:

$$\frac{1}{\sigma}\frac{\partial}{\partial r} \approx \frac{1}{\sigma_0}\frac{\partial}{\partial r_0}\ , \tag{2.15}$$

$$\left|\frac{\partial P}{\partial r}\right| \gg \left|\frac{1}{r}\frac{\partial P}{\partial \phi}\right|, \qquad \left|\frac{\partial P}{\partial r}\right| \gg \left|\frac{1}{r}\frac{P}{\phi}\right|, \tag{2.16}$$

where P is the stress tensor, we can eliminate J_1 between equations (2.10a) and (2.10c) and obtain

$$\frac{\partial}{\partial\psi_0}\left[(\omega - m\,\Omega)^2\frac{\partial^2 r_1}{\partial\psi_0^2} + \kappa^2 r_1\right] = \frac{\partial}{\partial\psi_0}\left[g_1 + g_D - \frac{1}{\sigma_0}\frac{\partial P_{rr}}{\partial r_0}\right] + \frac{2\Omega}{(\omega - m\,\Omega)\sigma_0}\frac{\partial P_{r\theta}}{\partial r_0}\ , \tag{2.17}$$

where g_1 is the effective perturbational quantity of the external force,

$$g_1(r_0\ ,\ \psi_0) = \frac{1}{r_0}\Psi_1(r_0)\cos\psi_0\ , \tag{2.18}$$

with

$$\Psi_1(r_0) \equiv -\,r_0\frac{\partial\Phi_1}{\partial r_0} + \frac{2m\,\Omega(r_0)\Phi_1(r_0)}{\omega - m\,\Omega(r_0)}\ , \tag{2.19}$$

and g_D is the radial self-gravity of the gaseous disk. To the asymptotic (WKBJ) approximation considered in the study, g_D may be expressed in terms of the surface density by an integral (Borderies, Goldreich and Tremaine 1983, Shu 1984):

$$g_D(r_0, \psi_0) = -\,2\,G\int_0^\infty \frac{\sigma(r', \psi_0)}{r - r'}dr'\ , \tag{2.20}$$

with

$$r = r_0 + r_1(r_0, \psi_0). \tag{2.21}$$

The surface density, σ, is to be determined by the equation of continuity in the Lagrangian coordinates (r_0, ψ_0):

$$\sigma(r, \psi) r dr d\psi = \sigma_0(r_0) r_0 dr_0 d\psi_0. \tag{2.22}$$

Again, we use the asymptotic (WKBJ) approximation in which the variation in r is much more rapid than that in ψ. Within this approximation, we have $d\psi \approx d\psi_0$. The Jacobian of the transformation may be approximated by

$$\frac{\partial(r, \psi)}{\partial(r_0, \psi_0)} \approx \frac{\partial r}{\partial r_0} = 1 + \frac{\partial r_1}{\partial r_0}. \tag{2.23}$$

Equation (2.22) becomes

$$\sigma(r, \psi) = \frac{\sigma_0(r_0)}{1 + \dfrac{\partial r_1}{\partial r_0}}, \tag{2.24}$$

to the order of accuracy with which we work. Equation (2.20) then may be written as

$$g_D = -2G\, \sigma_0(r_0) \int_0^\infty \frac{dr'_0}{r_0 + r_1(r_0, \psi_0) - r'_0 - r_1(r'_0, \psi_0)}. \tag{2.25}$$

Replacing g_D by equation (2.25) in equation (2.17) gives an integro-differential equation for r_1 alone:

$$\frac{\partial}{\partial \psi_0}\left[(\omega - m\,\Omega)^2 \frac{\partial^2 r_1}{\partial \psi_0^2} + \kappa^2 r_1\right] = \frac{\partial}{\partial \psi_0}\left[\frac{1}{r_0}\Psi_1(r_0)\cos\psi_0\right.$$

$$\left. -2G\,\sigma_0 \int_0^\infty \frac{dr'_0}{r_0 + r_1(r_0, \psi_0) - r'_0 - r_1(r'_0, \psi_0)} - \frac{1}{\sigma_0}\frac{\partial P_{rr}}{\partial r_0}\right] + \frac{2\Omega}{(\omega - m\,\Omega)\sigma_0}\frac{\partial P_{r\theta}}{\partial r_0}.$$

(2.26)

Equation (2.26) is a singular non-linear integro-differential equation for r_1 (P_{rr} and $P_{r\theta}$ depend on r_1 implicitly) with two independent variables (r_0, ψ_0). Our next task is to reduce it to an equation of a single independent variable.

2. 2. The Integro-Differential Equation

It is convenient at this point to introduce a number of dimensionless variables. One of the fundamental dimensionless parameters to appear in the equation is a small quantity,

$$\epsilon \equiv \frac{2\pi G\, \sigma_0(r_L)}{r_L \tilde{D}}, \tag{2.27}$$

where r_L is the distance from the center to one of the Lindblad resonances, σ_0 is the surface density at r_L and $\tilde{D}$ is defined as

$$\tilde{D} \equiv \left| r_0 \frac{dD}{dr_0} \right|_{r_0 = r_L}, \tag{2.28}$$

with D defined as

$$D \equiv \kappa^2(r_0) - [\omega - m\,\Omega(r_0)]^2 . \tag{2.29}$$

We define a dimensionless Lagrangian variable,

$$x_0 = \frac{r_0 - r_L}{r_L}, \tag{2.30}$$

so that for small X_0 we can expand

$$D \approx \pm \tilde{D} x_0, \tag{2.31a}$$

where the upper sign corresponds to the inner Lindblad resonance, while the lower

sign, the outer Lindblad resonance.

The natural dimensionless distances in the problem, however, should be (see SYL)

$$\xi_0 = \epsilon^{-1/2} x_0 , \tag{2.31b}$$

$$X = \epsilon^{-1/2} r_L^{-1} r_1 . \tag{2.31c}$$

Written in terms of them, we have

$$\frac{\partial}{\partial \psi_0}\left[\epsilon^{-1/2}\frac{\kappa^2}{\tilde{D}}\left(\frac{\partial^2 X}{\partial \psi_0^2} + X\right)\right] = \frac{\partial}{\partial \psi_0}\left[\mp \xi_0 X \pm f \cos\psi_0 \right.$$

$$\left. -\frac{1}{\pi}\int_{-\infty}^{\infty} \frac{d\,\xi_0'}{\xi_0 + X - \xi_0' - X'} - \frac{\partial \tilde{P}_{rr}}{\partial \xi_0}\right] \mp \frac{2\Omega}{\kappa}\frac{\partial \tilde{P}_{r\theta}}{\partial \xi_0} , \tag{2.32}$$

where

$$\tilde{P} = \frac{\epsilon^{-1/2} P}{2\pi G r_L\, \sigma_0^2(r_L)} , \tag{2.33}$$

and

$$f = \frac{|\Psi_1(r_L)|}{2\pi G r_L\, \sigma_0(r_L)} . \tag{2.34}$$

Equation (2.32) may be solved by a series expansion,

$$X = X_1 + \epsilon^{1/2} X_2 + \cdots \tag{2.35}$$

Clearly, the lowest approximation gives us

$$\frac{d^2 X_1}{d\,\psi_0^2} + X_1 = 0 , \tag{2.36}$$

which yields a solution of the form

$$X_1 = A(\xi_0)\cos[\psi_0 - \Phi(\xi_0)]\,. \tag{2.37}$$

It was shown (SYL and Shu et al.) that the conditions for X_2 free from secular terms in the series expansion can be used to reduce the problem to an integro-differential equation of a single independent variable ξ_0 for a complex dependent variable,

$$Z = A(\xi_0)\, e^{i\,\Phi(\xi_0)}\,. \tag{2.38}$$

The equation is, then,

$$\frac{dF}{d\,\xi_0} + \frac{1}{\pi}\int_{-\infty}^{\infty} I(q^2)\frac{Z(\xi_0') - Z(\xi_0)}{(\xi_0' - \xi_0)^2}d\,\xi_0' \pm \xi_0 Z(\xi_0) = \pm f\ , \tag{2.39}$$

in which

$$I(q^2) \equiv \frac{2}{q^2}[(1 - q^2)^{-1/2} - 1]\,, \tag{2.40}$$

$$q^2 = \left|\frac{Z(\xi_0') - Z(\xi_0)}{\xi_0' - \xi_0}\right|^2\,, \tag{2.41}$$

and

$$F \equiv \frac{1}{\pi}\oint(\tilde{P}_{rr} \pm i\ \frac{2\Omega}{\kappa}\tilde{P}_{r\theta})\, e^{i\,\psi_0}\, d\,\psi_0\,. \tag{2.42}$$

Equation (2.39) is the fundamental integro-differential of our formulation.

2. 3. The Pressure and Viscous Term

The term $dF\,/\,d\,\xi_0$ in equation (2.39) contains the contribution from the pressure and the viscosity. It is necessary to express it explicitly in terms of Z. The lengthy derivation can be found in Appendix A. The results are summarized here.

We assume the coefficients of viscosity to be constant and the stress-strain relation to be of classic Newtonian type. Thus

$$P_{rr} = -P + 2\mu\frac{\partial u}{\partial r} + (\mu' - \frac{2}{3}\mu)(\frac{u}{r} + \frac{\partial u}{\partial r} + \frac{1}{r}\frac{\partial v}{\partial \theta}) \tag{2.43a}$$

$$P_{r\theta} = \mu(\frac{\partial v}{\partial r} - \frac{v}{r} + \frac{1}{r}\frac{\partial u}{\partial \theta}) \tag{2.43b}$$

where

$$u = \frac{dr_1}{dt} \tag{2.44a}$$

$$v = r(\Omega - \Omega_P) + r\frac{d\phi}{dt} \tag{2.44b}$$

Under the approximation assumed, we may neglect the ϕ derivatives in equation (3.43) such that

$$P_{rr} \approx -P + (\frac{4}{3}\mu + \mu')\frac{\partial u}{\partial r}, \tag{2.45a}$$

$$P_{r\theta} \approx \mu r\frac{\partial}{\partial r}(\frac{v}{r}). \tag{2.45b}$$

Following the derivation in Appendix A, we reach the final results,

$$F \equiv \frac{\epsilon^{-1/2}a^2}{2\pi G r_L\, \sigma_0(r_L)}\, F_1 = \frac{\epsilon^{-1/2}a^2}{2\pi G r_L\, \sigma_0(r_L)}\,[\,\mathrm{Re}(F_1) + i\ \mathrm{Im}(F_1)\,], \tag{2.46}$$

where

$$\mathrm{Re}(F_1) = I(q_0^2)\frac{dZ(\xi_0)}{d\xi_0}, \tag{2.47}$$

$$\mathrm{Im}(F_1) = \mp \frac{\kappa}{\sigma_0(r_L)a^2} \{(\frac{4}{3}\mu+\mu')[I_0(q_0)-I_2(q_0)] + \mu I(q_0^2)\} \frac{dZ(\xi_0)}{d\xi_0}, \quad (2.48)$$

with

$$I_n(q_0) \equiv \frac{1}{2\pi}\int_{-\pi}^{\pi} \frac{\cos(n\Theta)d\Theta}{1+q_0\cos\Theta} = \frac{1}{q_0^n(1-q_0^2)^{1/2}}[(1-q_0^2)^{1/2}-1]^n ,$$

$$n = 1, 2, \cdots \quad (2.49)$$

$$I(q_0^2) \equiv -\frac{2}{q_0} I_1(q_0) = \frac{2}{q_0^2}[(1-q_0^2)^{-1/2} - 1] \quad (2.50)$$

and

$$q_0 \equiv \left|\frac{dZ}{d\xi_0}\right|. \quad (2.51)$$

It is convenient for the present purpose to introduce a new dimensionless parameter

$$2\tilde{k}_0 = \left[\frac{2\pi G r_L \sigma_0(r_L)}{a^2\epsilon^{-1/2}}\right]^{2/3} = \frac{2\pi G \sigma_0}{a^2}\frac{r_L}{\gamma} \quad (2.52a)$$

where

$$\gamma = \left(\frac{r_L \tilde{D}^{1/2}}{a}\right)^{2/3}. \quad (2.52b)$$

Thus, equation (2.46) becomes

$$F = (2\tilde{k}_0)^{-2/3}[I_0(q_0^2) \mp i\, b(q_0^2)]\frac{dZ(\xi_0)}{d\xi_0} \quad (2.53)$$

where

$$b(q_0^2) \equiv \frac{\kappa}{\sigma_0(r_L)a^2}\{(\frac{4}{3}\mu+\mu')[I_0(q_0)-I_2(q_0)] + \mu I(q_0^2)\}, \qquad (2.54a)$$

the limiting value of it as $q_0 \to 0$ is

$$b_0 = \frac{\kappa}{\sigma_0(r_L)a^2}(\frac{7}{3}\mu + \mu'). \qquad (2.54b)$$

Using new variables

$$Z' \equiv (2\tilde{k}_0)^{1/2} Z \ , \qquad (2.55)$$

$$\xi_0' \equiv (2\tilde{k}_0)^{1/2} \xi_0 \ , \qquad (2.56)$$

the fundamental integro-differential equation takes the following form,

$$\frac{d}{d\xi_0'}\{[I(q_0^2) \mp ib(q_0^2)]\frac{dZ'}{d\xi_0'}\} - \frac{2\tilde{k}_0}{\pi}\int_{-\infty}^{\infty} I(q^2)\frac{Z'(\xi_0'')-Z'(\xi_0')}{(\xi_0''-\xi_0')^2}d\xi_0'' \mp \xi_0' Z'(\xi_0')$$

$$= \mp f' , \qquad (2.57)$$

where

$$f' = \frac{|\Psi_1|}{a^2\gamma} . \qquad (2.58)$$

Therefore, we obtain a non-linear integro-differential equation of second order. The equation can not be solved with usual techniques. Again, we adopt the method of solutions used by SYL, in which a non-linear differential equation is constructed out of equation (2.57). This differential equation will give results which, as shown in SYL, satisfactorily approximate the integro-differential equation.

CHAPTER III

PHYSICAL PARAMETERS

In deriving the integro-differential equation for the non-linear waves in the preceding chapter, we have used a number of approximations and introduced several dimensionless parameters. Justifications for using these approximations were given for the waves in Saturn's rings (SYL). In this chapter, we want to re-evaluate these approximations together with the dimensionless parameters for other similar problems in astrophysics, to which, we hope, our theory can be applied.

For a self-gravitating gaseous disk, there are four basic time scales which characterize the physics of the problem. The rate of disk rotation specifies a dynamic time scale , which we denote as t_R ,

$$t_R \approx \Omega^{-1} \text{ or } \kappa^{-1} . \tag{3.1}$$

The rotation, for most of the problems considered here, depends mainly on the gravity of the central mass or the background disk stars. The only exception is the case of barred galaxies, whose motions are fully self-supported. The time scale associated with self-gravity may be measured by

$$t_G \approx (G\,\sigma_0 / r)^{-1/2} , \tag{3.2}$$

where G is the gravitational constant, σ_0 is the surface density of the gaseous disk and r represents a typical radial distance. This indeed is the equivalent Jean's time for disk systems. An intrinsic time scale in the gas is the acoustic time,

$$t_A \approx r / a \ , \tag{3.3}$$

where a is the sound speed and r is, again, a typical radial distance. Using a distance on the scale of the size of a disk for r, in defining t_G and t_A is entirely appropriate, since the effects of gravity and pressure are to be measured against the rotation, which becomes important on the scale of r. Viscosity gives rise to another time scale in the system, which we define as

$$t_V \approx \frac{(\Delta r)^2}{\nu} \ , \tag{3.4}$$

where ν is the kinematic viscosity and Δr is the typical distance over which a wave train is being attenuated. Although these four time scales represent the four basical physical components in the dynamics of a self-gravitating gaseous disk, they do not appear separately in the problem. It is their combinations that govern the nature of the problem.

In the case of Saturn's rings, the sound speed is negligibly small. The waves have no acoustic component. The collective effects of gravity organize ring particles into spiral waves in balance with the rotation. The waves of this kind are characterized by parameter ϵ [see equation (2.27)]

$$\epsilon = \frac{2\pi G \, \sigma_0}{r_L \, \tilde{D}} \approx \frac{t_R^2}{t_G^2} \ , \tag{3.5}$$

where $\tilde{D} \approx (3\kappa)^2$ [see equations (2.28) and (2.29)], and r_L is the radius for the Lindblad resonance. The term, "density waves", has been used in the past to refer to such waves.

As for the 3-kpc arm, the effects of self-gravity are relatively unimportant.

The waves are essentially acoustic in nature. We call them "acoustic waves" in the limit of zero self-gravity. The parameter

$$\gamma = \left[\frac{r_L \tilde{D}^{1/2}}{a}\right]^{2/3} \approx \left[\frac{t_A}{t_R}\right]^{2/3} \tag{3.6}$$

appears in the problem (see Yuan 1984).

When the small yet non-negligible effects of self-gravity are taken into account for the gas in the 3-kpc arm problem, the waves are modified by gravity effects. Another two parameters, Q and $\tilde{k}_0$, necessarily come into the picture. The problem no longer differs from the general problem in which all three non-dissipative factors — rotation, pressure and self-gravity are involved. The problems of the proto-stellar disk of the solar nebula, the circumstellar disk of a binary and the spiral structure of normal galaxies and barred galaxies all belong to this category.

The quantity

$$Q \equiv \frac{\kappa a}{\pi G \sigma_0} \approx \frac{t_G^2}{t_A t_R} \tag{3.7}$$

introduced by Toomre (1963) to set the stability criterion for a self-gravitating disk is extremely useful for the classification of waves. It is clear from equation (3.7) that Saturn's rings correspond to the case of $Q = 0$ and the 3-kpc arm without self-gravitation, to the other extreme, the case of $Q = \infty$. All other cases lie somewhere between these extremes. For instance, for the self-excited waves in spiral galaxies, Q remains nearly unity throughout the disk except in regions close to the center where the surface density of the ever reduced disk component causes

Q to rise sharply. When self-gravity is taken into account for the 3-kpc arm, Q would remain much greater than 1 but finite. The values of Q are expected to be the same also for cases of the proto-stellar disk and the circumstellar disk of a binary.

The quantity $\tilde{k}_0$ is another parameter involving the three non-dissipative time scales. Unlike Q which does not appear explicitly in the integro-differential equation, $\tilde{k}_0$ is the parameter in front of the integral [see equation (2.57)]. Therefore, $\tilde{k}_0$ directly measures the self-gravity against the pressure and rotation. Using the definition (5.25), we may re-write

$$\tilde{k}_0 = \frac{k_0 r_L}{\gamma} = \frac{\pi G \sigma_0}{a^2} \cdot \frac{r_L}{(\frac{r_L \tilde{D}^{1/2}}{a})^{2/3}}$$

$$\approx \frac{t_A^{4/3} t_R^{2/3}}{t_G^2} \tag{3.8}$$

where k_0 is the basic wavenumber used in the density wave theory of galactic spirals (e. g., Lin and Lau 1979). For Saturn's rings, $\tilde{k}_0$ approaches infinity. Equation (2.57) reduces to the integral equation of SYL. For the 3-kpc arm, $\tilde{k}_0$ is about 0.1. For a barred galaxy, $\tilde{k}_0$ would be of the order of unity. As for the proto-stellar disk or the circumstellar disk, although the precise value of $\tilde{k}_0$ is not known without a realistic disk model, it seems reasonable to assume $0.1 \leqslant \tilde{k}_0 \leqslant 1$.

In deriving the integro-differential equation, three basic assumptions are used: (1) The excursion of a fluid particle, represented by r_1, is small compared with r_0; (2) The parameter ϵ is small such that we may expand our solutions in

series of $\epsilon^{1/2}$ and (3) The WKBJ approximation is assumed to be valid. Thus, the perturbation quantities vary rapidly with r but slowly with ψ, or $|rk| \gg m$ with k being the wave number in the r - direction and m is equal to 2 for an oval distortion. The last assumption is equivalent to stating that the resulting waves have a tightly wound spiral pattern. This requirement, which is a confirmed posteriori in analysis, has been used in almost all analytical works on the density wave theory and has repeatedly proven to be a satisfactory working hypothesis. Therefore, it is the first two assumptions that we want to examine carefully.

The first assumption holds perfectly for Saturn's rings, where r_0 is about $10^5\ km$ and r_1 is about $10\ km$. For the 3-kpc arm, the validity of this assumption is weaker. In that case, $r_0 = 3\ kpc$ and the excursion, according to the calculations of Yuan (1984), is $r_1 \approx 0.3\ kpc$. Thus, for analyzing the 3-kpc arm problem using the present formulation, we shall keep in mind that the quantitative results are limited to an accuracy of $\pm 10\,\%$. The same degree of accuracy may be expected for galaxy problems as well, since a typical epicycle of a star would have a size about one-tenth of its orbital radius. For the proto-stellar disk or the circumstellar disk, in which the disk mass is tiny in comparison with the mass of the central star or stars, the situation is somewhat improved. It is more likely to be closer to the case of Saturn's rings than to that of galactic disks. Unfortunately, it is difficult to make a more definite estimate without a realistic model.

The parameter ϵ in the second assumption is about 10^{-8} for Saturn's rings. The series in $\epsilon^{1/2}$ is therefore fully justified. For the 3-kpc arm, if we take $\sigma_0 = 5\ M_\odot / pc^2$ for the gas and $\tilde{D} = (188)^2\ km^2/\ sec^2\text{–}kpc^2$, ϵ is

approximately equal to 0.001. The series expansion in $\epsilon^{1/2} = 0.03$ yields an accuracy much less than in the case of Saturn's rings, but it is small enough to justify our derivation. Again, using the same reasoning that the proto-stellar and the circumstellar disks are more likely to be similar to the case of Saturn's rings than that of the galactic disks, we should expect that the series expansion is also justified for them. The assumption, unfortunately, does not hold so well for the barred galaxy problems unless the galaxy has a relatively large bulge and the surface density of its disk component near the Lindblad resonances is relatively small.

The following table summarizes the above discussions. The numerical values in the table are calculated according to SYL for Saturn's rings, Yuan (1984) for the 3-kpc arm, Cassen and Summers (1983) for the proto-stellar disk of the solar nebula (the minimum-mass model), and for barred galaxies we use

$$\sigma_0 = 50\ M_\odot / pc^2\ , \quad r_0 = 11\ kpc\ , \quad r_1 = 1\ kpc\ ,$$

$$\kappa = 14\ km/sec-kpc\ , \quad a = 40\ km/sec\ , \quad \tilde{D} = 2538\ km^2/sec^2-kpc^2\ ,$$

based on unpublished observations of NGC1300 (Shane and Yuan 1977).

Table 3.1

	r_1/r_0	ϵ	Q	$\tilde{k}_0$	γ
Saturn's rings	10^{-5}	10^{-8}	0	∞	∞
3–kpc arm	10^{-1}	10^{-3}	10	0.1	10
proto–stellar disk	10^{-2}	10^{-2}	$\gg 1$	$0.1 \sim 1$	–
barred galaxies	10^{-1}	10^{-1}	1	2	–

The viscosity plays an important role in damping the density waves or acoustic waves, in all cases except for the barred galaxies. The coefficients of viscos-

ity for Saturn's rings have been studied in great detail by Shu et al. (SS; Shu et al.) and by Borderies, Goldreich and Tremaine (1983). They have showed that the kinematic viscosity ν depends non-linearly on the streamline-crossing parameter q [see equation (2.41)] and the random velocity of the ring particles. The values of viscosity for the gas in the proto-stellar or circumstellar disks or in the Galaxy are unknown, although most researchers believe that in both cases the viscosity arises from turbulent motions of the gas. It can be estimated by order-of-magnitude arguments, which give $\nu = a\ l$ with l the scale length for turbulent motions and a , the sound speed. Very little can be said beyond this. In the derivation of the integro-differential equation, we have simply assumed ν to be constant and adopted the classic stress-strain relation.

CHAPTER IV

EXCITATION AND PROPAGATION OF THE WAVES IN THE DISK

4. 1. The Linear Equation

In principle, all the information about the density and/or acoustic waves driven by a periodic disturbance is contained in the integro-differential equation derived in Chapter II. Solving that equation with proper boundary conditions should let us understand not only the mechanism that is responsible for generating the waves, but also the way the waves propagate. The solution to equation (2.57), however, can not be obtained easily. It involves a complete treatment of a non-linear singular integral for which no standard technique is available at present. In order to make the problem mathematically manageable, we follow SYL in replacing the integro-differential equation heuristically by a differential equation which (1) in the linear limit ($q_0 \to 0$) reduces to the linear form of the integro-differential equation, and (2) reproduces the amplitude relation and the non-linear dispersion relation in the asymptotic limit $\xi_0 \gg 0$, i. e., in regions where waves are fully developed and propagate essentially in free forms. Equation (2.57), however, is far more complicated than the governing equation in SYL and Shu et al. It turns out that the second requirement can not be easily satisfied so that the heuristic differential equation reproduces in the WKBJ limit the amplitude relation and the non-linear dispersion relation simultaneously. Since the amplitude relation states the conservation of angular momentum carried by the waves, it clearly

surpasses the importance of the WKBJ dispersion relation. Therefore, we shall instead choose a differential equation which meets the linearization requirement and satisfies the amplitude relation.

To write down such a differential equation is not overly difficult if we follow SYL. The process, however, must be guided by a careful study of the properties of these waves. A great deal of knowledge about the density and/or acoustic waves, fortunately, can be obtained by analyzing the linear equation of the free waves and its dispersion relation. As we recall, the appearance of the streamline crossing parameter q , defined in equation (2.41) as

$$q^2 = \left| \frac{Z(\xi_0') - Z(\xi_0)}{\xi_0' - \xi_0} \right|^2 ,$$

and its limit $q_0 = |dZ / d\xi_0|$ in equation (2.57), is the source of non-linearity. In the limit of small displacements, i. e., when q and q_0 approach zero, those functions of q^2 or q_0^2 in equation (2.57) become constant,

$$I(q^2) \to 1 , \quad I(q_0^2) \to 1, \quad b(q_0^2) \to \frac{\kappa}{\sigma_0(r_L)a^2}\left(\frac{7}{3}\mu + \mu'\right) \equiv b_0 . \tag{4.1}$$

Equation (2.57) then takes a simple form,

$$(1 \mp i\, b_0)\frac{d^2Z}{d\xi_0^2} - \frac{2\tilde{k}_0}{\pi}\int_{-\infty}^{\infty} \frac{dZ / d\xi_0'}{\xi_0' - \xi_0} d\xi_0' \mp \xi_0 Z = \mp f' , \tag{4.2}$$

in which we have dropped the primes of Z and ξ_0 for convenience, but we should keep in mind that ξ_0 really stands for ξ_0' when we transform our results back to the dimensional forms. After performing Cauchy integration, we have

$$(1 \mp i\, b_0) \frac{d^2 Z}{d \xi_0^2} + i\, 2 \tilde{k}_0 \frac{dZ}{d \xi_0} \mp \xi_0 Z = \mp f', \tag{4.3}$$

where the upper signs correspond to the inner Lindblad resonance and the lower sings, the outer Lindblad resonance. We note that the positive sign in the second term corresponds to trailing waves.

4. 2. Linear Dispersion Relation

The fundamental properties of the density waves can be understood by studying the motions of the free waves in which the inhomogeneous forcing term f' and the viscous term containing b_0 may be ignored. It is easy to show that equation (4.3) would lead to the well-known linear dispersion relation (e. g. Lin and Lau 1979),

$$a^2 k^2 - 2\pi G\ \sigma_0\ |k\ | + \kappa^2 (1 - \nu^2) = 0\,, \tag{4.4}$$

in which k is the local radial wavenumber such that the perturbation quantity is

$$r_1 = \hat{r}_1 e^{i \int k dr}\,, \tag{4.5}$$

and ν is the effective frequency, defined as

$$\nu^2 = \frac{m^2 (\Omega - \Omega_P)^2}{\kappa^2} = \frac{(m\,\Omega - \omega)^2}{\kappa^2}\,. \tag{4.6}$$

The absolute value of k which appears in the second term of equation (4.4) suggests that there are two types of waves possible: trailing waves for $k < 0$ and leading waves for $k > 0$. It has been shown on physical grounds that trailing waves give the correct physical results both for Saturn's rings and for the 3-kpc arm. If $k < 0$, equation (4.4) has two roots,

$$\frac{ak}{\kappa} = -Q^{-1} \pm (Q^{-2} + \nu^2 - 1)^{1/2} . \tag{4.7}$$

Equation (4.7) is one of the most important results because it reveals the nature of the spiral density waves. First, it states that waves can only exist when $Q^{-2} + \nu^2 - 1 > 0$. Second, it implies that in the regions $\nu^2 - 1 > 0$ only short waves are allowed, i. e., those corresponding to the negative square root. Third, both long waves and short waves can exist between the Lindblad resonances which are located where

$$\nu^2 - 1 = 0 , \tag{4.8}$$

and the Q-barriers which are located where

$$Q^{-2} + \nu^2 - 1 = 0 . \tag{4.9}$$

In the above discussions, we have taken $n = 1$ in the more general definition of the Lindblad resonances,

$$m (\Omega - \Omega_p) = \pm n \kappa , \tag{4.10}$$

where the + sign corresponds to the inner Lindblad resonance and the − sign, the outer Lindblad resonance. The term "inner" and "outer" are in reference to the co-rotation which occurs at

$$\Omega(r) - \Omega_p = 0 . \tag{4.11}$$

A plot of $Q^{-2} + \nu^2 - 1$ versus r proves to be very useful in illustrating various features of the excitation and propagation of the waves. These curves are drawn schematically in Figure 4.1, corresponding to $Q = \infty, 2, 1$. The lower light curve (for $Q = \infty$) indeed represents the case of the 3-kpc arm with no self-gravity. It intersects the abscissa at the inner and outer Lindblad resonances, where

$\nu^2 - 1 = 0$. Since Q approaches ∞, these two points are also the Q-barriers, according to equation (4.9). Waves, in this case only short waves, can be found in regions outside the outer Lindblad resonance or inside the inner Lindblad resonance. Between the two Lindblad resonances, solutions become evanescent. The heavy curve with $Q = 2$ intersects the abscissa at the Q-barriers, which now lie between the two Lindblad resonances. Both long waves and short waves can exist between a Q-barrier and its neighboring Lindblad resonance. The evanescent region again lies between the two Q-barriers. Beyond the outer Lindblad resonance or inside the inner Lindblad resonance, only short waves are allowed. The curve (which is not drawn in the figure) with $Q = 10$ corresponding to the case in which the acoustic effect is modified by the effect of self-gravity such as the 3-kpc arm with self-gravity, the proto-stellar disk of the solar nebula or the circumstellar disk of a binary, will lie above the curve with $Q = \infty$ and below the curve with $Q = 2$. The top light curve with $Q = 1$ touches the abscissa at the co-rotation. The two Q-barriers, in this case, move to the co-rotation point simultaneously and coincide there. The curve corresponds to a typical situation found in a disk galaxy in which $Q = 1$ throughout the disk except near the inner Lindblad resonance, where Q becomes much greater than one as the surface density of the disk diminishes rapidly. A dashed line is drawn to illustrate this situation. Another Q-barrier results from this, occurring at the intersection of the dashed line and the abscissa. Both long and short waves exist between this Q-barrier and the co-rotation, or the double Q-barrier as noted above.

The curve, corresponding to the waves in Saturn's rings, lies far above the r-axis and is not drawn here. There is no Q-barrier in this case. Short waves can

exist on both sides of the Lindblad resonances, but long waves are only allowed between the two Lindblad resonances. The short waves in this case have wavelengths even smaller than the size of the ring particles (see e.g. Shu 1984). Physically, they can not possibly exist. Furthermore, since the sources of disturbance, i. e., the moons, in the majority of cases lie beyond the rings, waves in Saturn's rings usually occur only at the inner Lindblad resonances. Thus, we have a simple case of long waves traveling in regions outside the inner Lindblad resonances and decaying rapidly inside it.

The linear dispersion relation written in equation (4.4) contains both trailing and leading waves. The group velocity, C_g , can be obtained by taking derivative of equation (4.4) with respect to k , which yields the well known result (Toomre 1969; Shu 1984),

$$C_g = -\frac{\partial \omega}{\partial k} = \frac{\pi G \sigma_0 - |k| a^2}{\omega - m \Omega} \text{sign}(k) . \tag{4.12}$$

Accordingly, long trailing waves ($k < 0$, $\pi G \sigma_0 - |k| a^2 > 0$) propagate outward from the inner Lindblad resonance (where $\omega - m \Omega = -k$) and inward from the outer Lindblad resonance (where $\omega - m \Omega = +k$). Conversely, long leading waves ($k > 0$, $\pi G \sigma_0 - |k| a^2 > 0$) propagate toward the Lindblad resonances. As the disturbance potential varies on the scale of size of the disk, it is capable of exciting only the long waves at the Lindblad resonances. The large torques exerted on the rings by the moons and vice versa transport themselves through the Lindblad resonances. The necessary conclusion is that only the long trailing waves are being excited at the Lindblad resonances by the disturbance and propagate towards the co-rotation, carrying angular momentum (Goldreich and

Tremaine 1978). The same argument, of course, can be applied to the 3-kpc arm problem and the waves in the gaseous disk surrounding a stellar mass. It thus suffices to consider only the excitation of long trailing waves in this study.

When a long wave is excited at the outer Lindblad resonances such as in the case of the 3-kpc arm, it will propagate inward until it reaches the Q-barrier beyond which lies the evanescent region. The wave which can not penetrate the Q-barrier will be reflected as a short trailing wave propagating outward. Indeed, according to equation (4.12), only short trailing waves are capable of propagating outward from the Q-barrier. Thus, we would expect to obtain a solution in which short trailing waves are seemingly emitted from the Q-barrier. We shall show in the next chapter that this conjecture is fully confirmed in the linear analysis. A phase shift in the linear asymptotic solution, again, found in the next chapter, can be identified as the phase contribution that the long waves must pay for traveling from the outer Lindblad resonance to the Q-barrier. The problem of the 3-kpc arm without self-gravity treated by Yuan (1984) is a special case of this physical picture in which the long waves excited at the outer Lindblad resonance are reflected immediately.

The dispersion relation between the effective frequency $|\nu|$ and the dimensionless wavenumber $|k|a/\kappa$ depicted in Figure 4.2 further demonstrates the overall picture of wave propagation discussed here. We may regard $|\nu|$ as a distance indicator, measured from the co-rotation where $|\nu| = 0$. The Lindblad resonances are located at $|\nu| = 1$. When $|\nu| > 1$, there is only one wavelength for each $|\nu|$ at a fixed Q, which undoubtedly corresponds to the short wave root of the dispersion relation. When $|\nu| < 1$, it is always possible to

have both long wave and short wave solutions between the Lindblad resonance and the Q-barrier. For a fixed Q, the Q-barrier is situated at a point on the $|\nu|$ axis, through which a vertical line is tangential to the dispersion relation curve. When $Q \leqslant 1$, both long waves and short waves exist throughout the region between $|\nu| = 0$ and $|\nu| = 1$. It is interesting to observe that the short wave branch of the dispersion relation curve extends indefinitely beyond the Lindblad resonance. This result is significantly different from the case in the stellar dynamic formulation, in which both long wave branch and short wave branch of the dispersion relation curve for a certain Q are bounded by the vertical lines of $Q = \infty$ passing through the Lindblad resonances, as depicted in Figure 4.3. Therefore, even short waves can not propagate beyond their corresponding Lindblad resonances. The spiral waves are completely confined to a region bounded by the Lindblad resonances, a result reported in the first paper of the density wave theory (Lin and Shu 1964)!

The foregoing analysis of the dispersion relation has made the boundary conditions obvious. We should seek a solution behaving like an outgoing wave on the one end, and decaying rapidly after passing the Q-barrier on the other end. Moreover, these boundary conditions are not limited to the context of the linear theory. They can be used for the general non-linear problem.

4. 3. Non-linear Dispersion Relation

The study of the linear dispersion relation gives us deep insight into the nature of the wave motions — how they are being excited and how they propagate afterwards. The linear analysis, however, breaks down quickly after the

wave travels a distance of the order of $(2\pi f^{2})^{-1/2}$, in dimensionless units, from the Q-barrier (SYL 1985). The wave motions soon become highly non-linear. Many properties of the fully developed non-linear waves in the regions far away from the Q-barrier can be extracted from a WKBJ analysis. Following SYL, we take for granted that the complex displacement Z has a slowly varying amplitude $A(\xi_0)$ and a rapidly varying phase $\Phi(\xi_0)$. Then, judging from the singular nature of the integral in equation (2.57), we suppose that the most important contribution to the integral comes from the immediate neighborhood of ξ_0. Thus, we expand $Z(\xi'_0)$ in Taylor series,

$$Z(\xi'_0) \approx Z(\xi_0) \exp[\, i \;\; K \;\; (\xi'_0 - \xi_0)]\,, \tag{4.13}$$

where

$$K \equiv \frac{d\,\Phi}{d\,\xi_0}\,, \tag{4.14}$$

which is negative for trailing waves. It can be shown that to the WKBJ approximation,

$$\frac{1}{\pi}\int_{-\infty}^{\infty} I(q^{2})\frac{Z(\xi'_0) - Z(\xi_0)}{(\xi'_0 - \xi_0)^{2}}\, d\,\xi'_0 \approx K \;\; Z(\xi_0) H(q_0^{2})\,, \tag{4.15}$$

in which

$$H(q_0^{2}) \equiv \frac{1}{\pi}\int_{-\infty}^{\infty} I(q^{2})\frac{\sin^{2}\zeta}{\zeta^{2}}\, d\,\zeta\,, \tag{4.16}$$

$$q^{2} = q_0^{2}\frac{\sin^{2}\zeta}{\zeta^{2}}\,, \tag{4.17}$$

$$q_0^2 \approx K^2 A^2 . \tag{4.18}$$

The function $H(q_0^2)$ can be expanded in series of q_0^2 and is evaluated in SYL. It approaches the following limits

$$H(q_0^2) \sim 1 \qquad \text{as} \quad q_0^2 \to 0 , \tag{4.19}$$

$$H(q_0^2) \sim -\frac{2\sqrt{3}}{\pi} \ln(1 - q_0^2) \qquad \text{as} \quad q_0^2 \to 1 . \tag{4.20}$$

Applying the same WKBJ approximation to other terms in equation (2.57), we obtain

$$-2\tilde{k}_0 K \; H(q_0^2) + \xi_0 - I(q_0^2) K^2 = 0 . \tag{4.21}$$

Equation (4.21) is the non-linear dispersion equation. The forcing term on the right hand side of equation (2.57) may be ignored because we are interested only in free waves. In any case, it is much smaller than terms like $\xi_0 Z$ where ξ_0 is numerically large. In the limit of $a = 0$, equation (4.21) reduces to the non-linear dispersion relation of a pure density wave (SYL). On the other hand, when the effect of self-gravity is ignored, the equation takes the form of a pure acoustic wave,

$$\xi_0 = I(q_0^2) K^2 . \tag{4.22}$$

Using the definition of I [equation (2.50)] and the fact that $q_0 = |K| A$ is approaching 1 for large ξ_0, i. e., waves become highly non-linear, we obtain the following approximations for equation (4.22):

$$K^2 = \frac{1}{A^2}\left(1 - \frac{4}{\xi_0^2 A^4}\right) . \tag{4.23}$$

As expected, the wavelength is proportional to A and only has a weak dependence

on ξ_0.

4. 4. Amplitude Relation

One of the most important results of SYL is the derivation of the conservation of angular momentum flux of the waves from the integral equation of the complex displacement. Similar results can be obtained from equation (2.57). First, the dimensionless torque, $\tilde{J}$, exerted by a satellite or a minor oval distortion on the disk up to a distance ξ_0 is

$$\tilde{J}(\xi_0) = \mp f' \int_{-\infty}^{\xi_0} \mathrm{Im}(Z)\, d\xi'_0 . \tag{4.24}$$

Second, the singular integral in equation (2.57), after multiplying by Z^* (Z conjugate) and taking the imaginary part, can be shown to be equivalent to the dimensionless angular momentum flux density of the waves in the disk. In other words, the angular momentum flux at ξ_0 due to self-gravity, $\tilde{L}_G(\xi_0)$, is

$$\tilde{L}_G(\xi_0) = \int_{-\infty}^{\xi_0} d\xi'_0 \frac{2\tilde{k}_0}{\pi} \int_{-\infty}^{\infty} \frac{I(q^2)}{(\xi''_0 - \xi'_0)^2} \mathrm{Im}\,[Z^*(\xi'_0) Z(\xi''_0)]\, d\xi''_0 . \tag{4.25}$$

The above equation under the WKBJ approximation, in the same sense of the preceding section, can be reduced to

$$\tilde{L}_G(\xi_0) = -2\tilde{k}_0 A^2(\xi_0) L(q_0^2), \tag{4.26}$$

where

$$L(q_0^2) = \frac{1}{\pi} \int_0^{\infty} I(q^2) \frac{\sin 2\zeta}{\zeta} d\zeta . \tag{4.27}$$

Function $L(q_0^2)$ has similar properties to $H(q_0^2)$. Its functional dependence on

q_0^2 is given in SYL. For the present purposes, we just note that

$$L(q_0^2) \sim \frac{1}{2}, \qquad \text{as } q_0^2 \to 0, \tag{4.28a}$$

$$L(q_0^2) \sim -\frac{2\sqrt{3}}{\pi}\ln(1 - q_0^2), \qquad \text{as } q_0^2 \to 1. \tag{4.28b}$$

With the new notation, we may re-write equation (2.57) after multiplying by Z^* and taking the imaginary part,

$$\frac{d}{d\xi_0}[2\tilde{k}_0 A^2 L + IA^2 K] = \pm f\,\mathrm{Im}(Z) + bq_0^2, \tag{4.29}$$

or, equivalently,

$$\tilde{L}(\xi_0) = \pm \tilde{J}(\xi_0) - \int_{-\infty}^{\xi_0} bq_0^2 d\xi''_0, \tag{4.30}$$

where

$$\tilde{L}(\xi_0) \equiv \tilde{L}_G(\xi_0) + \tilde{L}_A(\xi_0) = -2\tilde{k}_0 A^2(\xi_0) L(q_0^2) - IA^2 K \tag{4.31}$$

is the total angular momentum flux, and

$$\tilde{L}_A(\xi_0) = -IA^2 K \tag{4.32}$$

is the acoustic part of the angular momentum flux. Note that K is negative for trailing waves. Equation (4.30) may be interpreted as the total angular momentum flux at ξ_0 is equal to the total torque exerted by the satellite or some minor distortion at the center on the disk, integrated from the evanescent region all the way up to ξ_0 minus the viscous damping over the same region. Without viscosity, equation (4.30),

$$2\tilde{k}_0 LA^2 + IA^2K = \mp\tilde{J}(\xi_0), \tag{4.33}$$

is called the amplitude relation in SYL.

Multiplying equation (4.21) by A^2 and equation (4.33) by K and adding them, we have

$$A^2\xi_0 = \mp\tilde{J}K \ . \tag{4.34}$$

For large ξ_0, equation (4.23) becomes

$$|K|A = 1 . \tag{4.35}$$

From equation (4.34) and (4.35), we obtain

$$|K| \to \left(\frac{\xi_0}{|\tilde{J}|}\right)^{1/3} \quad \text{and} \quad A \to \left(\frac{|\tilde{J}|}{\xi_0}\right)^{1/3} \quad \text{as} \quad \xi_0 \to \infty . \tag{4.36}$$

These two relations are exactly the same as in SYL. Thus, the acoustic effect does not change the results of pure density waves that $A \sim \xi_0^{-1/3}$ and $|K| \sim \xi_0^{1/3}$ for large ξ_0. This is in contrast to the results of the linear theory where $|K| \sim \xi_0^{1/2}$ and $A \sim \xi_0^{-3/4}$.

4. 5. Replacement By A Differential Equation

The non-linear singular integro-differential equation (2.57) cannot be solved by the usual known mathematical techniques. In order to make it mathematically manageable, we follow the procedure of SYL in replacing it with a differential equation. This differential equation has the following properties: It reduces to the linear differential equation (4.3) in the linear limit and it reproduces the non-linear amplitude relation, equation (4.33), and finally the non-linear dispersion

relation, equation (4.21), in the WKBJ asymptotic limit. The presence of the stress tensor term of pressure and viscosity, however, has made this extremely difficult. (This is a point overlooked in Shu et al.). It seems unlikely that there exists a simple way to construct an equation satisfying all the three requirements. The best we can do is to obtain an equation that satisfies the linear equation requirement and one of the two non-linear relation requirements. Since the amplitude relation results directly from the consideration of conservation of angular momentum of the waves, we decide to have it satisfied first. The equation of our choice is

$$\frac{d}{d\xi_0}[(I \mp i\, b)\frac{dZ}{d\xi_0}] + i\, 4\tilde{k}_0 L^{1/2}\frac{d}{d\xi_0}(L^{1/2}Z) \mp \xi_0 Z = \mp f' . \tag{4.37}$$

It is easy to show that equation (4.37) approaches equation (4.3) in the limit $q_0 \to 0$, and also it assumes the non-linear amplitude relation (4.33) by multiplying Z^*, integrating from $-\infty$ to ξ_0, and taking the imaginary part. When considering free waves, it takes the following non-linear dispersion relation,

$$-4\tilde{k}_0 KH + \xi_0 - IK^2 = 0 . \tag{4.38}$$

The only difference of this equation from equation (4.21) is a factor of 2 in front of the first term. In the case of pure acoustic waves, i. e., when the first term vanishes, (4.38) would be the same as equation (4.21) in the same limit. To the limit of pure density waves, the discrepancy of factor 2 shows up. We could have, like Shu et al., chosen a factor $\frac{2L}{H}$ to put in front of the term $\xi_0 Z$ in equation (3.37), for which equation (3.37) would still satisfy the two requirements as before, but leads to a dispersion relation,

$$-4\tilde{k}_0 KH + 2\xi_0 - IK^2 = 0 . \tag{4.39}$$

Equation (4.39) would reverse the results of equation (4.38) in the two limits. Since our primary interest is to modify the 3-kpc problem by including the self-gravity effects, equation (4.37) is more appropriate.

CHAPTER V

THE LINEAR THEORY

5. 1. The Reduced Differential Equation

In Chapter IV we have shown that when the streamline crossing parameter q is small, the fundamental integro-differential equation (2.57) reduces to the following linear differential equation [see (4.3)]:

$$(1 \mp i\, b_0) \frac{d^2 Z}{d \xi_0^2} + i 2 \tilde{k}_0 \frac{dZ}{d \xi_0} \mp \xi_0^2 Z = \mp f \ , \tag{5.1}$$

where we have rewritten f ' as f for simplicity, and as before,

$$b_0 = \frac{\kappa}{\sigma_0(r_L) a^2} (\frac{7}{3}\mu + \mu') \geqslant 0 \tag{5.2}$$

is the parameter linearly related to the coefficients of viscosity [see (2.54b)],

$$f = \frac{|\Psi_1|}{a^2 \gamma} \tag{5.3}$$

is the external force at one of the Lindblad resonances due to a satellite or a central distortion [see (2.58)], and

$$2\tilde{k}_0 \equiv \left[\frac{2\pi G r_L \sigma_0(r_L)}{a^2 \epsilon^{-1/2}} \right]^{2/3} \geqslant 0 \tag{5.4}$$

is a parameter associated with the self-gravity of the disk mass. In equation (5.1), the upper signs refer to the inner Lindblad resonance and the lower signs, the outer Lindblad resonance.

Equation (5.1) determines the motions of linear density and/or acoustic waves and it takes into consideration all three factors: pressure, viscosity and self-gravity. From the discussions in the preceding chapter, the following two boundary conditions should be imposed:

(i) $Z(\xi_0) \sim 0$ as $\xi_0 \to -\infty$, (5.5a)

(ii) $Z(\xi_0)$ behaves like an outgoing wave with

bounded amplitude as $\xi_0 \to +\infty$. (5.5b)

To be specific, we will concentrate on the problems associated with the outer Lindblad resonance. Problems associated with the inner Lindblad resonance can be treated similarly. Corresponding to the outer Lindblad resonance, equation (5.1) reduces to

$$(1 + i\, b_0) \frac{d^2 Z}{d \xi_0^2} + i 2 \tilde{k}_0 \frac{dZ}{d \xi_0} + \xi_0 Z = f \ . \tag{5.6}$$

In order to reduce equation (5.6) to the standard form so that the Airy functions can be employed, we reverse the direction of the independent variable by introducing

$$\eta_0 = -\xi_0 , \tag{5.7}$$

so that equation (5.6) becomes

$$(1 + i\, b_0) \frac{d^2 Z}{d \eta_0^2} - i 2 \tilde{k}_0 \frac{dZ}{d \eta_0} - \eta_0 Z = f \ . \tag{5.8}$$

We further introduce the following transformations :

$$\tan\beta = b_0 , \tag{5.9}$$

$$Z_1 = \cos^{-1/3}\beta \, e^{i\beta/3} Z , \tag{5.10}$$

$$\eta_1 = \cos^{1/3}\beta \, e^{-i\beta/3} \eta_0 , \tag{5.11}$$

and

$$\tilde{k} = \cos^{2/3}\beta \, e^{-i2/3\,\beta} \tilde{k}_0 . \tag{5.12}$$

Now equation (5.8) can take the following form :

$$\frac{d^2 Z_1}{d\eta_1^2} - i2\tilde{k}\frac{dZ_1}{d\eta_1} - \eta_1 Z_1 = f . \tag{5.13}$$

To eliminate the first order derivative term we further introduce new transformations,

$$\eta_2 = \eta_1 - \tilde{k}^2 \tag{5.14}$$

and

$$Z_2 = e^{-i\tilde{k}\eta_2} Z_1 , \tag{5.15}$$

to obtain

$$\frac{d^2 Z_2}{d\eta_2^2} - \eta_2 Z_2 = f \; e^{-i\tilde{k}\eta_2} . \tag{5.16}$$

We can obtain the real η_1-axis by rotating the real η_0-axis counterclockwise by $\beta/3$ and stretching it by a factor of $\cos^{1/3}\beta$. The real η_2-axis is obtained by translation using equation (5.14) so it is parallel to the real η_1-axis (see Figure 5.1).

From Figure 5.1, we see that the real η_0-axis on which the boundary conditions are specified may be expressed in the η_2-plane as

$$\eta_2 = \eta_{20} + \alpha\, e^{-i\beta/3} \tag{5.17}$$

where η_{20} is the intersection (indicated by T) of the imaginary axis of the η_2-plane and the real η_0-axis. As we shall see later, T is the turning point or the Q-barrier separating the wavy part and the evanescent part of the solution, for the inviscid case. From the geometry of Figure 5.1, we obtain

$$\eta_{20} = i\, \tilde{k}_0^2 \cos^{4/3}\beta\, [\sin(4\beta/3) - \cos(4\beta/3)\tan(\beta/3)]\,. \tag{5.18}$$

The quantity α in equation (5.17) is a real variable, measured from point T. It is convenient to write

$$\alpha \equiv \cos^{1/3}\beta\, \eta_3\,, \tag{5.19}$$

$$\eta_3 \equiv \eta_0 - \eta_{00}\,, \tag{5.20}$$

where η_{00} is the distance from the origin of the real η_0-axis to T (OT in Figure 5.1),

$$\eta_{00} = \frac{\tilde{k}_0^2\, \cos\beta \cos(4\beta/3)}{\cos(\beta/3)}\,, \tag{5.21}$$

and η_3 is the distance from any point P on the real η_0-axis to T. When the real η_0 value varies from $-\infty$ to $+\infty$, η_3 will change accordingly to cover the whole real η_0-axis.

Any point P on the real η_0-axis can also be written in polar coordinates in the η_2-plane as

$$\eta_2 \equiv \alpha_1 \, e^{-i\,\beta_1/3} . \tag{5.22}$$

Note that

$$\alpha_1 \sim \alpha , \quad \beta_1 \sim \beta , \qquad as \quad |\eta_0| \to \infty . \tag{5.23}$$

In terms of η_2 and Z_2, we may translate the boundary conditions (5.5a) and (5.5b) into the following:

(i) $Z_2(\eta_2) \sim 0 \qquad$ as $\eta_2 \to +\infty^{-i\beta/3}$, (5.24a)

(ii) $Z_2(\eta_2)$ behaves like an outgoing wave with

bounded amplitude as $\eta_2 \to -\infty^{-i\beta/3}$. (5.24b)

The particular solution of (5.16) can be written as

$$Z_{2p}(\eta_2) = -\pi f \; [\, I_b(\eta_2)\mathrm{Ai}(\eta_2) + I_a(\eta_2)\mathrm{Bi}(\eta_2) \,] \tag{5.25}$$

where

$$I_a(\eta_2) \equiv \int_{\eta_2}^{\infty e^{-i\beta/3}} \mathrm{Ai}(\eta_2') \, e^{-i\,\tilde{k}\,\eta_2'} \, d\,\eta_2' , \tag{5.26a}$$

and

$$I_b(\eta_2) \equiv \int_{\eta_{20}}^{\eta_2} \mathrm{Bi}(\eta_2') \, e^{-i\,\tilde{k}\,\eta_2'} \, d\,\eta_2' , \tag{5.26b}$$

where Ai and Bi are the Airy functions and the integrals are to be carried out along the real η_0-axis. By substituting the asymptotic expansions of I_a and I_b as $\eta_2 \to +\infty e^{-i\beta/3}$ [see (B19) and (B64)],

$$I_a \sim \frac{\pi^{-1/2}\eta_2^{-3/4} e^{-\frac{2}{3}\eta_2^{3/2} - i\tilde{k}\eta_2}}{2(1 + i\tilde{k}\eta_2^{-1/2})}, \tag{5.27a}$$

$$I_b \sim \frac{\pi^{-1/2}\eta_2^{-3/4} e^{\frac{2}{3}\eta_2^{3/2} - i\tilde{k}\eta_2}}{1 - i\tilde{k}\eta_2^{-1/2}} - C_{\tilde{k}}(\eta_{20}), \tag{5.27b}$$

and the the asymptotic expansions of Ai and Bi in the same limit (Abramowitz and Stegun 1965),

$$\mathrm{Ai}(\eta_2) \sim \frac{1}{2}\pi^{-1/2}\eta_2^{-1/4} e^{-\frac{2}{3}\eta_2^{3/2}}, \quad \mathrm{Bi}(\eta_2) \sim \pi^{-1/2}\eta_2^{-1/4} e^{\frac{2}{3}\eta_2^{3/2}}, \tag{5.27c}$$

into (5.25), we find as $\eta_2 \to +\infty e^{-i\beta/3}$,

$$Z_{2p} \sim -\pi f \left[\pi^{-1}\eta_1^{-1} e^{-i\tilde{k}\eta_2} - C_{\tilde{k}}(\eta_{20})\frac{1}{2}\pi^{-1/2}\eta_2^{-1/4} e^{-\frac{2}{3}\eta_2^{3/2}}\right], \tag{5.28}$$

where $C_{\tilde{k}}(\eta_{20})$ is a constant, so that we have verified that the particular solution (5.25) satisfies the boundary condition (i).

The general solution of (5.16) may be written as

$$Z_2(\eta_2) = Z_{2p}(\eta_2) - \pi f \left[C_1 \mathrm{Ai}(\eta_2) + C_2 \mathrm{Bi}(\eta_2)\right] \tag{5.29}$$

where C_1 and C_2 are the arbitrary constants. Since $|\mathrm{Bi}(\eta_2)| \sim \infty$ as $\eta_2 \to \infty e^{-i\beta/3}$, we have to set $C_2 = 0$ to satisfy boundary condition (i). The constant C_1 shall be determined by boundary condition (ii), but before we can do that we must turn first to the asymptotic solution to equation (5.16).

5. 2. Asymptotic Solutions

5. 2. 1. Case with neither Self-gravity nor Viscosity

This simplest case corresponds to the situation when both the self-gravity of the disk mass and the viscosity can be ignored leaving the effects of the pressure only. For this case, the new variables introduced in section 5.1. assume their limiting values :

$$\beta = \tilde{k} = \eta_{00} = \eta_{20} = 0 , \tag{5.30a}$$

$$\eta_2 = \eta_1 = \eta_0 = \eta_3 , \tag{5.30b}$$

$$Z_2 = Z_1 = Z , \tag{5.30c}$$

and equation (5.8) reduces to the inhomogeneous Airy equation

$$\frac{d^2 Z(\eta_0)}{d\eta_0^2} - \eta_0 Z(\eta_0) = f . \tag{5.31}$$

Yuan (1984) first treated equation (5.31) in the context of the 3-kpc arm problem in the Galaxy. To be more general, we extend η_0 to its complex plane. The solution of (5.31) is known (Abramowitz and Stegun 1965):

$$Z(\eta_0) = -\pi f \left[\mathrm{Gi}(\eta_0) + C_1 \mathrm{Ai}(\eta_0) + C_2 \mathrm{Bi}(\eta_0) \right], \tag{5.32}$$

where Ai and Bi are the Airy functions satisfying the homogeneous Airy equation. The particular solution Gi can be written in terms of Ai and Bi :

$$\mathrm{Gi}(\eta_0) = \frac{1}{3}\mathrm{Bi}(\eta_0) + \int_0^{\eta_0} [\mathrm{Bi}(\eta_0')\mathrm{Ai}(\eta_0) - \mathrm{Ai}(\eta_0')\mathrm{Bi}(\eta_0)] \, d\eta_0' , \tag{5.33a}$$

or

$$\mathrm{Gi}(\eta_0) = I_b\,\mathrm{Ai}(\eta_0) + I_a\,\mathrm{Bi}(\eta_0) \tag{5.33b}$$

where I_a and I_b are defined in (5.26) with $\tilde{k} = \beta = 0$. The asymptotic expansions of Ai, Bi and Gi for large $|\eta_0|$ and $|\arg \eta_0| < \pi$ are

$$\mathrm{Ai}(\eta_0) \sim \frac{1}{2}\pi^{-1/2}\eta_0^{-1/4}\, e^{-\frac{2}{3}\eta_0^{3/2}}, \quad \mathrm{Bi}(\eta_0) \sim \pi^{-1/2}\eta_0^{-1/4}\, e^{\frac{2}{3}\eta_0^{3/2}}, \tag{5.34}$$

$$\mathrm{Gi}(\eta_0) \sim \pi^{-1}\,\eta_0^{-1}. \tag{5.35}$$

Hence, we must set $C_2 = 0$ to meet the boundary condition (i).

To meet the boundary condition (ii), let us consider the asymptotic expansions of Ai and Bi for large $|\eta_0|$ and $|\arg \eta_0| > \frac{1}{3}\pi$ (Abramowitz and Stegun 1965):

$$\mathrm{Ai}(\eta_0) \sim \pi^{-1/2}(-\eta_0)^{-1/4}\sin\left[\frac{2}{3}(-\eta_0)^{3/2} + \frac{\pi}{4}\right], \tag{5.36a}$$

$$\mathrm{Bi}(\eta_0) \sim \pi^{-1/2}(-\eta_0)^{-1/4}\cos\left[\frac{2}{3}(-\eta_0)^{3/2} + \frac{\pi}{4}\right]. \tag{5.36b}$$

From Appendix B we obtain

$$I_a \sim 1 - \pi^{-1/2}(-\eta_0)^{-3/4}\cos\left[\frac{2}{3}(-\eta_0)^{3/2} + \frac{\pi}{4}\right] \tag{5.37a}$$

$$I_b \sim -\pi^{-1/2}(-\eta_0)^{-3/4}\sin\left[\frac{2}{3}(-\eta_0)^{3/2} + \frac{\pi}{4}\right] \tag{5.37b}$$

Substituting (5.37a) and (5.37b) into (5.33b) gives

$$\mathrm{Gi}(\eta_0) \sim \pi^{-1/2}(-\eta_0)^{-1/4}\cos\left[\frac{2}{3}(-\eta_0)^{3/2} + \frac{\pi}{4}\right] - \pi^{-1}(-\eta_0)^{-1} \tag{5.37c}$$

We notice that we must take $C_1 = -i$ such that the solution

$$-\pi^{-1} f^{-1} Z(\eta_0) = \mathrm{Gi}(\eta_0) - i\ \mathrm{Ai}(\eta_0) \tag{5.38}$$

will decrease like η_0^{-1} as it approaches the central region from the outer Lindblad resonance and, together with the phase term $e^{-i\psi_0}$ (see Chapter II), will give a two-arm trailing-wave pattern in the rotating frame from the outer Lindblad resonance. Then, the asymptotic solution to equation (5.8) is

$$Z(\eta_0) \sim -f\ \eta_0^{-1}, \qquad as\ \eta_0 \to +\infty; \tag{5.39a}$$

$$Z(\eta_0) \sim -\pi^{1/2} f\ (-\eta_0)^{-1/4} e^{-i\,\Sigma_1(-\eta_0)} + f\ (-\eta_0)^{-1} \quad as\ \eta_0 \to -\infty, \tag{5.39b}$$

where

$$\Sigma_1(-\eta_0) \equiv \frac{2}{3}(-\eta_0)^{3/2} + \frac{\pi}{4}. \tag{5.40}$$

Therefore, the asymptotic solution to equation (5.6) is

$$Z(\xi_0) \sim f\ \xi_0^{-1}, \qquad as\ \xi_0 \to -\infty; \tag{5.41a}$$

$$Z(\xi_0) \sim -\pi^{1/2} f\ \xi_0^{-1/4} e^{-i\,\Sigma_1(\xi_0)} + f\ \xi_0^{-1} \quad as\ \xi_0 \to +\infty. \tag{5.41b}$$

The real part of $Z(\xi_0)$ in equation (5.41b) is plotted by dotted line in Figure 5.2 in comparison with the results of the exact numerical integration. The agreement is excellent. The imaginary part of $Z(\xi_0)$ in equation (5.41b) is plotted in Figure 5.3, again in comparison with the results of the exact numerical integration, and also with excellent agreement.

5. 2. 2. Case with Viscosity, without Self-gravity

Next we consider the case in which the self-gravity can be ignored leaving only the pressure and the viscosity. For this case,

$$\tilde{k} = \eta_{00} = \eta_{20} = 0 , \tag{5.42}$$

and

$$\eta_2 = \eta_1 , \eta_3 = \eta_0 , Z_2 = Z_1 , \tag{5.43}$$

and therefore, equation (5.16) becomes

$$\frac{d^2 Z_2}{d \eta_2^2} - \eta_2 Z_2 = f \ . \tag{5.44}$$

Again this is the inhomogeneous Airy equation but the independent variable is now complex. We similarly conclude that $C_2 = 0$ in order to meet the boundary condition (i) and $C_1 = -i$ to meet the boundary condition (ii) after examing the asymptotic expansions of Airy functions of a complex argument η_2 as $\eta_2 \to \pm \infty e^{-i\beta/3}$ [see (5.34) – (5.37)], since now

$$|\arg \eta_2| = \frac{\beta}{3} < \frac{\pi}{6} \qquad \text{for } \textit{positive } \eta_0 ,$$

and

$$|\arg \eta_2| = \pi - \beta/3 > \frac{5\pi}{6} \qquad \text{for } \textit{negative } \eta_0$$

are always within the domain of the asymptotic formulae. Therefore, the solution to (5.16) has the same form as (5.38).

The asymptotic solution to (5.44) as $\eta_2 \to -\infty e^{-i\beta/3}$ is

$$Z_2(\eta_2) \sim -\pi^{1/2} f\ (-\eta_2)^{-1/4}\, e^{-i\,\Sigma_1(-\eta_2)} + f\ (-\eta_2)^{-1} \tag{5.45}$$

where

$$\Sigma_1(-\eta_2) \equiv \frac{2}{3}(-\eta_2)^{3/2} + \frac{\pi}{4}\,. \tag{5.46}$$

Hence, the asymptotic solution to (5.8) as $\eta_0 \to -\infty$ is

$$Z(\eta_0) \sim -\pi^{1/2} f\ \cos^{1/4}\beta(-\eta_0)^{-1/4}\, e^{-\frac{2}{3}(-\eta_0)^{3/2}\cos^{1/2}\beta\,\sin(\beta/2)}$$

$$\cdot\, e^{i\,[-\frac{2}{3}(-\eta_0)^{3/2}\cos^{1/2}\beta\,\cos(\beta/2) - \pi/4 - \beta/4]} + f\ (-\eta_0)^{-1} \tag{5.47a}$$

Therefore, the asymptotic solution to (5.6) as $\xi_0 \to +\infty$ is

$$Z(\xi_0) \sim -\pi^{1/2} f\ \cos^{1/4}\beta\ \xi_0^{-1/4}\, e^{-\frac{2}{3}\xi_0^{3/2}\cos^{1/2}\beta\,\sin(\beta/2)}$$

$$\cdot\, e^{i\,[-\frac{2}{3}\xi_0^{3/2}\cos^{1/2}\beta\,\cos(\beta/2) - \pi/4 - \beta/4]} + f\ \xi_0^{-1}\,. \tag{5.47b}$$

From (5.47) we see that exponential damping occurs when η_0 becomes large negative or ξ_0 becomes large positive and that there is also a phase shift and a wavelength change due to the viscosity.

The asymptotic results in equation (5.47b) are depicted by dotted lines in Figures 5.4 and 5.5 in comparison with the real and imaginary parts of the results from the exact numerical integration.

5. 2. 3. Case with Self-gravity, without Viscosity

Now we include the effects of the self-gravity as well as the pressure but

neglect the viscosity. This case requires the various parameters to take values as follows:

$$\beta = 0 , \tilde{k} = \tilde{k}_0 , \eta_{00} = \tilde{k}_0^2 , \eta_{20} = 0 , \tag{5.48}$$

$$\eta_1 = \eta_0 , \eta_2 = \eta_0 - \tilde{k}_0^2 = \eta_3 , \tag{5.49}$$

$$Z_1 = Z , Z_2 = Z\ e^{-i\ \tilde{k}_0 \eta_3} , \tag{5.50}$$

and equation (5.16) reduces to

$$\frac{d^2 Z_2}{d\ \eta_3^2} - \eta_3 Z_2 = f\ \ e^{-i\ \tilde{k}_0 \eta_3} . \tag{5.51}$$

Notice that the turning point has been moved from $\eta_0 = 0$ to $\eta_0 = \tilde{k}_0^2$, and keep in mind that η_3 measures the distance from the turning point. The general solution of (5.51) is

$$Z_2(\eta_3) = -\pi f\ [I_b(\eta_3)\mathrm{Ai}(\eta_3) + I_a(\eta_3)\mathrm{Bi}(\eta_3) + C_1\mathrm{Ai}(\eta_3) + B_1\mathrm{Bi}(\eta_3)], \tag{5.52}$$

where

$$I_a(\eta_3) = \int_{\eta_3}^{\infty} \mathrm{Ai}(\eta_3')\, e^{-i\ \tilde{k}_0 \eta_3'}\, d\ \eta_3' , \tag{5.53}$$

$$I_b(\eta_3) = \int_{0}^{\eta_3} \mathrm{Bi}(\eta_3')\, e^{-i\ \tilde{k}_0 \eta_3'}\, d\ \eta_3' . \tag{5.54}$$

Since $\mathrm{Bi}(\eta_3)$ goes up exponentially as $\eta_3 \to +\infty$, we must set $C_2 = 0$. The asymptotic expansions of I_a and I_b as $\eta_3 \to -\infty$ are derived in Appendix B; the results are:

$$I_a \sim (P.C.)_a + \pi^{-1/2}(-\eta_3)^{-3/4} e^{-i\tilde{k}_0\eta_3} \frac{[-\cos\Sigma_1(-\eta_3) + i\tilde{k}_0(-\eta_3)^{-1/2}\sin\Sigma_1(-\eta_3)]}{1-\tilde{k}_0^2(-\eta_3)^{-1}} \tag{5.55}$$

where

$$(P.C.)_a = \begin{cases} e^{i\tilde{k}_0^3/3} & \text{if } \eta_3 < -\tilde{k}_0^2 \\ 0 & \text{if } -\tilde{k}_0^2 < \eta_3 < 0 \end{cases} \tag{5.56}$$

and

$$I_b \sim (P.C.)_b - C_{\tilde{k}_0} - \pi^{-1/2}(-\eta_3)^{-3/4} e^{-i\tilde{k}_0\eta_3} \frac{[\sin\Sigma_1(-\eta_3) + i\tilde{k}_0(-\eta_3)^{-1/2}\cos\Sigma_1(-\eta_3)]}{1-\tilde{k}_0^2(-\eta_3)^{-1}} \tag{5.57}$$

where

$$(P.C.)_b = \begin{cases} i\, e^{i\tilde{k}_0^3/3} & \text{if } \eta_3 < -\tilde{k}_0^2 \\ 0 & \text{if } -\tilde{k}_0^2 < \eta_3 < 0 \end{cases} \tag{5.58}$$

and $C_{\tilde{k}_0}$ is the constant integral,

$$C_{\tilde{k}_0} = \frac{1}{\pi}\int_0^\infty \left\{ \frac{r + i\tilde{k}_0}{r^2+\tilde{k}_0^2} - \frac{(2r-\sqrt{3}\tilde{k}_0) - i\tilde{k}_0}{(2r-\sqrt{3}\tilde{k}_0)^2+\tilde{k}_0^2} - \frac{(2r+\sqrt{3}\tilde{k}_0) - i\tilde{k}_0}{(2r+\sqrt{3}\tilde{k}_0)^2+\tilde{k}_0^2} \right\} e^{-r^3/3}\, dr \tag{5.59}$$

which can be calculated numerically. It can be seen directly from (5.59) by noticing

$$\frac{1}{\pi}\lim_{\tilde{k}_0\to 0} \frac{\tilde{k}_0}{r^2+\tilde{k}_0^2} = \delta(r), \tag{5.60}$$

where $\delta(r)$ is the Dirac function, that

$$\mathrm{Re}(C_{\tilde{k}_0}) \sim 0, \qquad \mathrm{Im}(C_{\tilde{k}_0}) \sim 1, \qquad as\ \tilde{k}_0 \to 0, \tag{5.61}$$

which is the case discussed in section 5.2.1.

Substituting (5.55) and (5.57) into (5.52) and recalling (5.36) and (5.37), we may conclude that in order to get an asymptotic solution as $\eta_3 \to -\infty$ and $\eta_3 < -\tilde{k}_0^2$ satisfying the boundary condition (ii), we have to choose C_1 such that

$$i\, e^{i\tilde{k}_0^3/3} - C_{\tilde{k}_0} + C_1 = -i\, e^{-\tilde{k}_0^3/3}, \tag{5.62}$$

or

$$C_1 = -2i\, e^{i\tilde{k}_0^3/3} + C_{\tilde{k}_0}. \tag{5.63}$$

The asymptotic solution to equation (5.51) as $\eta_3 \to -\infty$ then is

$$Z_2(\eta_3) \sim \begin{cases} -\pi^{1/2} f\,(-\eta_3)^{-1/4} e^{i\tilde{k}_0^3/3 - i\Sigma_1(-\eta_3)} + f\,(-\eta_0)^{-1} e^{-i\tilde{k}_0\eta_3} & \text{if } \eta_3 < -\tilde{k}_0^2 \\ 2i\,\pi^{1/2} f\,(-\eta_3)^{-1/4} e^{i\tilde{k}_0^3/3} \sin\Sigma_1(-\eta_3) + f\,(-\eta_0)^{-1} e^{-i\tilde{k}_0\eta_3} & \text{if } -\tilde{k}_0^2 < \eta_3 < 0 \end{cases} \tag{5.64}$$

Hence, the asymptotic solution to equation (5.8) as $\eta_3 \to -\infty$ is

$$Z(\eta_3) \sim \begin{cases} -\pi^{1/2} f\,(-\eta_3)^{-1/4} e^{i\tilde{k}_0^3/3 - i\Sigma_1(-\eta_3) + i\tilde{k}_0\eta_3} + f\,(-\eta_0)^{-1} & \text{if } \eta_3 < -\tilde{k}_0^2 \\ 2i\,\pi^{1/2} f\,(-\eta_3)^{-1/4} e^{i\tilde{k}_0^3/3 + i\tilde{k}_0\eta_3} \sin\Sigma_1(-\eta_3) + f\,(-\eta_0)^{-1} & \text{if } -\tilde{k}_0^2 < \eta_3 < 0 \end{cases} \tag{5.65a}$$

Therefore, the asymptotic solution to equation (5.6) as $\xi_3 \equiv \xi_0 + \tilde{k}_0^2 \to +\infty$ is

$$Z(\xi_3) \sim \begin{cases} -\pi^{1/2} f\,\xi_3^{-1/4} e^{i\tilde{k}_0^3/3 - i\Sigma_1(\xi_3) - i\tilde{k}_0\xi_3} + f\,\xi_0^{-1} & \text{if } \xi_3 > +\tilde{k}_0^2 \\ 2i\,\pi^{1/2} f\,\xi_3^{-1/4} e^{i\tilde{k}_0^3/3 - i\tilde{k}_0\xi_3} \sin\Sigma_1(\xi_3) + f\,\xi_0^{-1} & \text{if } 0 < \xi_3 < \tilde{k}_0^2 \end{cases} \tag{5.65b}$$

where we have defined

$$\xi_3 \equiv -\eta_3 = \xi_0 + \tilde{k}_0^2 \ , \tag{5.65c}$$

and where Σ_1 has been defined in (5.46), or

$$\Sigma_1(\xi_3) \equiv \frac{2}{3}\xi_3^{3/2} + \frac{\pi}{4} \ . \tag{5.65d}$$

For small $\tilde{k}_0^2$ ($= 0.15^2$), we plot the asymptotic results (5.65b) by dotted lines in Figure 5.6 for real part and in Figure 5.7 for imaginary part. For large $\tilde{k}_0^2$ ($= 3^2$), the asymptotic solution as $\xi_3 \to +\infty$ has two expressions for different regions according to equation (5.65b) (one is for $\xi_3 > 9$, or $\xi_0 > 0$; the other is for $0 < \xi_3 < 9$, or $-9 < \xi_0 < 0$, in this example). They are depicted in Figures 5.8 and 5.9, again for the real and imaginary parts respectively. The results from the exact numerical integration are plotted by solid curves in these Figures. It can be seen clearly from these figures that the asymptotic solutions approach the exact numerical solutions very well except in the vicinity of $\xi_3 = \tilde{k}_0^2$, where the poles of the integrands of I_a and I_b coincide with the saddle points involved in the steepest-descent method, as we point out in Appendix B.

5. 2. 4. The General Case

We now consider the general case when all the three factors – pressure, self-gravity and viscosity are included (see section 5.1). The asymptotic solution of equation (5.16) is treated along the real η_0-axis which intersects the positive imaginary η_2 axis at point η_{20} (point T ; see Figure 5.1).

The general solution to (5.16) can be written as

$$Z_2(\eta_2) = -\pi f \left[I_b \, \mathrm{Ai}(\eta_2) + I_a \, \mathrm{Bi}(\eta_2) + C_1 \mathrm{Ai}(\eta_2) + C_2 \mathrm{Bi}(\eta_2) \right] \qquad (5.66)$$

where I_a and I_b are given by (5.26a) and (5.26b). As mentioned in section 5.1, we must set $C_2 = 0$ to satisfy boundary condition (i). To determine C_1, we have to use boundary condition (ii). To do so, we must first determine the asymptotic expansions of the integrals $I_a(\eta_2)$ and $I_b(\eta_2)$. We use the integral representations of Ai and Bi (Abramowitz and Stegun 1965),

$$\mathrm{Ai}(\eta_2) = \frac{1}{2\pi} \int_{-\infty}^{\infty} e^{i t^3/3 + i \eta_2 t} \, dt \ , \qquad (5.67)$$

$$\mathrm{Bi}(\eta_2) = \frac{1}{\pi} \int_0^{\infty} \left[e^{-t^3/3 + \eta_2 t} + \frac{1}{2i} \left(e^{i t^3/3 + i \eta_2 t} - e^{-i t^3/3 - i \eta_2 t} \right) \right] dt \ , \qquad (5.68)$$

and then choose the appropriate contours of integration , employ the method of steepest-descent, and carefully take into account of the pole contributions in various cases. The detailed analysis is presented in Appendix B. The problem is complicated, not only because all variables have become complex, but also because we want to include the cases when $\tilde{k}_0^2$ is large. We derive the asymptotic expressions for different regions: for $\eta_0 < 0$, and for $0 < \eta_0 < \eta_{00}$, where η_{00} is a quantity proportional to $\tilde{k}_0^2$ defined in (5.21). We can show that at the point separating these two regions, $\eta_0 = 0$, the poles in the integrands of both I_a and I_b coincide with the saddle points involved in the steepest-descent method, so the steepest-descent method fails near that point. However, away from it, the method satisfactorily produces asymptotic expressions on both sides.

The asymptotic expansions of I_a and I_b as $\eta_2 \to -\infty e^{-i\beta/3}$ are found to be (see Appendix B):

$$I_a = \int_{\eta_2}^{\infty e^{-i\beta/3}} \mathrm{Ai}(\eta_2')\, e^{-i\tilde{k}\eta_2'}\, d\eta_2'$$

$$\sim (P.C.)_a + \pi^{-1/2}(-\eta_2)^{-3/4} e^{-i\tilde{k}\eta_2} \frac{[-\cos\Sigma_1(-\eta_2) + i\tilde{k}(-\eta_2)^{-1/2}\sin\Sigma_1(-\eta_2)]}{1-\tilde{k}^2(-\eta_2)^{-1}} \tag{5.69}$$

where

$$(P.C.)_a = \begin{cases} e^{i\tilde{k}^3/3} & \text{if } \eta_0 < 0 \\ 0 & \text{if } 0 < \eta_0 < \eta_{00} \end{cases} \tag{5.70}$$

and

$$I_b = \int_{\eta_{20}}^{\eta_2} e^{-i\tilde{k}\eta_2'} \mathrm{Bi}(\eta_2')\, d\eta_2' = C_{\tilde{k}}(\eta_2) - C_{\tilde{k}}(\eta_{20})$$

$$\sim (P.C.)_b - C_{\tilde{k}}(\eta_{20})$$

$$- \pi^{-1/2}(-\eta_2)^{-3/4} e^{-i\tilde{k}\eta_2} \frac{[\sin\Sigma_1(-\eta_2) + i\tilde{k}(-\eta_2)^{-1/2}\cos\Sigma_1(-\eta_2)]}{1-\tilde{k}^2(-\eta_2)^{-1}} \tag{5.71}$$

where

$$(P.C.)_b = \begin{cases} i\, e^{i\tilde{k}^3/3} & \text{if } \eta_0 < 0 \\ 0 & \text{if } 0 < \eta_0 < \eta_{00} \end{cases} \tag{5.72}$$

$$C_{\tilde{k}}(\eta_{20}) = \frac{e^{-i\tilde{k}\eta_{20}}}{\pi} \int_0^{\infty} \left[\frac{e^{-t^3/3 + \eta_{20}t}}{t - i\tilde{k}} - \frac{e^{it^3/3 + i\eta_{20}t}}{2(t-\tilde{k})} - \frac{e^{-it^3/3 - i\eta_{20}t}}{2(t+\tilde{k})}\right] dt$$

(5.73)

The asymptotic expansions of Airy functions Ai and Bi of a complex argument η_2 as $|\eta_2| \to \infty$ and where $|arg(-\eta_2)| < \frac{2}{3}\pi$ are known to be (Abramowitz and Stegun 1965)

$$Ai(\eta_2) \sim \pi^{-1/2}(-\eta_2)^{-1/4} \sin\Sigma_1(-\eta_2) \tag{5.74}$$

$$Bi(\eta_2) \sim \pi^{-1/2}(-\eta_2)^{-1/4} \cos\Sigma_1(-\eta_2) \tag{5.75}$$

and our $|\arg \eta_2|$ value for $\eta_0 < \eta_{00}$ is well within the domain in which (5.74) and (5.75) are vaild (see Figure 5.1).

Substituting (5.69), (5.71), (5.74), (5.75) and $C_2 = 0$ into (5.66) gives the asymptotic expansion of $Z_2(\eta_2)$ as $\eta_2 \to -\infty e^{-i\beta/3}$:

$$\begin{aligned} Z_2(\eta_2) \sim & -\pi f \{(P.C.)_b - C_{\tilde{k}}(\eta_{20}) + C_1 \\ & - \pi^{-1/2}(-\eta_2)^{-3/4} e^{-i\tilde{k}\eta_2} \frac{[\sin\Sigma_1(-\eta_2) + i\tilde{k}(-\eta_2)^{-1/2}\cos\Sigma_1(-\eta_2)]}{1 - \tilde{k}^2(-\eta_2)^{-1}}\} \\ & \cdot \{\pi^{-1/2}(-\eta_2)^{-1/4} \sin\Sigma_1(-\eta_2)\} \\ & -\pi f \{(P.C.)_a + \pi^{-1/2}(-\eta_2)^{-3/4} e^{-i\tilde{k}\eta_2} \frac{[-\cos\Sigma_1(-\eta_2) + i\tilde{k}(-\eta_2)^{-1/2}\sin\Sigma_1(-\eta_2)]}{1 - \tilde{k}^2(-\eta_2)^{-1}}\} \\ & \cdot \{\pi^{-1/2}(-\eta_2)^{-1/4} \cos\Sigma_1(-\eta_2)\} . \end{aligned} \tag{5.76}$$

In (5.76), we have to choose C_1 such that when $\eta_2 \to -\infty e^{-i\beta/3}$ and $\eta_0 < 0$,

$$(P.C.)_b - C_{\tilde{k}}(\eta_{20}) + C_1 = -i\ (P.C.)_a \tag{5.77}$$

to meet the wavy boundary condition (ii).

Substituting (B70) and (B72) for $\eta_0 < 0$ into (5.77), we determine the value of the constant C_1:

$$C_1 = -2i\ e^{i\tilde{k}^3/3} + C_{\tilde{k}}(\eta_{20}). \tag{5.78}$$

Now we can reduce (5.76) to

$$Z_2(\eta_2) \sim \begin{cases} -\pi^{1/2} f\ (-\eta_2)^{-1/4}\, e^{i\tilde{k}^3/3 - i\Sigma_1(-\eta_2)} + f\ (-\eta_1)^{-1}\, e^{-i\tilde{k}\eta_2} & \text{if } \eta_0 < 0 \\ 2i\,\pi^{1/2} f\ (-\eta_2)^{-1/4}\, e^{i\tilde{k}^3/3} \sin\Sigma_1(-\eta_2) + f\ (-\eta_1)^{-1} e^{-i\tilde{k}\eta_2} & \text{if } 0 < \eta_0 < \eta_{00} \end{cases} \tag{5.79}$$

Substituting (5.79) into (5.15) gives

$$Z_1(\eta_2) \sim \begin{cases} -\pi^{1/2} f\ (-\eta_2)^{-1/4}\, e^{i\tilde{k}^3/3 - i\Sigma_1(-\eta_2) + i\tilde{k}\eta_2} + f\ (-\eta_1)^{-1} & \text{if } \eta_0 < 0 \\ 2i\,\pi^{1/2} f\ (-\eta_2)^{-1/4}\, e^{i\tilde{k}^3/3 + i\tilde{k}\eta_2} \sin\Sigma_1(-\eta_2) + f\ (-\eta_1)^{-1} & \text{if } 0 < \eta_0 < \eta_{00} \end{cases} \tag{5.80}$$

Finally, we substitute (5.80) into (5.10) and obtain the asymptotic solution of (5.8) as $\eta_2 \to -\infty\, e^{-i\beta/3}$ or $\eta_3 \equiv \eta_0 - \eta_{00} \to -\infty$

$$Z(\eta_2) \sim -\pi^{1/2} f\ (-\eta_2)^{-1/4} \cos^{1/3}\beta\, e^{i[\tilde{k}^3/3 + \tilde{k}\eta_2 - \Sigma_1(-\eta_2) - \beta/3]}$$

$$+ f\ (-\eta_0)^{-1}, \qquad \text{for } \eta_0 < 0, \tag{5.81}$$

and

$$Z(\eta_2) \sim -\pi^{1/2} f\ (-\eta_2)^{-1/4} \cos^{1/3}\beta\, e^{i[\tilde{k}^3/3 + \tilde{k}\eta_2 - \beta/3]} [e^{-i\Sigma_1(-\eta_2)} - e^{i\Sigma_1(-\eta_2)}]$$

$$+ f\ (-\eta_0)^{-1}, \qquad \text{for } 0 < \eta_0 < \eta_{00}. \tag{5.82}$$

Therefore, the asymptotic solution to equation (5.6) as $\xi_3 \equiv \xi_0 - \xi_{00} \to +\infty$ is

$$Z(\xi_2) \sim -\pi^{1/2} f\ \xi_2^{-1/4} \cos^{1/3}\beta\ e^{i\,[\tilde{k}^3/3 - \tilde{k}\,\xi_2 - \Sigma_1(\xi_2) - \beta/3]}$$

$$+ f\ \xi_0^{-1}, \qquad \text{for } \xi_0 > 0, \tag{5.83a}$$

and

$$Z(\xi_2) \sim -\pi^{1/2} f\ \xi_2^{-1/4} \cos^{1/3}\beta\ e^{i\,[\tilde{k}^3/3 - \tilde{k}\,\xi_2 - \beta/3]} [e^{-i\,\Sigma_1(\xi_2)} - e^{i\,\Sigma_1(\xi_2)}]$$

$$+ f\ \xi_0^{-1}, \qquad \text{for } \xi_{00} < \xi_0 < 0, \tag{5.83b}$$

where we have defined

$$\xi_{00} \equiv -\eta_{00}, \quad \xi_2 \equiv -\eta_2, \quad \xi_3 \equiv -\eta_3, \tag{5.84a}$$

and where Σ_1 has been defined in (5.46) or (5.65d),

$$\Sigma_1(\xi_2) \equiv \frac{2}{3}\xi_2^{3/2} + \frac{\pi}{4}. \tag{5.84b}$$

When $\tilde{k}_0^2$ is small we can further approximate (5.82) for the case when $\xi_0 > 0$ as

$$Z(\xi_3) \sim -\pi^{1/2} f\ \xi_3^{-1/4} \cos^{1/4}\beta\ e^{i\,\Sigma} + f\ (\xi_3 + \xi_{00})^{-1}$$

$$= -\pi^{1/2} f\ \xi_3^{-1/4} \cos^{1/4}\beta\ e^{-\mathrm{Im}(\Sigma) + i\,\mathrm{Re}(\Sigma)} + f\ \xi_0^{-1} \tag{5.85}$$

where ξ_3, given by (5.84a), measures the distance from the turning point,

$$\xi_3 = \xi_0 - \xi_{00} , \tag{5.86}$$

and

$$\mathrm{Re}(\Sigma) \equiv \tilde{k}_0^3 \cos^2\beta \{ \frac{1}{3}\cos(2\beta) + [\sin(4\beta/3) - \cos(4\beta/3)\tan(\beta/3)]\sin(2\beta/3)\}$$

$$- \frac{2}{3}\xi_3^{3/2}\cos^{1/2}\beta\cos(\beta/2) - \tilde{k}_0\xi_3\cos^2\beta$$

$$+ \tilde{k}_0^2\xi_3^{1/2}\cos^{3/2}\beta[\sin(4\beta/3) - \cos(4\beta/3)\tan(\beta/3)]\sin(\beta/6)$$

$$- \frac{\pi}{4} - \frac{\beta}{4} , \tag{5.87}$$

$$\mathrm{Im}(\Sigma) \equiv - \tilde{k}_0^3 \cos^2\beta \{ \frac{1}{3}\sin(2\beta) - [\sin(4\beta/3) - \cos(4\beta/3)\tan(\beta/3)]\cos(2\beta/3)\}$$

$$+ \frac{2}{3}\xi_3^{3/2}\cos^{1/2}\beta\sin(\beta/2) + \frac{1}{2}\tilde{k}_0\xi_3\sin(2\beta)$$

$$+ \tilde{k}_0^2\xi_3^{1/2}\cos^{3/2}\beta[\sin(4\beta/3) - \cos(4\beta/3)\tan(\beta/3)]\cos(\beta/6) . \tag{5.88}$$

From this solution it is clear that exponential damping will occur when ξ_3 becomes large and positive and that there is a phase shift and a wavelength change due to self-gravity as well as viscosity.

The results of equation (5.85) for $\tilde{k}_0 = 0.15$ and $b_0 = 0.127$ (corresponding to an effective kinematic viscosity $\nu = \nu' = 0.2$ in the 3-kpc arm problem) are plotted by dotted line in Figures 5.10 and 5.11, and show very little difference from the results obtained by means of the exact numerical integration.

5. 3. Numerical Solutions

In section 5.2 we obtained the general solution of equation (5.16), with the arbitrary constants C_1 and C_2 [see equation (5.66)]. We have set $C_2 = 0$ because of boundary condition (i) [see (5.24a)]. The other arbitrary constant, C_1, is determined by boundary condition (ii) [see (5.24b)] such that the solution behaves like a bounded outgoing wave as $\eta_2 \to -\infty e^{-i\beta/3}$. At this limit, we can safely calculate C_1 from the asymptotic solutions obtained in the previous sections as [see (5.78)]:

$$C_1 = -2i\ e^{i\tilde{k}^3/3} + C_{\tilde{k}}(\eta_{20}). \tag{5.89}$$

Therefore, Z_2 equals

$$Z_2(\eta_2) = -\pi f\ \{[I_b(\eta_2) - 2i\ e^{i\tilde{k}^3/3} + C_{\tilde{k}}(\eta_{20})]\ \mathrm{Ai}(\eta_2) + I_a(\eta_2)\mathrm{Bi}(\eta_2)\} \tag{5.90}$$

with the Airy functions given by their integral representations (5.67) and (5.68):

$$\mathrm{Ai}(\eta_2) = \frac{1}{2\pi}\int_{-\infty}^{\infty} e^{i t^3/3 + i\eta_2 t}\, dt\ , \tag{5.91a}$$

$$\mathrm{Bi}(\eta_2) = \frac{1}{\pi}\int_0^{\infty}\left[e^{-t^3/3 + \eta_2 t} + \frac{1}{2i}\left(e^{i t^3/3 + i\eta_2 t} - e^{-i t^3/3 - i\eta_2 t}\right)\right] dt\ , \tag{5.91b}$$

and with I_a and I_b given by equations (B4), (B16) and (B41) as follows:

$$I_a = -\frac{e^{-i\tilde{k}\eta_2}}{2\pi i}\int_{-\infty}^{\infty} \frac{e^{i t^3/3 + i\eta_2 t}}{t - \tilde{k}}\, dt\ , \tag{5.92a}$$

$$I_b = C_{\tilde{k}}(\eta_2) - C_{\tilde{k}}(\eta_{20}). \tag{5.92b}$$

Therefore, equation (5.90) can be rewritten as

$$Z_2(\eta_2) = -\pi f \{[C_{\tilde{k}}(\eta_2) - 2i\, e^{i\tilde{k}^3/3}]\,\mathrm{Ai}(\eta_2) + I_a(\eta_2)\mathrm{Bi}(\eta_2)\} \tag{5.93}$$

where $C_{\tilde{k}}(\eta_2)$ is given by (5.73) or (5.59) with η_2 substituted for η_{20}:

$$C_{\tilde{k}}(\eta_2) = \frac{e^{-i\tilde{k}\eta_2}}{\pi}\int_0^\infty \left[\frac{e^{-t^3/3+\eta_2 t}}{t - i\tilde{k}} - \frac{e^{it^3/3+i\eta_2 t}}{2(t-\tilde{k})} - \frac{e^{-it^3/3-i\eta_2 t}}{2(t+\tilde{k})}\right] dt$$

$$\text{for } \beta \neq 0, \tag{5.94a}$$

$$C_{\tilde{k}}(\eta_2) = C_{\tilde{k}_0} =$$

$$\frac{1}{\pi}\int_0^\infty \left\{\frac{r + i\tilde{k}_0}{r^2+\tilde{k}_0^2} - \frac{(2r-\sqrt{3}\tilde{k}_0)-i\tilde{k}_0}{(2r-\sqrt{3}\tilde{k}_0)^2+\tilde{k}_0^2} - \frac{(2r+\sqrt{3}\tilde{k}_0)-i\tilde{k}_0}{(2r+\sqrt{3}\tilde{k}_0)^2+\tilde{k}_0^2}\right. e^{-r^3/3}\, dr$$

$$\text{for } \beta = 0. \tag{5.94b}$$

Differentiating (5.93) gives

$$Z'_2(\eta_2) = -\pi f \{[C_{\tilde{k}}(\eta_2) - 2i\, e^{i\tilde{k}^3/3}]\mathrm{A'i}(\eta_2) + I_a(\eta_2)\mathrm{B'i}(\eta_2)\} \tag{5.95}$$

where we have used the facts that

$$C'_{\tilde{k}}(\eta_2) = I'_b(\eta_2), \tag{5.96a}$$

and

$$I'_b(\eta_2)\mathrm{Ai}(\eta_2) + I'_a(\eta_2)\mathrm{Bi}(\eta_2) = 0. \tag{5.96b}$$

(5.93) is the exact solution to (5.16) that satisfies the boundary conditions specified by equations (5.24a) and (5.24b); in principle, it can be calculated numerically for any point η_2, but computer time becomes a constraint. In practice, we calculate $Z_2(\eta_2)$ and $Z'_2(\eta_2)$ by (5.93) and (5.95) for only one value of η_2. It turns out that the asymptotic solutions discussed in the early sections can also

provide accurate initial values for the Runge-Kutta scheme, if we choose the initial point in the regions where the asymptotic solutions are well valid. But in our calculation, we still use the initial values obtained by calculating (5.93) and (5.95) numerically at the initial point, so that we not only have more accurate initial values, but also have more freedom to choose the initial point.

After we obtain the accurate initial values of Z_2 and its derivative by solving equation (5.16) at one point of η_2, we go back to the original variable Z and its derivative at the same point, now in the η_0 or ξ_0 coordinate, use them as the initial values, and employ the Runge-Kutta method to integrate equation (5.8) or equation (5.6) directly. We choose to use the original equation (5.8) or (5.6), partly because in the numerical integration, the advantage of using the standard form, i. e., equation (5.16) disappears and partly because for equation (5.8) or (5.6), we can express our results directly. To be specific, we integrate equation (5.6) directly. Going back to Z, we have

$$Z(\xi_0) = \cos^{1/3}\beta\, e^{-i\beta/3 + i\tilde{k}\eta_2} Z_2 \tag{5.97a}$$

where η_2 is to be expressed in terms of ξ_0 as

$$\eta_2 = -\cos^{1/3}\beta\, e^{-i\beta/3}\xi_0 - \tilde{k}^2 \tag{5.97b}$$

Differentiating (5.97a) with respect to ξ_0 gives

$$Z'(\xi_0) = \cos^{2/3}\beta\, e^{-i\frac{2}{3}\beta + i\tilde{k}\eta_2} [Z'_2(\eta_2) + i\tilde{k} Z_2(\eta_2)] \tag{5.98}$$

where η_2 is to be expressed in terms of ξ_0 according to equation (5.97b), and where we have used

$$\frac{d\,\eta_2}{d\,\xi_0} = -\cos^{1/3}\beta\, e^{-i\,\beta/3}\,. \tag{5.99}$$

Equations (5.97) and (5.98) give the initial values to integrate equation (5.6) from an arbitrary initial point ξ_0.

To integrate equation (5.6) numerically by, say, the Runge-Kutta method, we may face parasitic problems. It is clearer to discuss the same difficulties encountered if we try to integrate equation (5.16) by the same method. Besides the boundary value solution discussed in section 5.2.4., equation (5.16) also admits other solutions. For instance, if we choose C_1 to satisfy the following equation:

$$(P.C.)_b - C_{\tilde{k}}(\eta_{20}) + C_1 = +\,i\,(P.C.)_a\,, \tag{5.100}$$

instead of (5.77), which we rewrite here,

$$(P.C.)_b - C_{\tilde{k}}(\eta_{20}) + C_1 = -\,i\,(P.C.)_a\,, \tag{5.101}$$

we would have the solution below (satisfying boundary conditions other than ours):

$$Z_2(\eta_2) \sim \begin{cases} -\pi^{1/2} f\,(-\eta_2)^{-1/4}\, e^{i\,\tilde{k}^{3/3}+i\,\Sigma_1(-\eta_2)} + f\,(-\eta_1)^{-1}\, e^{-i\,\tilde{k}\,\eta_2} & \text{if } \eta_0 < 0 \\ f\,(-\eta_1)^{-1} e^{-i\tilde{k}\,\eta_2} & \text{if } 0 < \eta_0 < \eta_{00} \end{cases} \tag{5.102}$$

If we compare solution (5.102) with the exponentially decreasing (with $-\eta_3$) solution (5.79) found in section 5.2.4., we see that (5.102) is a solution which increases exponentially (with $-\eta_3$) due the sign change before Σ_1 in the exponent of (5.102) for $\eta_0 < 0$. Inaccuracy in initial values or round-off errors in the intermediate steps may produce undesirable quantities of the type of equation (5.100)

and cause an exponential growth in the calculation and eventually ruin a good solution. These undesirable quantities are called parasitic components.

If the general solution of the equation has an exponentially increasing term which is not that one we are looking for, we will have parasitic problem. When $b_0 = 0$, $i\Sigma_1$ becomes pure imaginary, the solution to (5.6) in the wave region is not exponential any more, so that we will have much less difficulties in the integration. But, in the evanescent region, we still have to face the parasitic problem, since from equations (5.28), (5.29), (5.10) and (5.15) we see there is an exponentially increasing imaginary part and an algebraically increasing real part in the solution far into the evanescent region. The inaccurate initial values and the round-off errors may produce an undesirable real term which is exponentially increasing, in addition to the desirable, algebraically varying term.

To suppress parasitic contributions, we must use very accurate initial values (described in the first part of this section) and double precision calculations for the Runge-Kutta method.

In Figures 5.2 and 5.3, we give the results of our numerical calculation for $\tilde{k}_0 = 0$, $b_0 = 0$ by solid lines, for the real and imaginary parts of Z respectively, in comparison with the asymptotic solution obtained in section 5.2.2 (by dotted lines). The agreement is excellent even for moderate values of ξ_0.

In Figures 5.4 and 5.5, we plot the results of our numerical calculation for $\tilde{k}_0 = 0$, $b_0 = 0.127$ by solid lines, for the real and imaginary parts of Z respectively, in comparison with the asymptotic solution obtained in section 5.2.2 (by dotted lines). The agreement is again excellent even for moderate values of ξ_0.

For $b = 0$ and small $\tilde{k}_0^2$ $(=0.15^2)$, we plot our numerical results by solid lines in Figure 5.6 for real part and in Figure 5.7 for imaginary part. They also have excellent agreement with the asymptotic solution (depicted by dotted lines) derived in section 5.2.3. For large $\tilde{k}_0^2$ $(=3^2)$, the asymptotic solution has two expressions for different regions (one is for $\xi_0 > 0$, another is for $-9 < \xi_0 < 0$). They are depicted by dotted lines in Figures 5.8 and 5.9, for real and imaginary parts of Z respectively. We notice that near the singularity $\xi_0 = 0$, both the two asymptotic expressions fail. It is the numerical solution we obtained in this section that can cover the whole region we are interested in. The numerical results are plotted in these two figures, by solid lines, for real and imaginary parts of Z respectively. The agreement between the exact numerical solution and the asymptotic expressions is also very well except in the vicinity of $\xi_0 = 0$, where we can only depend on the numerical solution.

The numerical results for the general case where both b_0 and $\tilde{k}_0$ are nonzero ($\tilde{k}_0 = 0.15$ and $b_0 = 0.127$ in this example, corresponding to the case in the 3-kpc arm problem) are depicted by solid lines in Figures 5.10 and 5.11, for real and imaginary parts of Z respectively, in comparison with the asymptotic solution (by dotted lines) derived in section 5.2.4. The agreement, again, is excellent even for moderate value of ξ_0 (> 3).

5. 4. Discussion

Perhaps, the most significant result of the linear theory is to confirm the conjecture that we put forward in Chapter IV: the long trailing waves are excited at the Lindblad resonance, and propagate, according to the dispersion relation,

towards the co-rotation radius. Before reaching co-rotation, they are reflected back at the Q -barrier as short trailing waves.

This picture is best revealed in the inviscid case with large $\tilde{k}_0^2$. The solutions presented in sections 5.2.3. and 5.3 are obtained by setting $C_2 = 0$ to eliminate the unbounded solution for large negative $\xi_3 \equiv \xi_0 + \tilde{k}_0^2$, and $C_1 = -2i\, e^{-i\tilde{k}_0^3/3} + C_{\tilde{k}_0}$ to ensure the solution of a bounded outgoing wave for large positive ξ_3 ($\xi_3 \gg \tilde{k}_0^2$). The solution found in the region $\xi_3 > \tilde{k}_0^2$ contains only the outgoing short trailing waves while the solution found in the region between the Q -barrier ($\xi_3 = 0$) and the outer Lindblad resonance ($\xi_3 = \tilde{k}_0^2$) is a combination of two waves [equation (5.65b)]. The first wave can be identified as the same outgoing short trailing wave appearing in the region $\xi_3 > \tilde{k}_0^2$, which we may write as

$$Z_s \sim -\pi^{1/2} f\, \xi_3^{-1/4}\, e^{i\left[\tilde{k}_0^3/3 - \tilde{k}_0\xi_3 - \frac{2}{3}\xi_3^{3/2} - \frac{\pi}{4}\right]}. \qquad (5.103a)$$

The other wave, indeed is a long trailing wave propagating inward towards the Q -barrier

$$Z_l \sim +\pi^{1/2} f\, \xi_3^{-1/4}\, e^{i\left[\tilde{k}_0^3/3 - \tilde{k}_0\xi_3 + \frac{2}{3}\xi_3^{3/2} + \frac{\pi}{4}\right]}. \qquad (5.103b)$$

Whether the wave is long or short is determined by the sign of the phase function $(2/3)(\xi_3)^{3/2}$. The positive sign is for long waves and the negative sign for short ones. The direction of the wave propagation is determined in agreement with that of the group velocity, discussed in section 4.2. Clearly, Z_l is the long wave that has been generated by resonance excitation at the outer Lindblad resonance. In principle, the asymptotic solution represented by equation (5.65b) does not hold at

$\xi_3 = \tilde{k}_0^2$, because the term $f\ \xi_0^{-1}$ becomes unbounded there. The wavy part of the solution, i. e., $Z_l + Z_s$, however, should hold through the point $\xi_3 = \tilde{k}_0^2$, for two reasons. First, the exact numerical integration shows the short wave solution changes smoothly from $\xi_3 < \tilde{k}_0^2$ to $\xi_3 > \tilde{k}_0^2$ according to equation (5.103a) (see Figures 5.8 and 5.9). Second, the short wave is responsible for the transport of angular momentum which depends only on Im(Z), and Im(Z) has no term of $f\ \xi_0^{-1}$. Therefore, we can safely calculate the phase of the wave solution by using the asymptotic solution $Z = Z_l + Z_s$. The phase of the long wave at $\xi_3 = \tilde{k}_0^2$ is equal to $\frac{\pi}{4}$, while the phase of the short wave at $\xi_0 = \tilde{k}_0^2$, $-\frac{4}{3}\tilde{k}_0^3 + \frac{3}{4}\pi$. Therefore, the phase difference is

$$\arg(Z_s) - \arg(Z_l) = -\frac{4}{3}\tilde{k}_0^3 + \frac{\pi}{2} \qquad at\ \xi_3 = \tilde{k}_0^2\ . \tag{5.104}$$

On the other hand, the total phase change may also be calculated from the dispersion relation, using the conjecture that the long wave originating from $\xi_3 = \tilde{k}_0^2$ propagates inward and is reflected out as a short wave. Thus,

$$\arg(Z_s) - \arg(Z_l) = \int_{r_L}^{r_Q} k_l\, dr + \int_{r_Q}^{r_L} k_s\, dr + \Phi_R \tag{5.105}$$

where k_l and k_s are the wavenumbers for long and short waves defined in equation (4.7), r_L and r_Q are the radii for the Lindblad resonance and the Q-barrier respectively and Φ_R is the phase change incurred at the Q-barrier due to reflection. By using equation (4.7) and the transformation $\eta = -x\ /\ x_{QL}$ with $x = (r - r_L)/\ r_L$ and $x_{QL} = |r_Q - r_L|\ /\ r_L$ [x_{QL} is also equal to $(\pi G\ \sigma_0)^2/\ (a^2 \tilde{D})$], it is easy to show that

$$\int_{r_L}^{r_Q} k_l \, dr = \tilde{k}_0^3 \int_0^1 (1 - \sqrt{1-\eta}) d\eta = \frac{\tilde{k}_0^3}{3}. \tag{5.106a}$$

$$\int_{r_Q}^{r_L} k_s \, dr = -\tilde{k}_0^3 \int_0^1 (1 + \sqrt{1-\eta}) d\eta = -\frac{5}{3}\tilde{k}_0^3 . \tag{5.106b}$$

Therefore,

$$\arg(Z_s) - \arg(Z_l) = -\frac{4}{3}\tilde{k}_0^3 + \Phi_R \tag{5.107}$$

By comparison, we have $\Phi_R = \frac{\pi}{2}$. The identification of $-\frac{4}{3}\tilde{k}_0^3$ from equations (5.104) and (5.107) dramatically confirms the conjecture we have put on test. Equation (5.65b) or the corresponding solution by means of the numerical integration represents the sum of a long trailing wave excited at the Lindblad resonance and a short trailing wave resulting from the reflection of the long wave at the Q -barrier. The amplitude of the wave does not change after the reflection. Only the phase experiences a change of $\frac{\pi}{2}$. The same amount of angular momentum is transmitted to the short wave and carried away by it.

The asymptotic solution of equation (5.65b) breaks down near $\xi_3 = \tilde{k}_0^2$ because of the term $f\ \xi_0^{-1}$. The numerical integration of equation (5.6) in section 5.3, using very accurate initial values, can be carried out without difficulty. Figures 5.8 and 5.9 show that the short wave propagates outward passing beyond the outer Lindblad resonance and the long wave decays rapidly there, just as we anticipated in section 4.2 (of Chapter IV). We can also see that the asymptotic expansions are in excellent agreement with the exact numerical solution, except in the neighborhood of $\xi_3 = \tilde{k}_0^2$.

When $\tilde{k}_0^2$ is small, the long waves have wavelengths much longer than $r_L - r_Q$. Their presence becomes unnoticeable. The short trailing waves appear to be the only wave in the entire region. Since they are reflected waves from the Q-barrier, they also appear as if they were generated from the Q-barrier.

Overall the self-gravity has three effects. First, it moves the spiral pattern of short trailing waves closer to the co-rotation radius by a distance of $\tilde{k}_0^2$. Waves start at the Q-barrier. Second, it causes the spiral pattern to turn an angle of $\tilde{k}_0^3 / 3$ in the positive sense of rotation. Third, it makes the wavelength shorter by increasing the dimensionless wavenumber by $\tilde{k}_0$ as compared to the case of pure acoustic waves.

The presence of viscosity complicates the calculation greatly. In general, viscosity tends to damp the waves with an exponential factor of $e^{-\frac{2}{3}\xi_0^{3/2}\cos^{1/2}\beta\sin\frac{\beta}{2}}$ In addition, it also plays two roles similar to the self-gravity. First, it causes a negative phase shift of $-\beta/4$. Second, it tends to increase the wavelength by stretching it with a factor of $\sec^{1/2}\beta\sec(\beta/2)$. Both of these tend to reduce the self-gravity effects. Strictly speaking, these results are only for the cases without self-gravity. However, when self-gravity is included, although the viscous terms appear extremely complicated in the solutions, the viscosity basically still plays the same role as before.

CHAPTER VI

THE NON-LINEAR THEORY

6. 1. The Non-linear Differential Equation

The fundamental integro-differential equation (2.57) determines the resonance excitation, propagation and damping of the density and/or acoustic waves. We would be able to extract all the information it contains if we could solve it directly, but unfortunately, there is no easy way of doing it. In Chapter IV, following the procedure of SYL, we heuristically replaced the integro-differential equation (2.57) by a non-linear differential equation (4.37):

$$\frac{d}{d\xi_0}[(I \mp i\, b)\frac{dZ}{d\xi_0}] + i\, 4\tilde{k}_0 L^{1/2}\frac{d}{d\xi_0}(L^{1/2}Z) \mp \xi_0 Z = \mp f', \qquad (6.1)$$

which approaches the same linear equation (4.3) in the linear limit $q_0 \to 0$ and assumes the same non-linear amplitude relation (4.33), as equation (2.57) does. If the self-gravity term is relatively small, as in the case of the 3-kpc arm with self-gravity, equation (6.1) produces a dispersion relation which is not equal to, but can approximate in the limit of $\tilde{k}_0 \to 0$, the non-linear dispersion relation (4.21) deduced from equation (2.57). If the self-gravity term is much more important than the acoustic term, as in the case of Saturn's rings, we would rather constructed the differential equation as

$$\frac{d}{d\xi_0}[(I \mp i\, b)\frac{dZ}{d\xi_0}] + i\, 4\tilde{k}_0 L^{1/2}\frac{d}{d\xi_0}(L^{1/2}Z) \mp \frac{2L}{H}\xi_0 Z = \mp f', \qquad (6.2)$$

such that it would still satisfy the linear equation requirement and the amplitude

relation requirement, and can produce a dispersion relation which, although still not equal to, approximates the dispersion relation (4.21) in the limit of pure density waves. But when self-gravity and acoustic effects are comparable, neither equation (6.1) nor equation (6.2) can even approximately satisfy the dispersion relation requirement. In any case, there is always a factor of 2 difference between the dispersion relations deduced from the integro-differential equation and the differential equation, which seems impossible to get rid of by adjusting the coefficients of the differential equation. SYL do not include the pressure and viscous term when constructing the differential equation, so their differential equation is equivalent to equation (6.2) without the second order derivative term, and all three requirements are satisfied. Shu et al. add the pressure and viscous term into SYL's differential equation and take for granted that all three requirements are still satisfied. Fortunately, since the pressure is small and the viscosity is treated as a given forcing function, no serious error is involved. Since the differential equation satisfying all three requirements simultaneously cannot be obtained in any simple way, we simply choose to have the linear equation requirement and the amplitude relation requirement (which is related to the conservation of angular momentum) satisfied for the present study. Furthermore, since we intend to apply our theory to the 3-kpc arm problem, we adopt equation (6.1) for the integro-differential equation (2.57).

6. 2. Numerical Solutions

6. 2. 1. Methods of Solution

To fix our ideas, we concentrate on the problem associated with the outer

Lindblad resonance here. Thus, equation (6.1) becomes

$$\frac{d}{d\xi_0}[(I + i\,b)\frac{dZ}{d\xi_0}] + i\,4\tilde{k}_0 L^{1/2}\frac{d}{d\xi_0}(L^{1/2}Z) + \xi_0 Z = + f'. \tag{6.3}$$

where I , b , and L are complicated but known functions of q_0^2 as defined in (2.40), (2.54a) and (4.27), and q_0 is defined as $q_0 = |dZ / d\xi_0|$ in (2.51). The presence of these functions makes equation (6.3) highly non-linear and hence makes the numerical integration of it a nontrivial problem. Even though the equation of the form of (6.3) is derived in Shu et al., they did not solve the full equation. The pressure term is dropped for the case of Saturn's rings. The viscous term is treated as a forcing term. Thus, the equation solved in Shu et al. is only a first order differential equation of a complex variable Z.

We solve the second order differential equation (6.3) by the Runge-Kutta method. It is desirable to write equation (6.3) as a set of first order differential equations:

$$\frac{d\Phi}{d\xi_0} = -\frac{q_0}{A} \tag{6.4a}$$

$$\frac{dA}{d\xi_0} = g \tag{6.4b}$$

$$\frac{dq_0}{d\xi_0} = \frac{f'(I\sin\Phi + b\cos\Phi) - (I^2+b^2)\frac{gq_0}{A} + 4\tilde{k}_0 L\,(Ig - bq_0) - bA\,\xi_0}{(Iq_0+bg)\frac{dI}{dq_0} - (Ig - bq_0)\frac{db}{dq_0} + (I^2+b^2) - 2\tilde{k}_0 IA\frac{dL}{dq_0}} \tag{6.4c}$$

$$I\frac{dg}{d\xi_0} = f'\cos\Phi + \frac{Iq_0^2}{A} - \frac{bq_0 g}{A} - 4\tilde{k}_0 Lq_0 - \xi_0 A - (g\frac{dI}{dq_0} + q_0\frac{db}{dq_0} + b)\frac{dq_0}{d\xi_0} \tag{6.4d}$$

where, following SYL and Shu et al. in carrying out the numerical calculation, we

have redefined q_0 to be $A(-d\Phi/d\xi_0)$ rather than $|dZ/d\xi_0|$, where $Z \equiv A\, e^{i\Phi}$. This slight readjustment is justifiable since a model equation is always arbitrary to some extent and it significantly reduces the numerical difficulties. With this readjustment, the q_0 value at the initial position of our choice is much smaller so that the solution of the linear equation can approximate the non-linear equation much better, and the parasitic components can be suppressed to some extent. We will discuss this further in the following paragraphs.

To solve the system of equations (6.4), by the Runge-Kutta method, correct initial values are needed. But it seems impossible to find the exact initial values due to the high nonlinearity of the equations. Fortunately, we can use the exact or asymptotic solutions of the linearized equation (4.3), found in Chapter V, to approximate the solution to the non-linear equation (6.3) at the initial point of our choice. We choose the initial point of the integration ξ_0 to be far away from the turning point along the negative direction; since the amplitude of waves decays rapidly into the evanescent region, q_0 is necessarily small there. With the non-linearity parameter q_0 small enough, the functions I, L and b approach their limiting values such that the linear solution near the thus chosen position can well approximate the non-linear solution, and provide the initial values we need.

If we consider only the smallness of the q_0 values, it is clear that taking values deeper into the evanescent region should give us better results. This, however, will cause greater contributions from the parasitic components to enter our numerical results. The reason is similar to that we mentioned in Chapter V, section 5.3. As we can visualize from the asymptotic solution of the linear theory,

the solution which satisfys our boundary conditions will have an exponentially increasing imaginary part and an algebraically varying real part for large negative ξ_3 (the distance from the turning point). But inaccurate initial values and round-off errors may produce a solution with an additional term which is real and exponentially increasing. The general solution of (6.3) does contain such a term, although our boundary condition requires the arbitrary coefficient in front of it be zero. It is the inaccurate initial values and the round-off errors that makes this coefficient nonzero. This unwanted real term increases exponentially and eventually become comparable to the real part of the desired solution, and hence ruins the whole solution. The farther away the starting point from the turning point, the more the parasitic components are amplified in the integration. To balance the above two considerations, therefore, we should choose an appropriate initial position which is far away enough from the Q-barrier such that the linear solutions are valid for equations (6.3) yet close enough not to produce large parasitic contributions. This requirement cannot be always satisfied, as in the case of large viscosity, where we also have an exponentially decreasing solution for large, positive ξ_3. We will devise special techniques to cope with these numerical difficulties in later sections.

6. 2. 2. Inviscid Solutions

When neglecting the effect of viscosity, $b = 0$ and the set of equations (6.4) reduces to

$$\frac{d\Phi}{d\xi_0} = -\frac{q_0}{A} \tag{6.5a}$$

$$\frac{dA}{d\xi_0} = g \tag{6.5b}$$

$$\frac{dq_0}{d\xi_0} = \frac{f'\sin\Phi - I\frac{gq_0}{A} + 4\tilde{k}_0 Lg}{I + q_0\frac{dI}{dq_0} - 2\tilde{k}_0 A\frac{dL}{dq_0}} \tag{6.5c}$$

$$I\frac{dg}{d\xi_0} = f'\cos\Phi + \frac{Iq_0^2}{A} - 4\tilde{k}_0 Lq_0 - \xi_0 A - g\frac{dI}{dq_0}\frac{dq_0}{d\xi_0} \tag{6.5d}$$

where f' represents the dimensionless periodic external forcing due to a satellite or a central distortion. In this subsection, we take $f' = 3$, corresponding to a 5% perturbational field relative to the mean field in the 3-kpc arm problem. Since $q_0 = A(-d\Phi/d\xi_0)$ and A increases with f', the value of $f' = 3$ brings about a pretty large q_0, hence a high non-linearity. According to the discussion in the previous section, before integrating equation (6.4) by the Runge-Kutta method, we have to make a proper choice of the starting position for the integration.

The first example here is for $\tilde{k}_0 = 0$ (neglecting self-gravity). It turns out that near $\xi_0 = \xi_3 \approx -6.5$, the linear solution can well approximate the solution of equation (6.4), and in the region of our interest the parasitic components are not significantly amplified. We start from $\xi_0 = -6$, using the linear solution (obtained from Chapter V) there as the initial values to integrate equation (6.4), by the Runge-Kutta method, up to $\xi_0 = 40$. The results are plotted in Figure 6.1, in which the dotted line represents the real part of Z, while the solid line, the imaginary part of Z. We see that when ξ_0 is large positive, as we expected, the real and imaginary parts of Z have a phase difference of $\pi/2$. There is a fluctuation

in the wave amplitude as we can see from the figure, which may be due to the non-linearity of the equation.

In our second example, we take $\tilde{k}_0 = 0.15$, corresponding to the 3-kpc problem with the self-gravity included. Since $\tilde{k}_0^2$ is small in this example, $\xi_3 \approx \xi_0$, we still choose $\xi_0 = 6$ as the starting point in the integration. The results are presented in Figure 6.2, again, with the dotted line representing the real part of Z, and the solid line, the imaginary part of Z. As compared with Figure 6.1, we observe a phase shift, a wavelength change, and a shorter wavelength for the amplitude fluctuation.

The results of this subsection will be used to find the corresponding velocities and surface densities in the 3-kpc arm problem in section 6.3.

6. 2. 3. Viscous Solutions

When viscosity must be considered, we have to integrate equation (6.4) with non-zero b_0. Now we are looking for a wave solution which will decay by viscous attenuation on the other side of the turning point, and the solution becomes even more sensitive to the initial values. Since our initial values from the linear theory are only approximate, the parasitic components entered from the beginning increase very quickly and are difficult to control. A larger b_0 value can cause a more rapidly growing false solution. If b_0 is large, the requirement set forth near the end of subsection 6.2.1 can not be satisfied. Even for the best starting position we can use, it is still too close to the turning point to ensure a small q_0 such that the linear solution can well approximate the non-linear solution of equation (6.4). On the other hand, it is already too far away from the turning

point to have the growth of the parasitic terms properly suppressed. To cope with this difficulty, we notice that deep into the wave region the amplitude of the wave, and hence q_0, also becomes small due to viscous attenuation. We therefore try to integrate from both sides of the turning point with both the starting positions far away from the turning point such that the q_0 values are relatively small. The parasitic components grow rapidly along both directions of integration for reason stated above. If the two solutions match before they are destroyed by the parasitic terms, we can obtain a good solution by combining these two solutions. In general, they do not match in the overlapped region unless our choice of the phase at the far end of ξ_0 happens to be correct. We can adjust the complex phase of the initial values there until they match. We will demonstrate this procedure in the following examples.

The first example is for $\tilde{k}_0 = 0.15$, $f' = 0.3$, corresponding to 0.5% perturbational field relative to the mean field in the 3-kpc arm problem. We integrate equations (6.4) from $\xi_0 = -6$, along the positive direction (see solid lines in Figures 6.3 and 6.4, for real and imaginary parts respectively), and also from $\xi_0 = 12$, along the negative direction (see dotted lines in Figures 6.3 and 6.4, for real and imaginary parts respectively), using the linear solution to approximate the initial values at both starting points. As we expected, the two solutions match perfectly, near $\xi_0 = 2.5$, and beyond that, the parasitic contributions manifest themselves. We can reasonably believe that the true solution is represented by the solid lines for $-6 < \xi_0 < 2.5$, and by dotted lines for $2.5 < \xi_0 < 12$ in Figures 6.3 and 6.4.

The second example is for $\tilde{k}_0 = 0.15$, $f' = 0.6$, corresponding to 1% perturbational field relative to the mean field in the 3-kpc arm problem. Similarly,

we integrate equations (6.4) from $\xi_0 = -6$ (see solid lines in Figures 6.5 and 6.6, for real and imaginary parts respectively), and from $\xi_0 = 12$ (see dotted lines in Figures 6.5 and 6.6, for real and imaginary parts respectively). A noticeable phase difference can be seen between the solid and the dotted lines in the overlapped region. Our experience in the numerical calculation tells us that this phase difference is not due to the parasitic contribution, but rather due to the non-linearity of the equation. With larger f's (hence higher non-linearity), larger phase differences are observed, as in the following example.

This third example is for $\tilde{k}_0 = 0.15$, $f' = 3$, which is needed in the 3-kpc arm problem to produce an expansion velocity of $53\ km - sec^2$. Very high non-linearity is involved with such a large f' value. Now, we integrate equations (6.4) from $\xi_0 = -6$, along the positive direction, using the linear solution as the initial values; we also integrate equations (6.4) from $\xi_0 = 12$, along the negative direction, but using a modified linear asymptotic solution at $\xi_0 = 12$ as the initial values. Since we believe that non-linearity causes a phase shift, we adjust the complex phase in the linear asymptotic solution (5.83) by trial and error, such that the two solution curves from opposite directions can match approximately. In Figures 6.7 and 6.8, for the real part and the imaginary part of Z respectively, we show the results of integrating along the positive direction by solid lines, and the results of integrating along the negative direction (with modified initial conditions) by dotted lines. The agreements of the two curves in the overlapped region is not entirely ideal, but it is certainly acceptable in view of the degree of approximations with which we have worked in this study. Furthermore, since we are particularly interested in the first peak of the solution which is not really affected by

the above procedure, the results we have just obtained undoubtedly can be used to interpret the 3-kpc phenomenon.

6. 3. The 3-kpc Arm Phenomenon

The 3-kpc arm is a coherent armlike feature of gas streaming radially toward us at a velocity of 53 km/sec in the central region of the Galaxy. The arm covers a galactocentric sector of about 90^0, and is located at a distance about 3.75 kpc (3 kpc in the old scale) from the galactic center. The mass associated with the high expansion velocity is estimated as about $4 \cdot 10^7 M_\odot$. It is one of the most spectacular phenomena observed in the Galaxy.

For years, people had favored a theory based on an expulsion model to account for the fast expansion of the arm (van der Kruit 1971; Sanders and Prendergast 1974). The model requires frequent explosions at the galactic center for an energy source. It then needs a replenishment mechanism, as the mass loss due to the 3-kpc arm is about $1 M_\odot$ / *year* from the central region. Both the energy and the mass problems are difficult to resolve in the expulsion model.

In 1984, Yuan showed that a minor distortion or a barlike structure, rotating at a typical angular speed in the central region of the Galaxy can excite an outgoing acoustic wave which has a close resemblance to the observed "3-kpc arm". This approach has definite advantages over the expulsion model: it does not require frequent explosions at the center. Therefore no energy problem exists. Nor there is any net outgoing mass flux in this approach since the average radial velocity is zero. Therefore no mass loss problem exists. Furthermore, observations of a central bar structure are not uncommon in disk galaxies. Thus, it is not unreasonable to

assume a minor oval distortion in the center of the Galaxy.

According to Yuan's model, a minor oval distortion in the center with the ratio of semi-major to semi-minor axes of 1:0.9 can produce a perturbational field of 10% of the mean field at $r = 3kpc$. The oval distortion rotates at $\Omega_P = 118\ km\ /\ sec - kpc$. The corresponding co-rotation and the outer Lindblad resonance are located respectively at $r = 1.6\ kpc$ and $r = 3\ kpc$. Using the 1965 Schmidt model and taking $a = 10\ km\ /\ sec$, we have $\kappa = 103\ km\ /\ sec - kpc$, $\tilde{D}^{1/2} = 188\ km\ /\ sec - kpc$ and $\gamma = 14.115$. The oval distortion generates two trailing spiral waves, with an expanding motion equal to 53 km/sec.

Yuan's theory was solved out with both linear and non-linear methods. The linear theory provides a physical picture of the wave generation. It is the non-linear theory that was used to explain the observational features. The non-linear theory, however, is based on numerical integration of the hydrodynamical equations. A local approximation was used to reduce the two-dimensional problem to a one-dimensional problem. Therefore, the theory, strictly speaking, is only valid near the resonance. Furthermore, since the one-order scheme was used, the numerical viscosity arising from the second-order terms automatically enters the calculations without a proper control. Although the results seem to be reasonable, it is certainly desirable to have some independent confirmations. Another important drawback is that the formulation in that paper cannot be extended to include the self-gravity effect.

The present formulation is free from these limitations. First, it is formulated for the entire disk. Second, the viscosity terms and the self-gravity terms are

explicitly expressed in the governing equation. Therefore, we can have a globally valid equation, including viscosity and self-gravity. Using the same model of Yuan, except for a perturbational field of 5% of the mean field and adopting the same viscosity estimated there ($\nu = 0.2\ km - kpc\ /\ sec$), we re-calculate the 3-kpc arm problem. We find that the results are in qualitative agreement.

For the convenience of illustration, we first calculate the inviscid case with and without self-gravity. In section 6.2.2, we calculated the complex Lagrangian displacement $Z(\xi_0)$, for $\tilde{k}_0 = 0$ and $\tilde{k}_0 = 0.15$ respectively. Once $Z(\xi_0)$ is known, we can obtain the physical displacement (in non-dimensional form) as [see equations (2.37) and (2.38)]:

$$X(\xi_0,\phi_0) = \mathrm{Re}\{Z(\xi_0)\, e^{-i\,\psi_0}\} \tag{6.6}$$

from which we can recover the surface density contrast [see equations (2.24), (2.30) and (2.31)]:

$$\frac{\sigma}{\sigma_0} = \frac{1}{1 + \dfrac{\partial X}{\partial \xi_0}} \tag{6.7}$$

The radial velocity can be obtained by using [see equation (2.14)]:

$$u = \frac{dr_1}{dt} = -[\omega - m\,\Omega(r_0)]\frac{\partial r_1}{\partial \psi_0} \tag{6.8}$$

The observed density contrast and velocity are functions of $\phi_0 = \psi_0 / m$ and the Eulerian distance r_1. In Figure 6.9 we plot the surface density in the case of $\tilde{k}_0 = 0$ while in Figure 6.10 we plot the surface density in the case of $\tilde{k}_0 = 0.15$ (corresponding to $\sigma_0 = 5.4\ M_\odot\ /\ pc^2$, the average surface density of the gas at 3-kpc). The direction of the profiles are chosen such that the radial velocity has its

highest value. The abscissa in the above figures has been transformed back to the Eulerian distance. The results are similar to those of SYL. The profiles are highly peaked. The valleys are shallow with minimum value equal to −0.3 in logarithmic scale, or equal to 0.5 in linear scale, which is expected. The waves for $\tilde{k}_0 = 0.15$ clearly have a shorter wavelength and a phase shift as compared to the waves of $\tilde{k}_0 = 0$. This is again a result expected from the linear theory. The corresponding radial velocity for both cases are plotted in Figures 6.11 and 6.12.

When the viscosity with $b_0 = 0.127$ is included, the calculations are highly complicated as noted in the preceding sections. With technique of matching from both sides, we found the complex Lagrangian dispacement $Z(\xi_0)$ in section 6.2.3 for $\tilde{k}_0 = 0.15$. Then we can calculate the surface density and radial velocity using equations (6.7) and (6.8). The results are shown in Figures 6.13 for density and 6.14 for radial velocity. We find that the present approach does not need a perturbational field as high as 10% of the mean field. A 5% field is capable of driving a wave of streaming velocity equal to 53 km/sec. Even with the 5% field, the density contrast in the first peak as well as the second one is much higher than the results of Yuan (1984). For the first peak, the present calculation gives a value of 10:1 while the early one gave 4:1 (see Figure 6.13). The spacings between the peaks in both cases are roughly the same. The last two profiles correspond to the direction $\phi_0 = \psi_0/2 = 67^0$, in which the velocity has the largest value. This is another place where the present result differs substantially from that of Yuan, which gives $\phi_0 = 100^0$. Thus, the calculations based on the more accurate formulation lead to a greater phase shift. Those for other ϕ_0 are not presented here. A contour map of the density with indications of radial velocities is drawn in Figure

6.15. It should be noted that the radial velocity in Figure 6.14 at large r has a nonzero value. This is a response to the long-range perturbational field, corresponding to $f'\xi_0^{-1}$ in the linear theory. This is not in contradiction to the result of Yuan (1984) since there the perturbational force is allowed to drop to zero beyond 5-kpc.

The overall agreement between the results of the two independent approaches has convinced us that those calculations are reliable and the mechanism proposed by Yuan for the 3-kpc arm is a feasible one. Since the self-gravity if small for the 3-kpc arm, the present result does not modify the early result significantly in that respect. On the other hand, since the non-linearity has been handled more accurately here, the required field strength of the perturbation can be reduced by a factor of two to produce the same result.

CHAPTER VII

SUMMARY

The purpose of this thesis is to develop a theory which can be used to study the structure and dynamics of a self-gravitating gaseous disk responding to a periodic perturbational potential. The potential is derived from either a satellite exterior to the disk or an asymmetric distribution of mass in the central regions. The perturbational potential will excite spiral waves at the Lindblad resonances by a mechanism referred to as resonance excitation. The waves will carry angular momentum from the satellite or distorted central mass to the disk and vice versa. The deposit (or removal) of the angular momentum into (or from) the disk has profound influence on the structure of the disk. Such wave motions will be important in the evolution of the system. The nature of these waves is the subject of our present study.

Since we seek to apply the theory to the 3-kpc arm problem in the Galaxy, the proto-stellar disk of the solar nebula, the circumstellar disk of a binary and possibly barred galaxies, acoustic effects are as important as self-gravity. The waves studied, therefore, consist of both a self-gravity mode and a acoustic mode. This problem is more difficult than that of Saturn's rings, which deals only with self-gravity, and also than the 3-kpc arm problem without self-gravity, which deals only with the acoustic effect. Since viscosity is also expected to be important in all these problems, excepting stellar components of barred galaxies, we have included viscous stresses of the classic type in our formulation. The resulting

equation is a second order integro-differential equation. The acoustic and viscous effects enter the equation through the second order differential term, while the self-gravity effect is associated with the non-linear singular integral. Both linear and non-linear analyses are carried out. In order to make the non-linear analysis mathematically possible, we have replaced the integro-differential equation by a differential equation, using heuristic arguments.

The mathematical formulation of the present problem is based on three assumptions: (1) the excursion of a fluid particle is small compared with the radial distance of the particle, i. e., $|r_1| < r_0$, (2) the quantity $\epsilon = \frac{2\pi G\, \sigma_0(r_L)}{r_L \tilde{D}}$ is so small that the solution may be expanded in series of $\epsilon^{1/2}$, and (3) the waves are tightly wound, i. e., $|kr| \gg m$, such that the WKBJ approximation may be applied. All three assumptions, which hold perfectly for Saturn's rings, are also found valid, but to a lesser degree for the 3-kpc arm problem, the proto-stellar disk in the solar nebula and the circumstellar disk of a binary. The second condition does not hold for barred galaxies. Thus, the present study cannot be applied to barred galaxies. However, the linear equation in this thesis can be derived from hydrodynamic equations as demonstrated in the work of Yuan (1984); therefore, the linear theory in this thesis also can be used to analyze the structure of barred galaxies.

Earlier research shows that the disk would respond violently to any minor disturbance such as in Saturn's rings or in the gas component of the galactic disk. Therefore, the validity of the linear theory is very limited in application. The linear theory itself has laid a solid foundation of understanding for the intricate

interplay of the highly complicated dynamical processes involved in this problem, including the excitation, propagation and attenuation of the waves and the transport of angular momentum. The solutions of the linear equation suggest the following scenario: The small but long-range external disturbance excites long trailing waves at the Lindblad resonances. These waves then propagate toward the co-rotation and are reflected as short trailing waves at the Q-barrier. The amplitude is not changed while there is a phase gain of $\frac{\pi}{2}$ in the reflection. The same amount of angular momentum density will be transferred to, and then carried away by, the short trailing waves in the disk. Where the angular momentum is deposited in the disk depends entirely on the viscosity. Large viscosity causes the deposition to be concentrated near the Q-barrier. This would eventually leads to the clearing of a gap next to the Q-barrier, as the local materials move away due to gain or loss of angular momentum. Small viscosity will cause the angular momentum to be distributed over a large region. The effect on the re-distribution of the disk materials would be less pronounced.

The linear solutions also reveal the roles that self-gravity plays in shaping the wave pattern. The effect of self-gravity will change a pure acoustic wave pattern in three ways: First, it displaces the wave pattern closer to the co-rotation radius, that is, it moves the wave from the Lindblad resonance to the Q-barrier. Second, it rotates the wave pattern by an angle of $\tilde{k}_0^3 / 3$ radians in the same sense as disk rotation. Third, it shortens the wavelength or packs the wave pattern more tightly. Besides damping waves, the viscosity also acts to rotate the wave pattern and change the wavelength, according to the linear theory, except that it tends to reduce those effects caused by self-gravity. In any case, these effects due to

viscosity are usually very weak, unless the viscosity is exceedingly large.

The resonance excitation mechanism is extremely effective. A small periodic disturbance is capable of exciting waves of large amplitude. This makes the linear theory quite inadequate when applied to real problems. Therefore, developing the non-linear theory is a real necessity. Following the work of SYL, we adopt a non-linear differential equation in our calculations, instead of solving the original non-linear singular integro-differential equation. Even with this differential equation, we can only claim limited success. Three free parameters are involved, namely, $\tilde{k}_0$, b_0 and f', representing respectively, the self-gravity, the viscosity and the strength of the perturbational field. In general, when all of them are large, i. e., when $\tilde{k}_0 > 2$, $b_0 > 0.2$ and $f' > 3$, the integration cannot be carried through. Parasitic components, which enter the calculation by inaccuracy in the initial values provided by the linear theory and round-off errors in intermediate steps of integration, may grow exponentially and take over the true solution. The most troublesome parameter is b_0. Without it, it is possible to obtain solutions with moderate $\tilde{k}_0$ and f'. Well within the above limits of the three parameters, we obtained satisfactory results. The calculated density is highly peaked and the wavelength roughly varies linearly with the amplitude, similar to the results of SYL. With $\tilde{k}_0 = 0.15$, $b_0 = 0.127$ (corresponding to $\nu = 0.2\ km - kpc\ /\ sec$) and $f' = 3$ (corresponding to 5% perturbational field relative to the mean field), we can reproduce, with minor differences, the 3-kpc arm results of Yuan (1984) and therefore verify his non-linear solution from a completely different approach.

APPENDIX A

DERIVATION OF THE PRESSURE AND VISCOUS TERM

In the fundamental integro-differential equation derived in Chapter II [see (2.39)],

$$\frac{dF}{d\xi_0} + \frac{1}{\pi}\int_{-\infty}^{\infty} I(q^2)\left[\frac{Z(\xi_0') - Z(\xi_0)}{(\xi_0' - \xi_0)^2}\right] d\xi_0' \pm \xi_0 Z(\xi_0) = \pm f \ , \tag{A1}$$

the effects of the pressure and viscosity are contained in the term $\frac{dF}{d\xi_0}$. It is necessary that it is spelled out. The function F is twice the complex Fourier coefficient of a combination of pressure tensor components:

$$F \equiv \frac{1}{\pi}\oint(\tilde{P}_{rr} \pm i\,\frac{2\Omega}{\kappa}\tilde{P}_{r\theta})\,e^{i\psi_0}\,d\psi_0 \tag{A2}$$

where the upper sign corresponds to the inner Lindblad resonance, while the lower sign, the outer Lindblad resonance, and $\tilde{\mathbf{P}}$ is the nondimensional pressure tensor,

$$\tilde{\mathbf{P}} = \frac{\epsilon^{-1/2}\mathbf{P}}{2\pi G r_L\,\sigma_0^2(r_L)} \tag{A3}$$

with $\mathbf{P}$, the pressure tensor. We consistently adopt the asymptotic approximation that, except for the periodic perturbational potential, the r derivative of a perturbed quantity times r is much larger than either the θ derivative of the quantity or the quantity itself. So we can approximate the components of $\mathbf{P}$ as follows:

$$P_{rr} = -P + 2\mu\frac{\partial u}{\partial r} + (\mu' - \frac{2}{3}\mu)(\frac{u}{r} + \frac{\partial u}{\partial r} + \frac{1}{r}\frac{\partial v}{\partial \theta})$$

$$\approx - P + (\frac{4}{3}\mu + \mu')\frac{\partial u}{\partial r}, \tag{A4}$$

$$P_{r\theta} = \mu(\frac{\partial v}{\partial r} - \frac{v}{r} + \frac{1}{r}\frac{\partial u}{\partial \theta}) \approx \mu r\frac{\partial}{\partial r}(\frac{v}{r}). \tag{A5}$$

We assume that both the coefficients of the shear and the bulk viscosity, μ and μ', are constant. Substituting (A4) and (A5) into (A2) gives

$$\frac{2\pi G r_L\, \sigma_0^2(r_L)}{\epsilon^{-1/2}} F =$$

$$\frac{1}{\pi}\oint[- P + (\frac{4}{3}\mu + \mu')\frac{\partial u}{\partial r} \pm i\frac{2\Omega}{\kappa}\mu r\frac{\partial}{\partial r}(\frac{v}{r})]\, e^{i\psi_0}\, d\,\psi_0 . \tag{A6}$$

Recall that

$$r = r_0 + r_1, \tag{A7}$$

$$r_1 = r_L\, \epsilon^{1/2} X , \tag{A8}$$

$$x_0 = \frac{r_0 - r_L}{r_L}, \tag{A9}$$

$$\xi_0 = \epsilon^{-1/2} x_0, \tag{A10}$$

and

$$\phi \equiv \theta - \Omega_p\, t \tag{A11}$$

where θ is the azimuthal angle in the inertial frame and ϕ is the azimuthal angle measured in a frame rotating with angular velocity $\Omega_p \equiv \omega / m$, which can be written as

$$\phi = \phi_0 + [\Omega(r_0) - \Omega_P]\, t + \phi_1(r_0, \psi_0) \tag{A12}$$

where ϕ_0 is a constant and ϕ_1 may be considered to be a small perturbation about the mean circular motion which can be measured by the angular variable

$$\psi_0 = m\,\phi_0 + [m\,\Omega(r_0) - \omega]\, t\ . \tag{A13}$$

From (A7) we see that

$$\frac{\partial}{\partial r} = \frac{1}{1 + \dfrac{\partial r_1}{\partial r_0}} \frac{\partial}{\partial r_0}\ . \tag{A14}$$

The first term on the right hand side of (A6) can be written as

$$I_1 \equiv -\frac{1}{\pi}\oint P\ e^{i\,\psi_0} d\,\psi_0 = -\frac{a^2}{\pi}\oint \sigma\, e^{i\,\psi_0} d\,\psi_0$$

$$= -\frac{a^2}{\pi}\oint \frac{\sigma_0(r_0)\, e^{i\,\psi_0}}{1 + \dfrac{\partial r_1(r_0, \psi_0)}{\partial r_0}}\, d\,\psi_0 = -\frac{a^2 \sigma_0(r_0)}{\pi}\oint \frac{e^{i\,\psi_0}}{1 + \dfrac{\partial X}{\partial \xi_0}}\, d\,\psi_0\ . \tag{A15}$$

In (A15) we have used the relation

$$P = a^2 \sigma(r)\,, \tag{A16}$$

and

$$\sigma(r) = \frac{\sigma_0(r_0)}{1 + \dfrac{\partial r_1(r_0, \psi_0)}{\partial r_0}}\,, \tag{A17}$$

which is derived from the Lagrangian form of the equation of continuity.

To determine the integral in (A15)

$$I_{11} \equiv \oint \frac{e^{i\,\psi_0}}{1 + \frac{\partial X}{\partial \xi_0}} d\,\psi_0 \,, \tag{A18}$$

we use the approximation [see equations (2.35) and (2.37)]

$$X \approx A(\xi_0)\cos[\,\psi_0 - \Phi(\xi_0)]\,, \tag{A19}$$

and write it as

$$X = C(\xi_0)\cos\psi_0 + S(\xi_0)\sin\psi_0 \tag{A20}$$

where

$$C \equiv A(\xi_0)\cos\Phi(\xi_0)\,, \qquad S \equiv A(\xi_0)\sin\Phi(\xi_0)\,, \tag{A21}$$

so we have

$$\frac{\partial X}{\partial \xi_0} = \frac{dC(\xi_0)}{d\,\xi_0}\cos\psi_0 + \frac{dS(\xi_0)}{d\,\xi_0}\sin\psi_0$$

$$= q_0\cos\Delta_0\cos\psi_0 + q_0\sin\Delta_0\sin\psi_0 = q_0\cos(\psi_0 - \Delta_0)\,, \tag{A22}$$

where q_0 and Δ_0 are defined as functions of ξ_0 and ξ_0' through

$$q_0\cos\Delta_0 \equiv \frac{dC(\xi_0)}{d\,\xi_0}\,, \qquad q_0\sin\Delta_0 \equiv \frac{dS(\xi_0)}{d\,\xi_0}\,. \tag{A23}$$

If we further define that

$$\Theta \equiv \psi_0 - \Delta_0\,, \tag{A24}$$

we will have

$$I_{11} = \oint \frac{\cos\psi_0 + i\,\sin\psi_0}{1 + q_0\cos(\psi_0 - \Delta_0)} d\,\psi_0 = \int_{-\pi}^{\pi} \frac{\cos(\Theta + \Delta_0) + i\,\sin(\Theta + \Delta_0)}{1 + q_0\cos\Theta}\, d\,\Theta$$

$$= \int_{-\pi}^{\pi} \frac{\cos\Theta\cos\Delta_0 - \sin\Theta\sin\Delta_0 + i\ [\sin\Theta\cos\Delta_0 + \cos\Theta\sin\Delta_0]}{1 + q_0\cos\Theta} d\,\Theta\,. \qquad \text{(A25)}$$

Noting that the odd parts of the integrand give zero contributions, while (Gradshteyn and Ryzhik)

$$I_n(q) \equiv \frac{1}{2\pi}\int_{-\pi}^{\pi} \frac{\cos(n\,\Theta) d\,\Theta}{1 + q\cos\Theta} = \frac{1}{q^n (1-q^2)^{1/2}}[(1-q^2)^{1/2} - 1]^n\ , \qquad \text{(A26)}$$

we obtain

$$I_{11} = \int_{-\pi}^{\pi} \frac{\cos\Theta\cos\Delta_0 + i\ \cos\Theta\sin\Delta_0}{1 + q_0\sin\Theta}\, d\,\Theta$$

$$= 2\pi\,[I_1(q_0)\cos\Delta_0 + i\ I_1(q_0)\sin\Delta_0\,] = 2\pi I_1(q_0)\, e^{i\Delta_0}\,. \qquad \text{(A27)}$$

Recalling the definition of $Z(\xi_0)$ (see Chapter II) :

$$Z(\xi_0) \equiv A(\xi_0)\, e^{i\Phi(\xi_0)} = C(\xi_0) + i\ S(\xi_0)\,, \qquad \text{(A28)}$$

and using the fact that

$$\frac{dZ(\xi_0)}{d\,\xi_0} = \frac{d}{d\,\xi_0}[C(\xi_0) + i\ S(\xi_0)] = q_0\, e^{i\,\Delta_0}\,, \qquad \text{(A29)}$$

we obtain

$$I_{11} = \oint \frac{e^{i\,\psi_0}}{1 + \frac{\partial X}{\partial \xi_0}} d\,\psi_0 = 2\pi \frac{I_1(q_0)}{q_0}\frac{dZ(\xi_0)}{d\,\xi_0} = -\pi I(q_0^2)\frac{dZ(\xi_0)}{d\,\xi_0}\,, \qquad \text{(A30)}$$

where we have defined

$$I(q_0^2) \equiv -\frac{2}{q_0} I_1(q_0) = \frac{2}{q_0^2}\,[(1 - q_0^2)^{-1/2} - 1\,]\,. \qquad \text{(A31)}$$

Substituting (A30) into (A15) gives

$$I_1 \equiv -\frac{1}{\pi}\oint P\ e^{i\psi_0}\, d\psi_0 = a^2\sigma_0(r_0) I(q_0^2)\frac{dZ(\xi_0)}{d\xi_0}\,. \tag{A32}$$

The second term on the right hand side of (A6) can be written as

$$I_2 \equiv \frac{1}{\pi}\left(\frac{4}{3}\mu + \mu'\right)\oint \frac{\partial u}{\partial r}\, e^{i\psi_0} d\psi_0 = \frac{1}{\pi}\left(\frac{4}{3}\mu + \mu'\right)\oint \frac{\partial}{\partial r}\frac{dr_1}{dt}\, e^{i\psi_0}\, d\psi_0$$

$$= \pm\frac{\kappa}{\pi}\left(\frac{4}{3}\mu + \mu'\right)\oint \frac{\partial}{\partial r}\frac{\partial r_1}{\partial \psi_0}\, e^{i\psi_0}\, d\psi_0 \tag{A33}$$

where we have used (see (A13))

$$\frac{d}{dt} = [\, m\ \Omega(r_0) - \omega\,]\,\frac{\partial}{\partial \psi_0}\,, \tag{A34}$$

and

$$m\ \Omega - \omega \approx \pm\kappa\,, \tag{A35}$$

where the upper sign corresponds to the inner Lindblad resonance, while the lower sign, the outer Lindblad resonance. κ is the epicyclic frequency.

The integral in (A33) can be rewritten as

$$I_{21} \equiv \oint \frac{\partial}{\partial r}\frac{\partial r_1}{\partial \psi_0}\, e^{i\psi_0}\, d\psi_0 = \oint \frac{1}{1 + \dfrac{\partial r_1}{\partial r_0}}\frac{\partial}{\partial r_0}\frac{\partial r_1}{\partial \psi_0}\, e^{i\psi_0}\, d\psi_0$$

$$= \oint \frac{1}{1 + \dfrac{\partial X}{\partial \xi_0}}\frac{\partial}{\partial \xi_0}\frac{\partial X}{\partial \psi_0}\, e^{i\psi_0}\, d\psi_0\,. \tag{A36}$$

Using (A22) and (A24), we see

$$\frac{\partial}{\partial \xi_0}\frac{\partial X}{\partial \psi_0} = \frac{\partial}{\partial \psi_0}\frac{\partial X}{\partial \xi_0} = -\,q_0 \sin(\psi_0 - \Delta_0)\,, \tag{A37}$$

and

$$\frac{\partial}{\partial \xi_0}\frac{\partial X}{\partial \psi_0} e^{i\psi_0} = -q_0 \sin\Theta\, e^{i(\Theta+\Delta_0)}. \tag{A38}$$

Again, we switch the integration in (A36) over a complete cycle in ψ_0 to one in Θ from $-\pi$ to π and notice that the odd parts of the integrand give zero contributions. (A36) becomes

$$I_{21} = \int_{-\pi}^{\pi} \frac{-q_0 \sin^2\Theta\,(-\sin\Delta_0 + i\cos\Delta_0)}{1+q_0\cos\Theta} d\Theta$$

$$= -\frac{i}{2} q_0 e^{i\Delta_0} \int_{-\pi}^{\pi} \frac{1-\cos 2\Theta}{1+q_0\cos\Theta} d\Theta = -i\pi [I_0(q_0) - I_2(q_0)] \frac{dZ(\xi_0)}{d\xi_0} \tag{A39}$$

where (A26) and (A29) have been used.

Substituting (A39) into (A33) gives

$$I_2 \equiv \frac{1}{\pi}\left(\frac{4}{3}\mu + \mu'\right) \oint \frac{\partial u}{\partial r} e^{i\psi_0} d\psi_0$$

$$= \mp i\kappa \left(\frac{4}{3}\mu + \mu'\right) [I_0(q_0) - I_2(q_0)] \frac{dZ(\xi_0)}{d\xi_0}. \tag{A40}$$

The third term on the right-hand side of (A6),

$$I_3 \equiv \pm \frac{1}{\pi} \oint i \frac{2\Omega}{\kappa} \mu r \frac{\partial}{\partial r}\left(\frac{v}{r}\right) e^{i\psi_0} d\psi_0, \tag{A41}$$

can be rewritten with the help of (A11) and (A12) which lead to

$$\frac{v}{r} = \frac{d\theta}{dt} = \Omega_p + \frac{d\phi}{dt} = \Omega(r_0) + \frac{d\phi_1(r_0, \psi_0)}{dt}. \tag{A42}$$

From one of our perturbational equations, (2.10b), for the orbit trajectories,

$$r_0^2 \frac{d\,\phi_1}{dt} = J_1 - 2r_0\Omega(r_0)r_1\,, \tag{A43}$$

where J_1 is the perturbational specific angular momentum, we see that (A42) can be written as

$$\frac{v}{r} = \Omega(r_0) + \frac{J_1}{r_0^2} - \frac{2}{r_0}\Omega(r_0)r_1 \approx \Omega(r_0) - \frac{2}{r_0}\Omega(r_0)r_1\,. \tag{A44}$$

In (A44) we used the assumption that

$$J_1 \ll J_0 = r_0^2\,\Omega(r_0) \tag{A45}$$

where J_0 is the equilibrium specific angular momentum.

Differentiating (A44) with respect to r_0 gives

$$\frac{\partial}{\partial r_0}\left(\frac{v}{r}\right) \approx \frac{d\,\Omega(r_0)}{dr_0} - \frac{2}{r_0}\Omega(r_0)\frac{\partial r_1}{\partial r_0}$$

$$= \frac{\kappa^2}{2r_0\Omega(r_0)} - \frac{2\Omega(r_0)}{r_0}\left(1 + \frac{\partial r_1}{\partial r_0}\right), \tag{A46}$$

where κ, the epicyclic frequency, is defined as

$$\kappa^2 = 4\Omega(r_0)^2\left[1 + \frac{r_0}{2\Omega(r_0)}\frac{d\,\Omega(r_0)}{dr_0}\right]. \tag{A47}$$

Substituting (A14) and (A46) into (A41) and using (A30) give

$$I_3 \equiv \pm\frac{1}{\pi}\oint i\frac{2\Omega}{\kappa}\mu r\frac{\partial}{\partial r}\left(\frac{v}{r}\right)e^{i\psi_0}\,d\,\psi_0\,,$$

$$\approx \pm\frac{1}{\pi}\oint \frac{i\,2\Omega(r_0)}{\kappa}\frac{\mu r_0}{1+\dfrac{\partial r_1}{\partial r_0}}\left[\frac{\kappa^2}{2\Omega(r_0)r_0} - \frac{2\Omega(r_0)}{r_0}\left(1+\frac{\partial r_1}{\partial r_0}\right)\right]e^{i\psi_0}\,d\,\psi_0$$

$$= \pm \frac{i\,\mu\kappa}{\pi} \oint \frac{e^{i\psi_0}}{1 + \dfrac{\partial r_1}{\partial r_0}}\, d\,\psi_0 \mp \frac{i\,\mu 4\Omega (r_0)^2}{\pi\kappa} \oint e^{i\psi_0}\, d\,\psi_0$$

$$= \pm \frac{i\,\mu\kappa}{\pi} \oint \frac{e^{i\psi_0}}{1 + \dfrac{\partial X}{\partial \xi_0}}\, d\,\psi_0 = \pm \frac{i\,\mu\kappa}{\pi}\, I_{11}$$

$$= \mp i\,\mu\kappa I\,(q_0^2) \frac{dZ\,(\xi_0)}{d\,\xi_0}\,. \tag{A48}$$

Finally, we substitute (A32), (A40) and (A48) into (A6) and obtain (approximately)

$$F \equiv \frac{\epsilon^{-1/2} a^2}{2\pi G r_L\, \sigma_0(r_L)}\, F_1 = \frac{\epsilon^{-1/2} a^2}{2\pi G r_L\, \sigma_0(r_L)} \left[\mathrm{Re}(F_1) + i\ \mathrm{Im}(F_1) \right] \tag{A49}$$

where

$$\mathrm{Re}(F_1) = I\,(q_0^2) \frac{dZ\,(\xi_0)}{d\,\xi_0}\,, \tag{A50}$$

$$\mathrm{Im}(F_1) = \mp \frac{\kappa}{\sigma_0(r_L) a^2} \left\{ \left(\frac{4}{3}\mu + \mu'\right) [I_0(q_0) - I_2(q_0)] + \mu I\,(q_0^2) \right\} \frac{dZ\,(\xi_0)}{d\,\xi_0} \tag{A51}$$

where the upper sign corresponds to the inner Lindblad resonance, while the lower sign, the outer Lindblad resonance.

In the linear limit when $q_0 \to 0$, from (A26) we have

$$I\,(q_0) \sim 1\,, \quad I_0(q_0) \sim 1\,, \quad I_2(q_0) \sim 0\,, \tag{A52}$$

so (A50) and (A51) can be approximated as

$$\mathrm{Re}(F_1) \approx \frac{dZ(\xi_0)}{d\xi_0}, \tag{A53}$$

and

$$\mathrm{Im}(F_1) \approx \mp \frac{\kappa}{\sigma_0(r_L)a^2}\left(\frac{7}{3}\mu+\mu'\right)\frac{dZ(\xi_0)}{d\xi_0} \tag{A54}$$

for $q_0 \ll 1$.

Substituting (A53) and (A54) into (A49), we obtain an expression for F in the linear limit when $q_0 \ll 1$:

$$F = \frac{\epsilon^{-1/2}a^2}{2\pi G r_L\, \sigma_0(r_L)}\left(1 \mp i\, b_0\right)\frac{dZ(\xi_0)}{d\xi_0} \tag{A55}$$

where

$$b_0 \equiv \frac{\kappa}{\sigma_0(r_L)a^2}\left(\frac{7}{3}\mu + \mu'\right). \tag{A56}$$

Substituting (A49) or (A56) into $\frac{dF}{d\xi_0}$ will give the pressure and viscous term in an explicit form.

APPENDIX B

ASYMPTOTIC EXPRESSIONS OF I_a AND I_b

I_a and I_b are defined in Chapter V as (see section 5.1)

$$I_a \equiv \int_{\eta_2}^{\infty e^{-i\beta/3}} \mathrm{Ai}(\eta_2')\, e^{-i\tilde{k}\eta_2'}\, d\eta_2' , \tag{B1}$$

and

$$I_b \equiv \int_{\eta_{20}}^{\eta_2} \mathrm{Bi}(\eta_2')\, e^{-i\tilde{k}\eta_2'}\, d\eta_2' . \tag{B2}$$

The following derivations of the asymptotic expressions of (B1) and (B2) are for the general case when $\tilde{k}_0 \neq 0$ and $\beta \neq 0$, but the results are also valid when either or both of $\tilde{k}_0$ and β become zero. Expressions derived directly for the cases when either or both of $\tilde{k}_0$ and β are zero are consistent with the results given below.

1. Asymptotic Expansion of I_a as $\eta_2 \to +\infty e^{-i\beta/3}$

The integral representation of Airy function Ai (η_2) is

$$\mathrm{Ai}(\eta_2) = \frac{1}{2\pi}\int_{-\infty}^{\infty} e^{i t^3/3 + i\eta_2 t}\, dt \tag{B3}$$

Substituting it into (B1) gives

$$I_a = \int_{\eta_2}^{\infty e^{-i\beta/3}} \mathrm{Ai}(\eta_2')\, e^{-i\tilde{k}\eta_2'}\, d\eta_2'$$

$$= \int_{\eta_2}^{\infty e^{-i\beta/3}} e^{-i\tilde{k}\eta_2'} \frac{1}{2\pi} \int_{-\infty}^{\infty} e^{i t^3/3 + i\eta_2' t} \, dt \, d\eta_2'$$

$$= \frac{1}{2\pi} \int_{-\infty}^{\infty} dt \; e^{i t^3/3} \int_{\eta_2}^{\infty e^{-i\beta/3}} e^{i(t-\tilde{k})\eta_2'} \, d\eta_2'$$

$$= \lim_{\alpha \to \infty} \frac{e^{-i\tilde{k}\alpha e^{-i\beta/3}}}{2\pi i} \int_{-\infty}^{\infty} \frac{e^{i t^3/3 + i\alpha e^{-i\beta/3} t}}{t - \tilde{k}} \, dt$$

$$- \frac{e^{-i\tilde{k}\eta_2}}{2\pi i} \int_{-\infty}^{\infty} \frac{e^{i t^3/3 + i\eta_2 t}}{t - \tilde{k}} \, dt \; . \qquad \text{(B4)}$$

To find the asymptotic expansion of the integral in the first term,

$$I_{a1}(\eta_2) \equiv \int_{-\infty}^{\infty} \frac{e^{i t^3/3 + i\alpha e^{-i\beta/3} t}}{t - \tilde{k}} \, dt \; , \qquad \text{(B5)}$$

as $\alpha \to +\infty$, we rewrite it in the complex z-plane as

$$I_{a1}(\eta_2) = \int_{-\infty}^{\infty} \frac{e^{i z^3/3 + i\alpha e^{-i\beta/3} z}}{z - \tilde{k}} \, dz \; . \qquad \text{(B6)}$$

To employ the method of steepest descent we introduce the transformation,

$$z = \alpha^{1/2} s \; , \qquad \text{(B7)}$$

and obtain

$$I_{a1}(\eta_2) = \int_{-\infty}^{\infty} \frac{e^{i\alpha^{3/2}(s^3/3 + e^{-i\beta/3} s)}}{s - \tilde{k}\alpha^{-1/2}} ds \; . \qquad \text{(B8)}$$

The saddle points are given by

$$\frac{d}{ds}\left[i \left(s^3/3 + e^{-i\beta/3} s \right) \right] = 0 , \tag{B9}$$

or

$$s^2 + e^{-i\beta/3} = 0 . \tag{B10}$$

Hence, they are located at $s = \pm i\, e^{-i\beta/6}$.

To determine the asymptotic expansion of (B8), we use the analyticity of the integrand (except at the pole $s = \tilde{k}\, \alpha^{-1/2}$ which is below the real axis when both $\tilde{k}_0$ and β are nonzero) and deform the contour of integration from the real axis into the contour Γ that passes through the saddle point $s = i\, e^{-i\beta/6}$ and that is a steepest-descent contour (see Figure B1). The deformation is possible since the integral decays exponentially in the region between the contours as $|s| \to \infty$. Thus we rewrite (B8) as

$$I_{a1}(\eta_2) = \int_{\Gamma} \frac{e^{i\alpha^{3/2}\left(s^3/3 + e^{-i\beta/3} s \right)}}{s - \tilde{k}\, \alpha^{-1/2}} ds . \tag{B11}$$

Along Γ, the exponent in (B11) near the saddle point $s = i\, e^{-i\beta/6}$ can be expanded as

$$i\, \alpha^{3/2}\left(s^3/3 + e^{-i\beta/3} s \right)$$

$$= -\frac{2}{3}\, \alpha^{3/2}\, e^{-i\beta/2} - \alpha^{3/2}\, e^{-i\beta/6} \left(s - i\, e^{-i\beta/6} \right)^2 , \tag{B12}$$

and the direction of the path Γ near the saddle point will be such that

$$\alpha^{3/2}\, e^{-i\beta/6} \left(s - i\, e^{-i\beta/6} \right)^2 = \tau^2 \tag{B13}$$

where τ^2 is real and positive. Hence

$$ds = \pm \alpha^{-3/4} e^{i\beta/12} d\tau . \tag{B14}$$

Figure B1 shows that the direction of the path of integration is $\beta/12$, so that we must take the positive sign in (B14). Hence, for the leading term, we substitute (B12) into (B11), take the limits of integration from $-\infty$ to ∞, and obtain

$$I_{a1}(\eta_2) = \int_\Gamma \frac{e^{i\alpha^{3/2}(s^3/3 + e^{-i\beta/3}s)}}{s - \tilde{k}\alpha^{-1/2}} ds$$

$$\sim \frac{e^{-\frac{2}{3}\alpha^{3/2} e^{-i\beta/2}}}{i\, e^{-i\beta/6} - \tilde{k}\alpha^{-1/2}} \alpha^{-3/4} e^{i\beta/12} \int_{-\infty}^{\infty} e^{-\tau^2} d\tau$$

$$= \frac{\pi^{1/2}\alpha^{-3/4} e^{-\frac{2}{3}\alpha^{3/2} e^{-i\beta/2} + i\beta/4}}{i - \tilde{k}\alpha^{-1/2} e^{i\beta/6}} \tag{B15}$$

Substituting (B15) into the first term of (B4) gives

$$\lim_{\alpha\to\infty} \frac{e^{-i\tilde{k}\alpha e^{-i\beta/3}}}{2\pi i} \int_{-\infty}^{\infty} \frac{e^{i t^3/3 + i\alpha e^{-i\beta/3} t}}{t - \tilde{k}} dt = 0 . \tag{B16}$$

To get (B16) we have used the fact that $\beta < \frac{\pi}{2}$.

Substituting $\eta_2 \equiv \alpha_1 e^{-i\beta_1/3}$ into the integral in the second term in (B4) gives

$$I_{a2}(\eta_2) \equiv \int_{-\infty}^{\infty} \frac{e^{i t^3/3 + i\alpha_1 e^{-i\beta_1/3} t}}{t - \tilde{k}} dt , \tag{B17}$$

which has the same form as I_{a1} with α_1 substituted for α and β_1 for β, hence

$$I_{a2}(\eta_2) \sim \frac{\pi^{1/2}\eta_2^{-3/4} e^{-\frac{2}{3}\eta_2^{3/2}}}{i - \tilde{k}\eta_2^{-1/2}} . \tag{B18}$$

Therefore,

$$I_a \equiv \int_{\eta_2}^{\infty e^{-i\beta/3}} \mathrm{Ai}(\eta_2')\, e^{-i\tilde{k}\eta_2'}\, d\eta_2'$$

$$\sim \frac{\pi^{-1/2}\eta_2^{-3/4}\, e^{-\frac{2}{3}\eta_2^{3/2} - i\tilde{k}\eta_2}}{2(1 + i\tilde{k}\eta_2^{-1/2})}, \tag{B19}$$

as $\eta_2 \to +\infty e^{-i\beta/3}$.

2. Asymptotic Expansion of I_a as $\eta_2 \to -\infty e^{-i\beta/3}$

Now we determine the asymptotic expansion for the integral in the second term on the right hand side of (B4),

$$I_{a2}(\eta_2) \equiv \int_{-\infty}^{\infty} \frac{e^{it^3/3 + i\eta_2 t}}{t - \tilde{k}}\, dt\ , \tag{B20}$$

as $\eta_2 \to -\infty e^{-i\beta/3}$.

We rewrite (B20) in the complex z-plane as

$$I_{a2}(\eta_2) = \int_{-\infty}^{\infty} \frac{e^{iz^3/3 + i\eta_2 z}}{z - \tilde{k}}\, dz\ . \tag{B21}$$

To employ the method of steepest descent we recall $\eta_2 \equiv \alpha_1 e^{-i\beta_1/3}$, introduce the transformation,

$$z = (-\alpha_1)^{1/2} s\ , \tag{B22}$$

and obtain

$$I_{a2}(\eta_2) = \int_{-\infty}^{\infty} \frac{e^{i(-\alpha_1)^{3/2}(s^3/3 - e^{-i\beta_1/3}s)}}{s - \tilde{k}(-\alpha_1)^{-1/2}}\, ds\ . \tag{B23}$$

The saddle points are given by

$$\frac{d}{ds}\left[i \left(s^3/3 - e^{-i\beta_1/3} s \right)\right] = 0 , \tag{B24}$$

or

$$s^2 - e^{-i\beta_1/3} = 0 . \tag{B25}$$

Hence, they are located at $s = \pm e^{-i\beta_1/6}$.

To determine the asymptotic expansion of (B23), we use the analyticity of the integrand (except at the pole $s = \tilde{k}(-\alpha_1)^{-1/2}$) and deform the contour of integration from the real axis into the contour consisting of Γ_1 and Γ_2 that passes through the saddle points and that is a steepest-descent contour (see Figure B2). The deformation is possible since the integral decays exponentially in the region between the contours as $|s| \to \infty$. Thus we rewrite (B23) as

$$I_{a2}(\eta_2) = \left\{ \int_{\Gamma_1} + \int_{\Gamma_2} \right\} \frac{e^{i(-\alpha_1)^{3/2}\left(s^3/3 - e^{-i\beta_1/3} s \right)}}{s - \tilde{k}(-\alpha_1)^{-1/2}} ds$$

$$+ \textit{Pole Contribution} . \tag{B26}$$

Along Γ_1, the exponent in (B26) near the saddle point $s = -e^{-i\beta_1/6}$ can be expanded as

$$i(-\alpha_1)^{3/2}\left(s^3/3 - e^{-i\beta_1/3} s \right)$$

$$= i\,\frac{2}{3}(-\alpha_1)^{3/2} e^{-i\beta_1/2} - i(-\alpha_1)^{3/2} e^{-i\beta_1/6}(s + e^{-i\beta_1/6})^2 , \tag{B27}$$

and the direction of the path Γ_1 near the saddle point will be such that

$$i(-\alpha_1)^{3/2} e^{-i\beta_1/6}(s + e^{-i\beta_1/6})^2 = \tau^2 \tag{B28}$$

where τ^2 is real and positive. Hence

$$ds = \pm(-\alpha_1)^{-3/4} e^{-i\pi/4 + i\beta_1/12} d\tau . \tag{B29}$$

Figure B2 shows that the direction of the path of integration is $-\pi/4 + \beta_1/12$, so that we must take the positive sign in (B29). Hence, for the leading term, we substitute (B27) into the first term of (B26), take the limits of integration from $-\infty$ to ∞, and obtain

$$\int_{\Gamma_1} \frac{e^{i(-\alpha_1)^{3/2}(s^3/3 - e^{-i\beta_1/3}s)}}{s - \tilde{k}(-\alpha_1)^{-1/2}} ds$$

$$\sim \frac{e^{i\frac{2}{3}(-\alpha_1)^{3/2} e^{-i\beta_1/2}}}{-e^{-i\beta_1/6} - \tilde{k}(-\alpha_1)^{-1/2}} (-\alpha_1)^{-3/4} e^{-i\pi/4 + i\beta_1/12} \int_{-\infty}^{\infty} e^{-\tau^2} d\tau$$

$$= \frac{i\pi^{1/2}(-\eta_2)^{-3/4} e^{i\Sigma_1(-\eta_2)}}{1 + \tilde{k}(-\eta_2)^{-1/2}} \tag{B30}$$

where

$$\Sigma_1(-\eta_2) \equiv \frac{2}{3}(-\eta_2)^{3/2} + \frac{\pi}{4} . \tag{B31}$$

Along Γ_2, the exponent in (B26) near the saddle point $s = e^{-i\beta_1/6}$ can be expanded as

$$i(-\alpha_1)^{3/2}(s^3/3 - e^{-i\beta_1/3}s)$$

$$= -i\frac{2}{3}(-\alpha_1)^{3/2} e^{-i\beta_1/2} + i(-\alpha_1)^{3/2} e^{-i\beta_1/6}(s - e^{-i\beta_1/6})^2 , \tag{B32}$$

and the direction of the path Γ_2 near the saddle point will be such that

$$-i(-\alpha_1)^{3/2}\, e^{-i\beta_1/6}(s - e^{-i\beta_1/6})^2 = \tau^2 \tag{B33}$$

where τ^2 is real and positive. Hence

$$ds = \pm(-\alpha_1)^{-3/4}\, e^{i\pi/4 + i\beta_1/12} d\tau\,. \tag{B34}$$

Figure B2 shows that the direction of the path of integration is $\pi/4 + \beta_1/12$, so that we must take the positive sign in (B34). Hence, for the leading term, we substitute (B32) into the second term of (B26), take the limits of integration from $-\infty$ to ∞, and obtain

$$\int_{\Gamma_2} \frac{e^{i(-\alpha_1)^{3/2}(s^3/3 - e^{-i\beta_1/3}s)}}{s - \tilde{k}(-\alpha_1)^{-1/2}} ds$$

$$\sim \frac{e^{-i\frac{2}{3}(-\alpha_1)^{3/2} e^{-i\beta_1/2}}}{e^{-i\beta_1/6} - \tilde{k}(-\alpha_1)^{-1/2}} (-\alpha_1)^{-3/4}\, e^{i\pi/4 + i\beta_1/12} \int_{-\infty}^{\infty} e^{-\tau^2} d\tau$$

$$= \frac{i\pi^{1/2}(-\eta_2)^{-3/4}\, e^{-i\Sigma_1(-\eta_2)}}{1 - \tilde{k}(-\eta_2)^{-1/2}}\,. \tag{B35}$$

The contribution to the integral I_{a2} from the pole $s = \tilde{k}(-\alpha_1)^{-1/2}$ depends on the location of the pole. We can show that when

$$\frac{\beta_1}{3} = \frac{4}{3}\beta\,, \quad \text{or} \quad \arg(\eta_2) = \pi - \frac{4}{3}\beta\,,$$

the pole coincides with the saddle point $s = e^{-i\beta_1/6}$, so our asymptotic approach fails near that vicinity; for

$$\frac{\beta_1}{3} < \frac{4}{3}\beta \qquad \text{or} \quad \arg(\eta_2) > \pi - \frac{4}{3}\beta\,,$$

the pole is within the region enclosed by the contours, while for

$$\frac{4}{3}\beta < \frac{\beta_1}{3} < \frac{\pi}{2} \quad or \quad \frac{\pi}{2} < \arg(\eta_2) < \pi - \frac{4}{3}\beta ,$$

the pole is outside the region enclosed by the contours, so the pole contribution is :

$$P.C. = \begin{cases} -i\,2\pi\, e^{i\,\tilde{k}^3/3 + i\,\tilde{k}\,\eta_2} & \text{if } \arg(\eta_2) > \pi - \frac{4}{3}\beta \\ 0 & \text{if } \frac{\pi}{2} < \arg(\eta_2) < \pi - \frac{4}{3}\beta \end{cases} \tag{B36}$$

Substituting (B30), (B35) and (B36) into (B26) gives

$$I_{a\,2}(\eta_2) \sim P.C. + i\,\pi^{1/2}(-\eta_2)^{-3/4}\left[\frac{e^{i\,\Sigma_1(-\eta_2)}}{1 + \tilde{k}\,(-\eta_2)^{-1/2}} + \frac{e^{-i\,\Sigma_1(-\eta_2)}}{1 - \tilde{k}\,(-\eta_2)^{-1/2}}\right]$$

$$= P.C. + 2\,\pi^{1/2}(-\eta_2)^{-3/4}\,\frac{\left[\tilde{k}\,(-\eta_2)^{-1/2}\sin\Sigma_1(-\eta_2) + i\,\cos\Sigma_1(-\eta_2)\right]}{1 - \tilde{k}^2(-\eta_2)^{-1}} \tag{B37}$$

where *P.C.* is given by (B36).

Substituting (B16) and (B37) into (B4) gives

$$I_a = \int_{\eta_2}^{\infty e^{-i\beta/3}} \mathrm{Ai}(\eta_2')\, e^{-i\,\tilde{k}\,\eta_2'}\, d\,\eta_2'$$

$$\sim (P.C.)_a + \pi^{-1/2}(-\eta_2)^{-3/4}\, e^{-i\,\tilde{k}\,\eta_2}\,\frac{\left[-\cos\Sigma_1(-\eta_2) + i\,\tilde{k}\,(-\eta_2)^{-1/2}\sin\Sigma_1(-\eta_2)\right]}{1 - \tilde{k}^2(-\eta_2)^{-1}} \tag{B38}$$

as $\eta_2 \to -\infty e^{-i\,\beta/3}$, where

$$(P.C.)_a = \begin{cases} e^{i\,\tilde{k}^3/3} & \text{if } \arg(\eta_2) > \pi - \frac{4}{3}\beta \\ 0 & \text{if } \frac{\pi}{2} < \arg(\eta_2) < \pi - \frac{4}{3}\beta \end{cases} \tag{B39}$$

3. Asymptotic Expansion of I_b as $\eta_2 \to +\infty e^{-i\beta/3}$

The integral representation of Airy function $\mathrm{Bi}(\eta_2)$ is

$$\mathrm{Bi}(\eta_2) = \frac{1}{\pi}\int_0^\infty [\, e^{-t^3/3+\eta_2 t} + \frac{1}{2i}(e^{i t^3/3 + i\eta_2 t} - e^{-i t^3/3 - i\eta_2 t})]\, dt \ , \tag{B40}$$

Substituting it into (B2) gives

$$I_b = \int_{\eta_{20}}^{\eta_2} e^{-i\tilde{k}\eta_2'} \mathrm{Bi}(\eta_2')\, d\eta_2'$$

$$= \frac{1}{\pi}\int_0^\infty dt\ e^{-t^3/3} \int_{\eta_{20}}^{\eta_2} e^{(t - i\tilde{k})\eta_2'} d\eta_2'$$

$$+ \frac{1}{2\pi i}\int_0^\infty dt\ e^{i t^3/3} \int_{\eta_{20}}^{\eta_2} e^{i(t - \tilde{k})\eta_2'} d\eta_2'$$

$$- \frac{1}{2\pi i}\int_0^\infty dt\ e^{-i t^3/3} \int_{\eta_{20}}^{\eta_2} e^{-i(t + \tilde{k})\eta_2'} d\eta_2'$$

$$= \frac{e^{-i\tilde{k}\eta_2}}{\pi}\int_0^\infty [\frac{e^{-t^3/3+\eta_2 t}}{t - i\tilde{k}} - \frac{e^{i t^3/3 + i\eta_2 t}}{2(t - \tilde{k})} - \frac{e^{-i t^3/3 - i\eta_2 t}}{2(t + \tilde{k})}]\, dt$$

$$- \frac{e^{-i\tilde{k}\eta_{20}}}{\pi}\int_0^\infty [\frac{e^{-t^3/3+\eta_{20} t}}{t - i\tilde{k}} - \frac{e^{i t^3/3 + i\eta_{20} t}}{2(t - \tilde{k})} - \frac{e^{-i t^3/3 - i\eta_{20} t}}{2(t + \tilde{k})}]\, dt$$

$$= C_{\tilde{k}}(\eta_2) - C_{\tilde{k}}(\eta_{20}) \tag{B41}$$

where we have defined

$$C_{\tilde{k}}(\eta_2) = \frac{1}{\pi} e^{-i\tilde{k}\eta_2} I_{b\,1}(\eta_2) , \tag{B42}$$

$$I_{b\,1}(\eta_2) = I_{b\,11}(\eta_2) - \frac{1}{2}[\, I_{b\,12}(\eta_2) + I_{b\,13}(\eta_2)\,] , \tag{B43}$$

$$I_{b\,11}(\eta_2) = \int_0^\infty \frac{e^{-t^3/3 + \eta_2 t}}{t - i\tilde{k}}\, dt , \tag{B44}$$

$$I_{b\,12}(\eta_2) = \int_0^\infty \frac{e^{i t^3/3 + i\eta_2 t}}{t - \tilde{k}}\, dt , \tag{B45}$$

and

$$I_{b\,13}(\eta_2) = \int_0^\infty \frac{e^{-i t^3/3 - i\eta_2 t}}{t + \tilde{k}}\, dt . \tag{B46}$$

In order to determine the asymptotic expansion of (B44) as $\eta_2 \to +\infty\, e^{-i\beta/3}$, we rewrite (B44) in the complex z-plane as

$$I_{b\,11}(\eta_2) = \int_0^\infty \frac{e^{-z^3/3 + \eta_2 z}}{z - i\tilde{k}}\, dz . \tag{B47}$$

To employ the method of steepest descent we recall

$$\eta_2 \equiv \alpha_1\, e^{-i\beta_1/3} , \tag{B48}$$

and introduce the transformation

$$z = \alpha_1^{1/2}\, s \tag{B49}$$

to obtain

$$I_{b\,11}(\eta_2) = \int_0^\infty \frac{e^{-\alpha_1^{3/2}(s^3/3 - e^{-i\beta_1/3} s)}}{s - i\tilde{k}\,\alpha_1^{-1/2}}\, ds . \tag{B50}$$

The saddle points are given by

$$\frac{d}{ds}\left[-\left(s^3/3 - e^{-i\beta_1/3}s\right)\right] = 0\,, \tag{B51}$$

or

$$s^2 - e^{-i\beta_1/3} = 0\,. \tag{B52}$$

Hence, they are located at $s = \pm e^{-i\beta_1/6}$.

To determine the asymptotic expansion of (B50), we use the analyticity of the integrand (except at the pole $s = i\,\tilde{k}\,\alpha_1^{-1/2}$) and deform the contour of integration into the contour containing Γ_1, that passes through the saddle point $s = e^{-i\beta_1/6}$ and that is a steepest-descent contour, and Γ_2, that consists of the lower half of the imaginary axis (see Figure B3). Thus we rewrite (B50) as

$$I_{b\,11}(\eta_2) = \int_{\Gamma_1} \frac{e^{-\alpha_1^{3/2}(s^3/3 - e^{-i\beta_1/3}s)}}{s - i\,\tilde{k}\,\alpha_1^{-1/2}}\,ds + \int_{\Gamma_2} \frac{e^{-z^3/3 + \eta_2 z}}{z - i\,\tilde{k}}\,dz \tag{B53}$$

In (B53), when writing the integral along Γ_2, we use the variable z instead of s for later convenience.

Along Γ_1, the exponent in the first term of (B53) near the saddle point $s = e^{-i\beta_1/6}$ can be expanded as

$$-\alpha_1^{3/2}(s^3/3 - e^{-i\beta_1/3}s)$$

$$= \frac{2}{3}\alpha_1^{3/2}\,e^{-i\beta_1/2} - \alpha_1^{3/2}\,e^{-i\beta_1/6}(s - e^{-i\beta_1/6})^2\,, \tag{B54}$$

and the direction of the path Γ_1 near the saddle point will be such that

$$\alpha_1^{3/2} e^{-i\beta_1/6}(s - e^{-i\beta_1/6})^2 = \tau^2 \tag{B55}$$

where τ^2 is real and positive. Hence

$$ds = \pm \alpha_1^{-3/4} e^{i\beta_1/12} d\tau . \tag{B56}$$

Figure B3 shows that the direction of the path of integration is $\beta_1/12$, so that we must take the positive sign in (B56). Hence, for the leading term, we substitute (B54) into the first term of (B53), take the limits of integration from $-\infty$ to ∞, and obtain

$$\int_{\Gamma_1} \frac{e^{-\alpha_1^{3/2}(s^3/3 - e^{-i\beta_1/3}s)}}{s - i\tilde{k}\alpha_1^{-1/2}} ds$$

$$\sim \frac{e^{\frac{2}{3}\alpha_1^{3/2} e^{-i\beta_1/2}}}{e^{-i\beta_1/6} - i\tilde{k}\alpha_1^{-1/2}} \alpha_1^{-3/4} e^{i\beta_1/12} \int_{-\infty}^{\infty} e^{-\tau^2} d\tau$$

$$= \frac{\pi^{1/2} \eta_2^{-3/4} e^{\frac{2}{3}\eta_2^{3/2}}}{1 - i\tilde{k}\eta_2^{-1/2}} \tag{B57}$$

as $\eta_2 \to +\infty e^{-i\beta/3}$.

Along Γ_2, the second integral in (B53) can be written as

$$\int_{\Gamma_2} \frac{e^{-z^3/3 + \eta_2 z}}{z - i\tilde{k}} dz = \int_0^{\infty} \frac{e^{it^3/3 + i\eta_2 t}}{t - \tilde{k}} dt . \tag{B58}$$

Substituting (B57) and (B58) into (B53) gives

$$I_{b\,11} \sim \frac{\pi^{1/2} \eta_2^{-3/4} e^{\frac{2}{3}\eta_2^{3/2}}}{1 - i\tilde{k}\eta_2^{-1/2}} + \int_0^{\infty} \frac{e^{it^3/3 + i\eta_2 t}}{t - \tilde{k}} dt . \tag{B59}$$

We notice that

$$-\frac{1}{2}[I_{b\,12}(\eta_2)+I_{b\,13}(\eta_2)]$$

$$=-\frac{1}{2}\int_0^{\infty}\left[\frac{e^{i\,t^3/3+i\,\eta_2 t}}{t-\tilde{k}}+\frac{e^{-i\,t^3/3-i\,\eta_2 t}}{t+\tilde{k}}\right]$$

$$=-\frac{1}{2}\left\{\int_0^{\infty}+\int_0^{-\infty}\right\}\frac{e^{i\,t^3/3+i\,\eta_2 t}}{t-\tilde{k}}\,dt\ . \tag{B60}$$

Substituting (B59) and (B60) into (B43) gives the asymptotic expansion of $I_{b\,1}(\eta_2)$:

$$I_{b\,1}(\eta_2)\sim\frac{\pi^{1/2}\,\eta_2^{-3/4}\,e^{\frac{2}{3}\eta_2^{3/2}}}{1-i\,\tilde{k}\,\eta_2^{-1/2}}-\frac{1}{2}\int_{-\infty}^{\infty}\frac{e^{i\,t^3/3+i\,\eta_2 t}}{t-\tilde{k}}dt\ . \tag{B61}$$

The integral in the second term of (B61) equals $I_{a\,2}(\eta_2)$, for which the asymptotic expansion as $\eta_2\to+\infty e^{-i\,\beta/3}$ is (B18). Substituting (B18) into (B61) gives:

$$I_{b\,1}(\eta_2)\sim\frac{\pi^{1/2}\,\eta_2^{-3/4}\,e^{\frac{2}{3}\eta_2^{3/2}}}{1-i\,\tilde{k}\,\eta_2^{-1/2}}-\frac{1}{2}\frac{\pi^{1/2}\eta_2^{-3/4}\,e^{-\frac{2}{3}\eta_2^{3/2}}}{i-\tilde{k}\,\eta_2^{-1/2}}\ .$$

$$\sim\frac{\pi^{1/2}\,\eta_2^{-3/4}\,e^{\frac{2}{3}\eta_2^{3/2}}}{1-i\,\tilde{k}\,\eta_2^{-1/2}} \tag{B62}$$

Substituting (B62) into (B42) gives

$$C_{\tilde{k}}(\eta_2)\ \sim\ \frac{\pi^{-1/2}\,\eta_2^{-3/4}\,e^{\frac{2}{3}\eta_2^{3/2}-i\,\tilde{k}\,\eta_2}}{1-i\,\tilde{k}\,\eta_2^{-1/2}}\ . \tag{B63}$$

Substituting (B63) into (B41) gives

$$I_b\ =\int_{\eta_{20}}^{\eta_2}e^{-i\,\tilde{k}\,\eta_2'}\,\mathrm{Bi}\,(\eta_2')\,d\,\eta_2'=C_{\tilde{k}}(\eta_2)-C_{\tilde{k}}(\eta_{20})$$

$$\sim \frac{\pi^{-1/2}\,\eta_2^{-3/4}\,e^{\frac{2}{3}\eta_2^{3/2} - i\,\tilde{k}\,\eta_2}}{1 - i\,\tilde{k}\,\eta_2^{-1/2}} - C_{\tilde{k}}(\eta_{20}), \tag{B64}$$

as $\eta_2 \to +\infty e^{-i\beta/3}$, where $C_{\tilde{k}}(\eta_{20})$ is given by (B63) with η_{20} substituted for η_2.

4. Asymptotic Expansion of I_b as $\eta_2 \to -\infty e^{-i\beta/3}$

In order to determine the asymptotic expansion of (B44) as $\eta_2 \to -\infty e^{-i\beta/3}$, we rewrite (B44) in the complex z-plane as

$$I_{b\,11}(\eta_2) = \int_0^\infty \frac{e^{-z^3/3 + \eta_2 z}}{z - i\,\tilde{k}}\,dz\ . \tag{B65}$$

To employ the method of steepest descent we recall $\eta_2 = \alpha_1 e^{-i\beta_1/3}$, and introduce the transformation $z = (-\alpha_1)^{1/2} s$ to obtain

$$I_{b\,11}(\eta_2) = \int_0^\infty \frac{e^{-(-\alpha_1)^{3/2}(s^3/3 + e^{-i\beta_1/3}s)}}{s - i\,\tilde{k}\,(-\alpha_1)^{-1/2}}\,ds\ . \tag{B66}$$

The saddle points are given by

$$\frac{d}{ds}\left[-(s^3/3 + e^{-i\beta_1/3}s)\right] = 0\,, \tag{B67}$$

or

$$s^2 + e^{-i\beta_1/3} = 0\,. \tag{B68}$$

Hence, they are located at $s = \pm i\,e^{-i\beta_1/6}$.

To determine the asymptotic expansion of (B66), we use the analyticity (except at the pole $s = i\,\tilde{k}\,(-\alpha_1)^{-1/2}$) of the integrand and deform the contour of integration

into the contour containing Γ_1, that passes through the saddle point $s = i\, e^{-i\beta_1/6}$ and that is a steepest-descent contour, and Γ_2, that consists of the upper half of the imaginary axis (see Figure B4). Thus we rewrite (B66) as

$$I_{b\,11}(\eta_2) = \int_{\Gamma_1} \frac{e^{-(-\alpha_1)^{3/2}(s^3/3 + e^{-i\beta_1/3}s)}}{s - i\,\tilde{k}(-\alpha_1)^{-1/2}} ds + \int_{\Gamma_2} \frac{e^{-z^3/3 + \eta_2 z}}{z - i\,\tilde{k}} dz$$

$$+ \textit{Pole Contribution} \,. \tag{B69}$$

When writing the integral along Γ_2 in (B69), , we use the variable z instead of s for later convenience.

Along Γ_1, the exponent in the first term of (B69) near the saddle point $s = i\, e^{-i\beta_1/6}$ can be expanded as

$$-(-\alpha_1)^{3/2}(s^3/3 + e^{-i\beta_1/3}s)$$

$$= -i\,\frac{2}{3}(-\alpha_1)^{3/2} e^{-i\beta_1/2} - i(-\alpha_1)^{3/2} e^{-i\beta_1/6}(s - i\, e^{-i\beta_1/6})^2 \,, \tag{B70}$$

and the direction of the path Γ_1 near the saddle point will be such that

$$i(-\alpha_1)^{3/2} e^{-i\beta_1/6}(s - i\, e^{-i\beta_1/6})^2 = \tau^2 \tag{B71}$$

where τ^2 is real and positive. Hence

$$ds = \pm(-\alpha_1)^{-3/4} e^{-i\pi/4 + i\beta_1/12} d\tau \,. \tag{B72}$$

Figure B4 shows that the direction of the path of integration is $-\pi/4 + \beta_1/12$, so that we must take the positive sign in (B72). Hence, for the leading term, we substitute (B70) into the first term of (B69), take the limits of integration from $-\infty$ to ∞, and obtain

$$\int_{\Gamma_1} \frac{e^{-(-\alpha_1)^{3/2}(s^3/3 + e^{-i\beta_1/3}s)}}{s - i\,\tilde{k}\,(-\alpha_1)^{-1/2}}\,ds$$

$$\sim \frac{e^{-i\frac{2}{3}(-\alpha_1)^{3/2}e^{-i\beta_1/2}}}{i\,e^{-i\beta_1/6} - i\,\tilde{k}\,(-\alpha_1)^{-1/2}}\,(-\alpha_1)^{-3/4}\,e^{-i\pi/4 + i\beta_1/12}\int_{-\infty}^{\infty} e^{-\tau^2}\,d\tau$$

$$= -\frac{i\,\pi^{1/2}(-\eta_2)^{-3/4}\,e^{-i\Sigma_1(-\eta_2)}}{1 - \tilde{k}\,(-\eta_2)^{-1/2}} \tag{B73}$$

where as before

$$\Sigma_1(-\eta_2) \equiv \frac{2}{3}(-\eta_2)^{3/2} + \frac{\pi}{4}\,. \tag{B74}$$

Along Γ_2, the second integral in (B69) can be written as

$$\int_{\Gamma_2} \frac{e^{-z^3/3 + \eta_2 z}}{z - i\,\tilde{k}}\,dz = \int_0^{\infty} \frac{e^{i\,t^3/3 + i\,\eta_2 t}}{t - \tilde{k}}\,dt\,. \tag{B75}$$

Again, it can be shown that when

$$\frac{\beta_1}{3} = \frac{4}{3}\beta\,, \quad or \quad \arg(\eta_2) = \pi - \frac{4}{3}\beta\,,$$

the pole $s = i\,\tilde{k}\,(-\alpha_1)^{-1/2}$ coincides with the saddle point $s = i\,e^{-i\beta_1/6}$, so our asymptotic approach fails in that vicinity; for

$$\frac{\beta_1}{3} < \frac{4}{3}\beta \quad or \quad \arg(\eta_2) > \pi - \frac{4}{3}\beta\,,$$

the pole is within the region enclosed by the contours, while for

$$\frac{4}{3}\beta < \frac{\beta_1}{3} < \frac{\pi}{2} \quad or \quad \frac{\pi}{2} < \arg(\eta_2) < \pi - \frac{4}{3}\beta\,,$$

the pole is outside the region enclosed by the contours, so the pole contribution to the integral $I_{b\,11}$ is

$$P.C. = \begin{cases} 2\pi i\ e^{i\,\tilde{k}^3/3 + i\,\tilde{k}\,\eta_2} & \text{if } \arg(\eta_2) > \pi - \frac{4}{3}\beta \\ 0 & \text{if } \frac{\pi}{2} < \arg(\eta_2) < \pi - \frac{4}{3}\beta \end{cases} \tag{B76}$$

Substituting (B73), (B75) and (B76) into (B69) gives

$$I_{b\,11}(\eta_2) \sim -\frac{i\,\pi^{1/2}(-\eta_2)^{-3/4}\,e^{-i\,\Sigma_1(-\eta_2)}}{1 - \tilde{k}\,(-\eta_2)^{-1/2}} + \int_0^\infty \frac{e^{i\,t^3/3 + i\,\eta_2 t}}{t - \tilde{k}}dt + P.C. \tag{B77}$$

where *P.C.* is given by (B76).

Substituting (B60) and (B77) into (B43) gives the asymptotic expansion of $I_{b\,1}(\eta_2)$:

$$I_{b\,1}(\eta_2) \sim -\frac{i\,\pi^{1/2}(-\eta_2)^{-3/4}\,e^{-i\,\Sigma_1(-\eta_2)}}{1 - \tilde{k}\,(-\eta_2)^{-1/2}} + \frac{1}{2}\int_{-\infty}^\infty \frac{e^{i\,t^3/3 + i\,\eta_2 t}}{t - \tilde{k}}dt + P.C. \tag{B78}$$

as $\eta_2 \to -\infty e^{-i\,\beta/3}$. In (B78) *P.C.* is given by (B76).

The integral in the second term of (B78) equals $I_{a\,2}(\eta_2)$, for which the asymptotic expansion as $\eta_2 \to -\infty e^{-i\,\beta/3}$ is (B37). Substituting (B37) into (B78) gives:

$$I_{b\,1}(\eta_2) \sim \frac{1}{2}P.C. + \frac{i}{2}\pi^{1/2}(-\eta_2)^{-3/4}\left[\frac{e^{i\,\Sigma_1(-\eta_2)}}{1 + \tilde{k}\,(-\eta_2)^{-1/2}} - \frac{e^{-i\,\Sigma_1(-\eta_2)}}{1 - \tilde{k}\,(-\eta_2)^{-1/2}}\right]$$

$$= \frac{1}{2}P.C. - \pi^{1/2}(-\eta_2)^{-3/4}\,\frac{[\sin\Sigma_1(-\eta_2) + i\,\tilde{k}\,(-\eta_2)^{-1/2}\cos\Sigma_1(-\eta_2)]}{1 - \tilde{k}^2(-\eta_2)^{-1}} \tag{B79}$$

where *P.C.* is given by (B76).

Substituting (B79) into (B41) gives

$$I_b = \int_{\eta_{20}}^{\eta_2} e^{-i\,\tilde{k}\,\eta_2'}\,\mathrm{Bi}\,(\eta_2')\,d\,\eta_2' = C_{\tilde{k}}\,(\eta_2) - C_{\tilde{k}}\,(\eta_{20})$$

$$\sim (P.C.)_b - C_{\tilde{k}}(\eta_{20})$$

$$- \pi^{-1/2}(-\eta_2)^{-3/4} e^{-i\tilde{k}\eta_2} \frac{[\sin\Sigma_1(-\eta_2) + i\tilde{k}(-\eta_2)^{-1/2}\cos\Sigma_1(-\eta_2)]}{1 - \tilde{k}^2(-\eta_2)^{-1}} \quad \text{(B80)}$$

as $\eta_2 \to -\infty e^{-i\beta/3}$, where

$$(P.C.)_b = \begin{cases} i\, e^{i\tilde{k}^3/3} & \text{if } \arg(\eta_2) > \pi - \frac{4}{3}\beta \\ 0 & \text{if } \frac{\pi}{2} < \arg(\eta_2) < \pi - \frac{4}{3}\beta \end{cases} \quad \text{(B81)}$$

FIGURE CAPTIONS

Figure 4.1

The quantity $Q^{-2} - 1 + \nu^2$ in the dispersion relation versus r. Between the two Q-barriers, the quantity is less than zero, there is no wave. Inside the inner Lindblad resonance (I.L.R. in the figure) or outside the outer Lindblad resonance (O.L.R. in the figure), only short wave exists. Between a Q-barrier and its neighboring Lindblad resonance, both long and short waves can exist.

Figure 4.2

The dimensionless wavenumber $|k|a/\kappa$ from the dispersion relation for gas, versus $|\nu|$. For $|\nu| > 1$, there is only short wave. For $|\nu| < 1$, both long and short waves exist. The short wave branch of the curve extends indefinitely beyond the Lindblad resonance.

Figure 4.3

The dimensionless wavenumber $|k|a/\kappa$ from the dispersion relation for stars, versus $|\nu|$. Both long wave branch and short wave branch of the dispersion relation curve for a certain Q are bounded by the vertical lines of $Q = \infty$ passing through the Lindblad resonances. even short waves can not propagate beyond their corresponding Lindblad resonances. The spiral waves are completely confined to a region bounded by the Lindblad resonances.

Figure 5.1

Relations among η_0, η_1 and η_2. The real η_1-axis can be obtained by rotating the real η_0-axis counterclockwise by $\beta/3$ and stretching it by a factor of $\cos^{1/3}\beta$. The real η_2-axis is obtained by translation using equation (5.14) so it is parallel to the real η_1-axis. T is the intersection of the real η_0-axis and the upper imaginary η_2-axis. It is the turning point (the Q-barrier) when $\beta = 0$. η_{00} and η_{20} are the coordinates of T in the η_0-plane and in the η_2-plane respectively. η_3 is the distance between an arbitrary point P on the real η_0-axis and T.

Figure 5.2

The real part of the complex Lagrangian displacement $Z(\xi_0)$ obtained from equation (5.6) when $\tilde{k}_0 = 0$, $b_0 = 0$. The dotted line represents the asymptotic solution while the solid, the numerical solution.

Figure 5.3

The imaginary part of the complex Lagrangian displacement $Z(\xi_0)$ obtained from equation (5.6) when $\tilde{k}_0 = 0$, $b_0 = 0$. The dotted line represents the asymptotic solution while the solid, the numerical solution.

Figure 5.4

The real part of the complex Lagrangian displacement $Z(\xi_0)$ obtained from equation (5.6) when $\tilde{k}_0 = 0$, $b_0 = 0.127$. The dotted line represents the asymptotic solution while the solid, the numerical solution.

Figure 5.5

The imaginary part of the complex Lagrangian displacement $Z(\xi_0)$ obtained from equation (5.6) when $\tilde{k}_0 = 0$, $b_0 = 0.127$. The dotted line represents the asymptotic

solution while the solid, the numerical solution.

Figure 5.6

The real part of the complex Lagrangian displacement $Z(\xi_0)$ obtained from equation (5.6) when $\tilde{k}_0 = 0.15$, $b_0 = 0$. The dotted line represents the asymptotic solution while the solid, the numerical solution.

Figure 5.7

The imaginary part of the complex Lagrangian displacement $Z(\xi_0)$ obtained from equation (5.6) when $\tilde{k}_0 = 0.15$,, $b_0 = 0$. The dotted line represents the asymptotic solution while the solid, the numerical solution.

Figure 5.8 and Figure 5.9

The real part (in Figure 5.8) or the imaginary part (in Figure 5.9) of the complex Lagrangian displacement $Z(\xi_0)$ obtained from equation (5.6) when $\tilde{k}_0 = 3$, $b_0 = 0$. The abscissa has two scales. The lower one is ξ_0 and the upper one is $\xi_3 = \xi_0 + \tilde{k}_0^2$. The dotted line represents the asymptotic solution while the solid, the numerical solution. Since $\tilde{k}_0^2$ is large, the asymptotic solution as $\xi_3 \to +\infty$ has two expressions for different regions according to equation (5.65b) (one is for $\xi_3 > 9$, or $\xi_0 > 0$; the other is for $0 < \xi_3 < 9$, or $-9 < \xi_0 < 0$, in the figure). It can be seen clearly from these figures that the asymptotic solutions approach the exact numerical solutions very well except in the vicinity of $\xi_3 = \tilde{k}_0^2$, where the poles of the integrands of I_a and I_b coincide with the saddle points involved in the steepest-descent method (see Appendix B). In this example, the turning point, or the Q-barrier, is located at $\xi_0 = -9$ or $\xi_3 = 0$. ξ_3 is the distance from the turning point. For the region $\xi_0 > 0$, only short wave exists while in the

region $-9 < \xi_0 < 0$, the short wave and the long wave co-exist and superpose.

Figure 5.10

The real part of the complex Lagrangian displacement $Z(\xi_0)$ obtained from equation (5.6) when $\tilde{k}_0 = 0.15$, $b_0 = 0.127$. The dotted line represents the asymptotic solution while the solid, the numerical solution.

Figure 5.11

The imaginary part of the complex Lagrangian displacement $Z(\xi_0)$ obtained from equation (5.6) when $\tilde{k}_0 = 0.15$, $b_0 = 0.127$. The dotted line represents the asymptotic solution while the solid, the numerical solution.

Figure 6.1

The real part (by the dotted line) and the imaginary part (by the solid line) of the Lagrangian displacement $Z(\xi_0)$ solved from the inviscid non-linear equations (6.5) with $\tilde{k}_0 = 0$, $f' = 3$. When ξ_0 is large positive the real and imaginary parts of Z have a phase difference of $\pi/2$. There is a fluctuation in the wave amplitude as we can see from the figure, which may be due to the non-linearity of the equation.

Figure 6.2

The real part (by the dotted line) and the imaginary part (by the solid line) of the Lagrangian displacement $Z(\xi_0)$ solved from the non-linear equations (6.5) with $\tilde{k}_0 = 0.15$, $f' = 3$. When ξ_0 is large positive the real and imaginary parts of Z have a phase difference of $\pi/2$. There is a fluctuation in the wave amplitude as we can see from the figure, which may be due to the non-linearity of the equation.

Figure 6.3

The real part of $Z(\xi_0)$ obtained by integrating the non-linear equation (6.4) with $\tilde{k}_0 = 0.15$, $b_0 = 0.127$ and $f' = 0.3$. The solid line represents the integration from $\xi_0 = -6$ and along the positive direction while the dotted line represents the integration from $\xi_0 = 12$ and along the negative direction. They match well in the overlapped region (near $\xi_0 = 2.5$). The true solution is represented by the solid line for $-6 < \xi_0 < 2.5$ and by the dotted line for $2.5 < \xi_0 < 12$. The parasitic contributions are obvious in the figure.

Figure 6.4

The imaginary part of $Z(\xi_0)$ obtained by integrating the non-linear equation (6.4) with $\tilde{k}_0 = 0.15$, $b_0 = 0.127$ and $f' = 0.3$. The solid line represents the integration from $\xi_0 = -6$ and along the positive direction while the dotted line represents the integration from $\xi_0 = 12$ and along the negative direction. They match well in the overlapped region (near $\xi_0 = 2.5$). The true solution is represented by the solid line for $-6 < \xi_0 < 2.5$ and by dotted line for $2.5 < \xi_0 < 12$. The parasitic contributions are obvious in the figure.

Figure 6.5 and Figure 6.6

The real part (in Figure 6.5) or the imaginary part (in Figure 6.6) obtained by integrating the non-linear equation (6.4) with $\tilde{k}_0 = 0.15$, $b_0 = 0.127$ and $f' = 0.6$, using initial values provided by the linear solution. The solid line represents the integration from $\xi_0 = -6$ and along the positive direction while the dotted line represents the integration from $\xi_0 = 12$ and along the negative direction. There is a noticeable phase difference between them in the overlapped region due to non-linearity. The parasitic contributions are obvious in the figure.

Figure 6.7 and Figure 6.8

The real part (in Figure 6.7) or the imaginary part (in Figure 6.8) obtained by integrating the non-linear equation (6.4) with $\tilde{k}_0 = 0.15$, $b_0 = 0.127$ and $f' = 3$, using initial values provided by the linear solution. The solid line represents the integration from $\xi_0 = -6$ and along the positive direction while the dotted line represents the integration from $\xi_0 = 14$ and along the negative direction. The phase difference between the two curves has been reduced by adjusting the initial complex phase provided by the linear solution at $\xi_0 = 14$, by trial and error. The combination of the solid and dotted lines can approximate the true solution.

Figure 6.9

The surface density contrast versus the Eulerian dimensional distance r from the center obtained by solving equations (6.4) with $\tilde{k}_0 = 0$, $b_0 = 0$ and $f' = 3$. The plot is made for the radial cut, $\phi_0 = 67^0$, along which the radial velocity has the highest value.

Figure 6.10

The surface density contrast versus the Eulerian dimensional distance r from the center obtained by solving equations (6.4) with $\tilde{k}_0 = 0.15$, $b_0 = 0$ and $f' = 3$. The plot is made for the radial cut, $\phi_0 = 67^0$, along which the radial velocity has the highest value.

Figure 6.11

The radial velocity in *km / sec* versus the Eulerian dimensional distance r from the center obtained by solving equations (6.4) with $\tilde{k}_0 = 0$, $b_0 = 0$ and $f' = 3$. The plot is made for the radial cut, $\phi_0 = 67^0$, along which the radial velocity has

the highest value.

Figure 6.12

The radial velocity in *km / sec* versus the Eulerian dimensional distance r from the center obtained by solving equations (6.4) with $\tilde{k}_0 = 0.15$, $b_0 = 0$ and $f' = 3$. The plot is made for the radial cut, $\phi_0 = 67^0$, along which the radial velocity has the highest value.

Figure 6.13

The surface density contrast versus the Eulerian dimensional distance r from the center obtained by solving equations (6.4) with $\tilde{k}_0 = 0.15$, $b_0 = 0.127$ and $f' = 3$. The plot is made for the radial cut, $\phi_0 = 67^0$, along which the radial velocity has the highest value.

Figure 6.14

The radial velocity in *km / sec* versus the Eulerian dimensional distance r from the center obtained by solving equations (6.4) with $\tilde{k}_0 = 0.15$, $b_0 = 0.127$ and $f' = 3$. A velocity of 53 km/sec is produced at the first peak. Beyond that, the velocity decays rapidly. The first peak of the velocity and the first peak of the density (see Figure 6.13) are at the same distance from the center. The plot is made for the radial cut, $\phi_0 = 67^0$, along which the radial velocity has the highest value.

Figure 6.15

The density contour map of the non-linear solution. The inner contour stands for $\rho / \rho_0 = 4$, and the outer contour for $\rho / \rho_0 = 2$. The arrows are radial velocities drawn to scale. The largest one is 53 km/sec. The oval distortion is drawn

schematically. The orientation is chosen such that the maximum radial velocity is toward us. The oval field is equal to 5% of the mean gravitational field at the outer Lindblad resonance which is located at $r = 3\,kpc$.

Figure B1

The contour consisting of Γ (solid line) in the complex s-plane that is needed to evaluate the integral I_{a1} as $\eta_2 \to +\infty e^{-i\beta/3}$. s_1 is the saddle point $i\,e^{-i\beta/6}$. Γ is the path of steepest-descent while the dotted line is the path of steepest-ascent. The pole $s_0 = \tilde{k}\,(-\alpha)^{-1/2}$ is below the real axis. In this figure we use $\beta = 84^0$.

Figure B2

The contour consisting of Γ_1 and Γ_2 in the complex s-plane that is needed to evaluate the integral I_{a2} as $\eta_2 \to -\infty e^{-i\beta/3}$. s_1 and s_2 are the saddle points $\pm e^{-i\beta_1/6}$. The solid lines are the paths of steepest-descent while the dotted lines are the paths of steepest-ascent. The pole $s_0 = \tilde{k}\,(-\alpha_1)^{-1/2}$ coincides with s_2 when $\xi_0 = 0$ (or $\beta_1 = 4\beta$ if $\beta \neq 0$). In this figure we use $\beta_1 = 84^0$.

Figure B3

The contour consisting of Γ_1, that passes through the saddle point $s_1 = e^{-i\beta_1/6}$ and that is a steepest-descent contour, and Γ_2, that consists of the lower half of the imaginary axis. This figure is for the asymptotic evaluation of $I_{b11}(\eta_2)$ as $\eta_2 \to +\infty e^{-i\beta/3}$. The solid line Γ_1 is the path of steepest-descent while the dotted line is the path of steepest-ascent. The pole $s_0 = i\,\tilde{k}\,\alpha_1^{-1/2}$ is above the real axis. In this figure we use $\beta_1 = 84^0$.

Figure B4

The contour consisting of Γ_1, that passes through the saddle point $s_1 = i\ e^{-i\beta_1/6}$ and that is a steepest-descent contour, and Γ_2, that consists of the upper half of the imaginary axis. This figure is for the asymptotic evaluation of $I_{b\,11}(\eta_2)$ as $\eta_2 \to -\infty e^{-i\beta/3}$. The dotted line is the path of steepest-ascent. The pole $s_0 = i\ \tilde{k}\,(-\alpha_1)^{-1/2}$ coincides with s_1 when $\xi_0 = 0$ (or $\beta_1 = 4\beta$ if $\beta \neq 0$.) In this figure we use $\beta_1 = 84^0$.

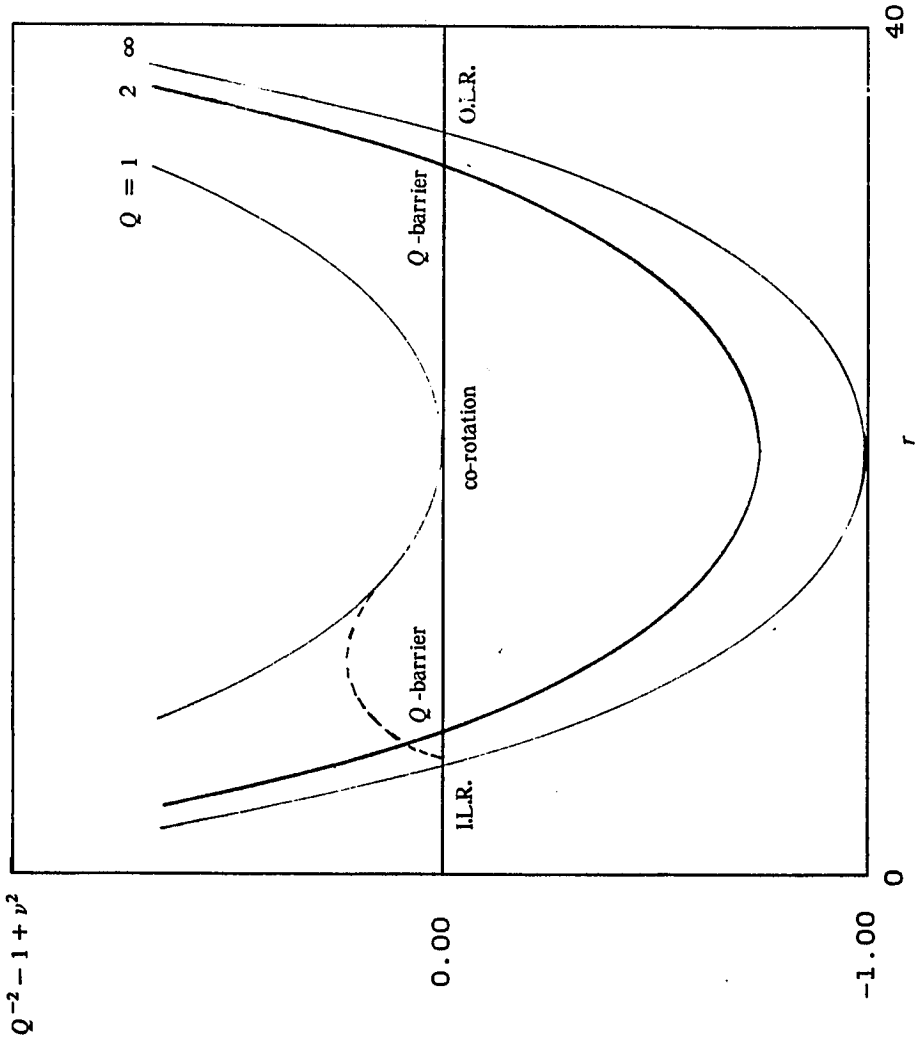

Figure 4.1

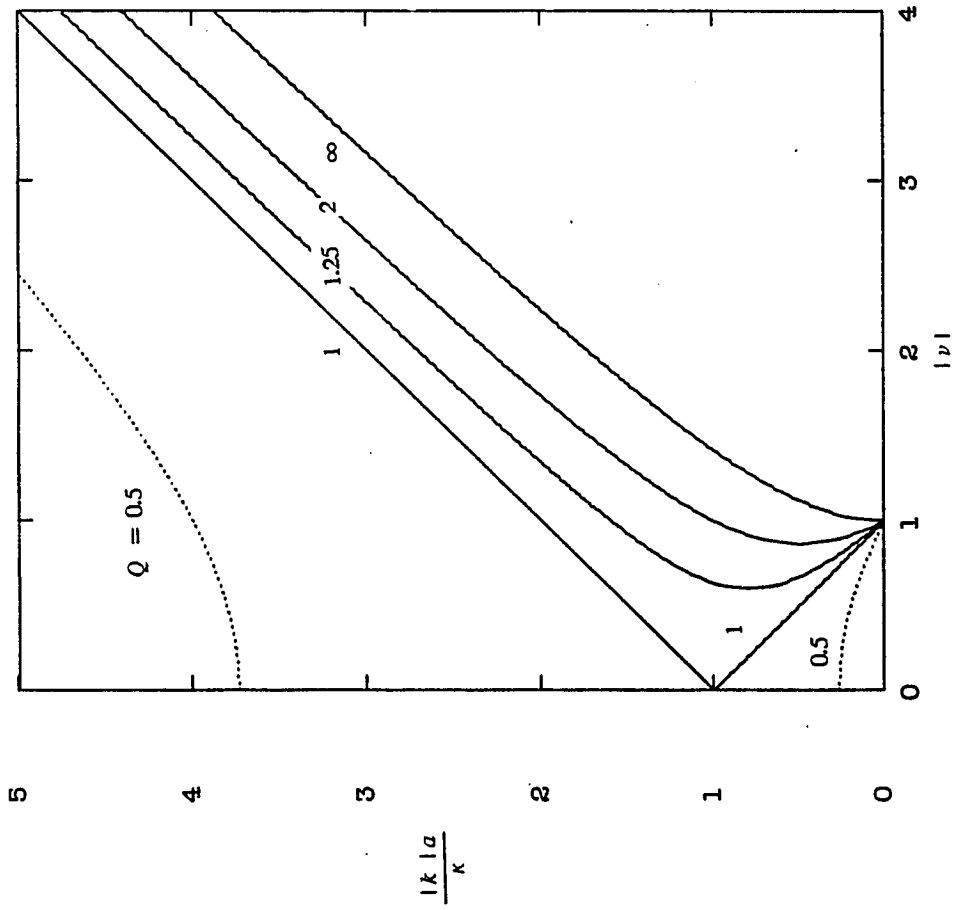

Figure 4.2

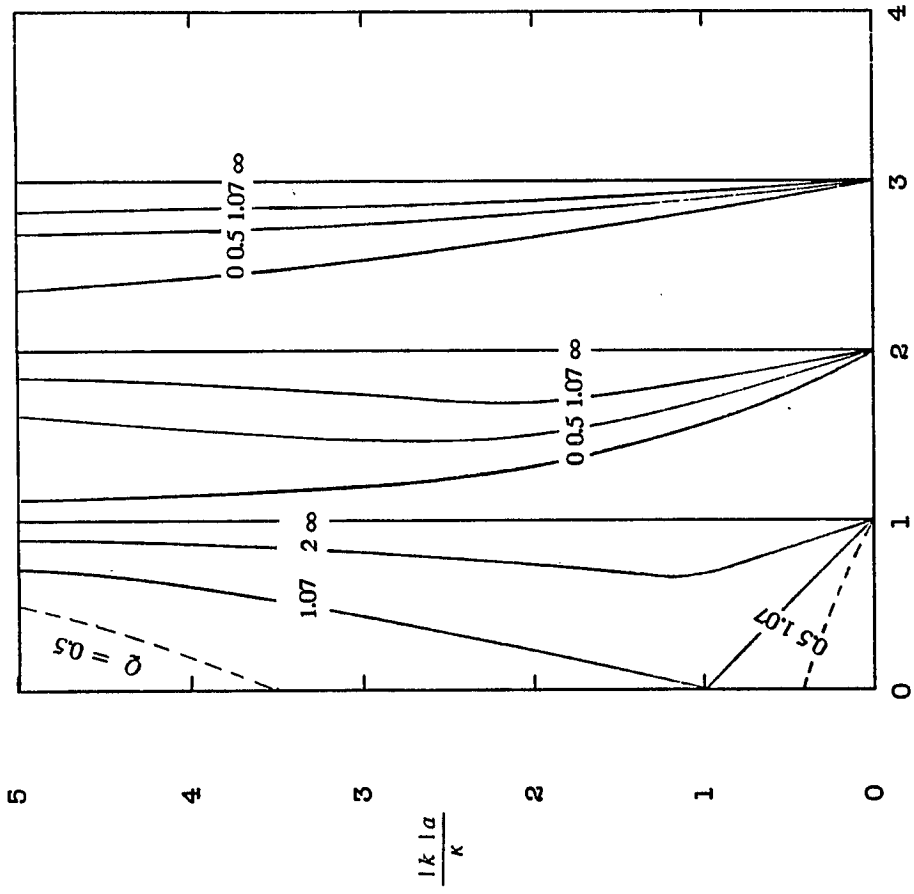

Figure 4.3

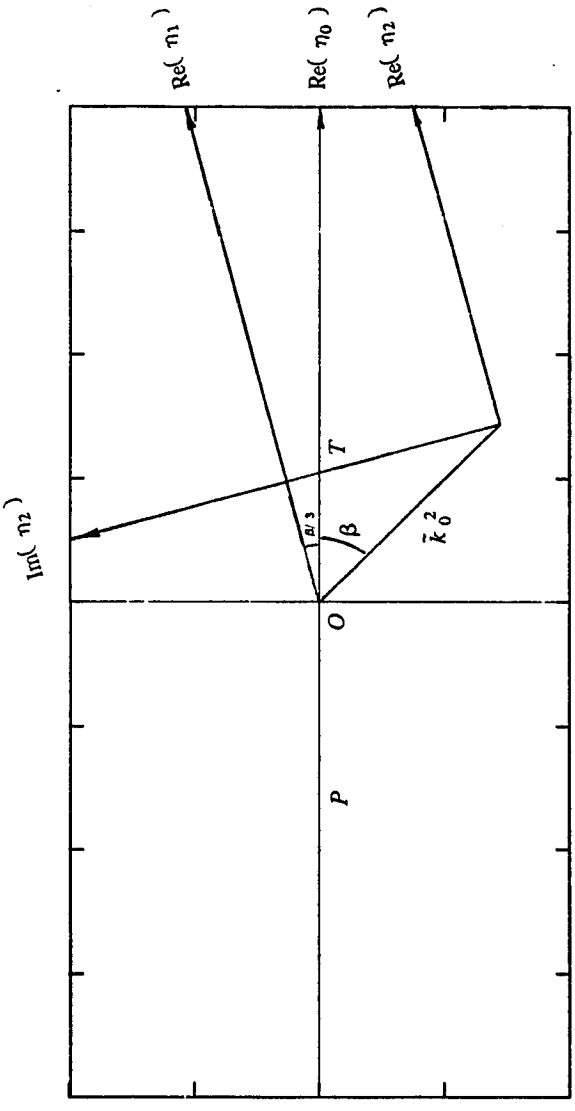

Figure 5.1

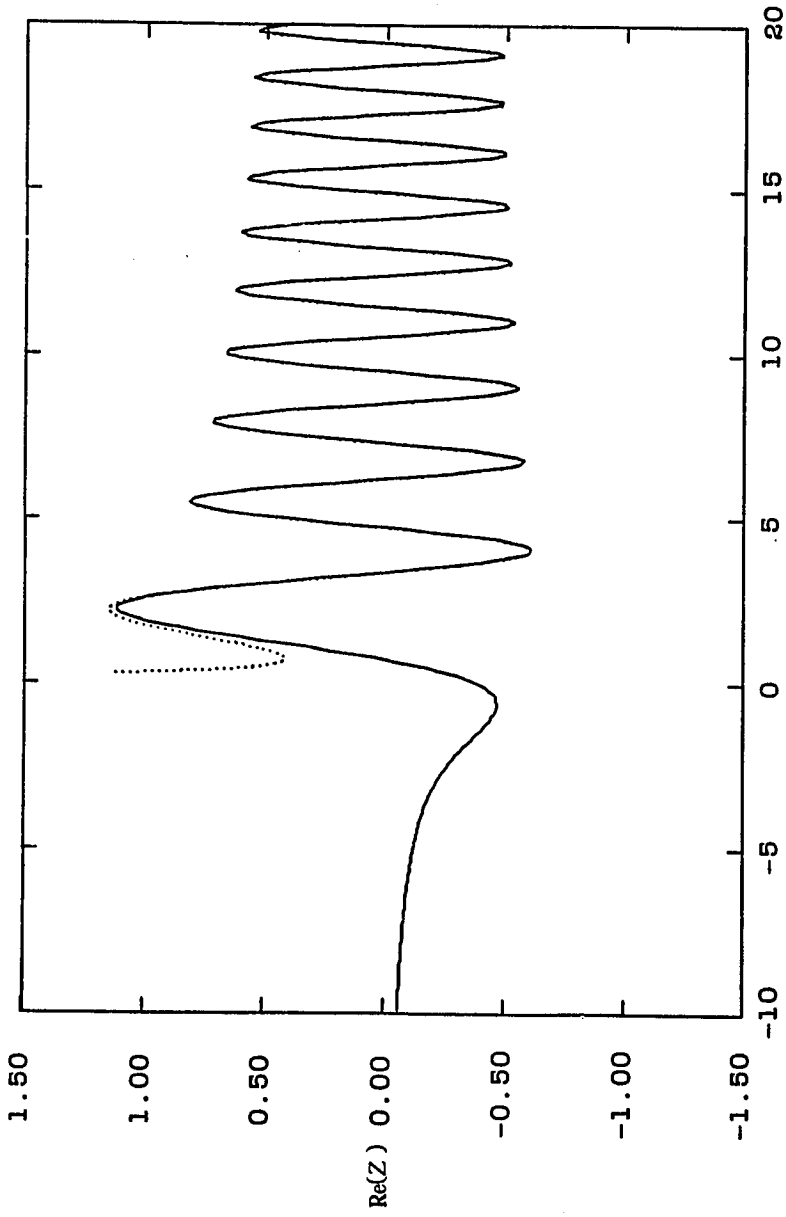

Figure 5.2

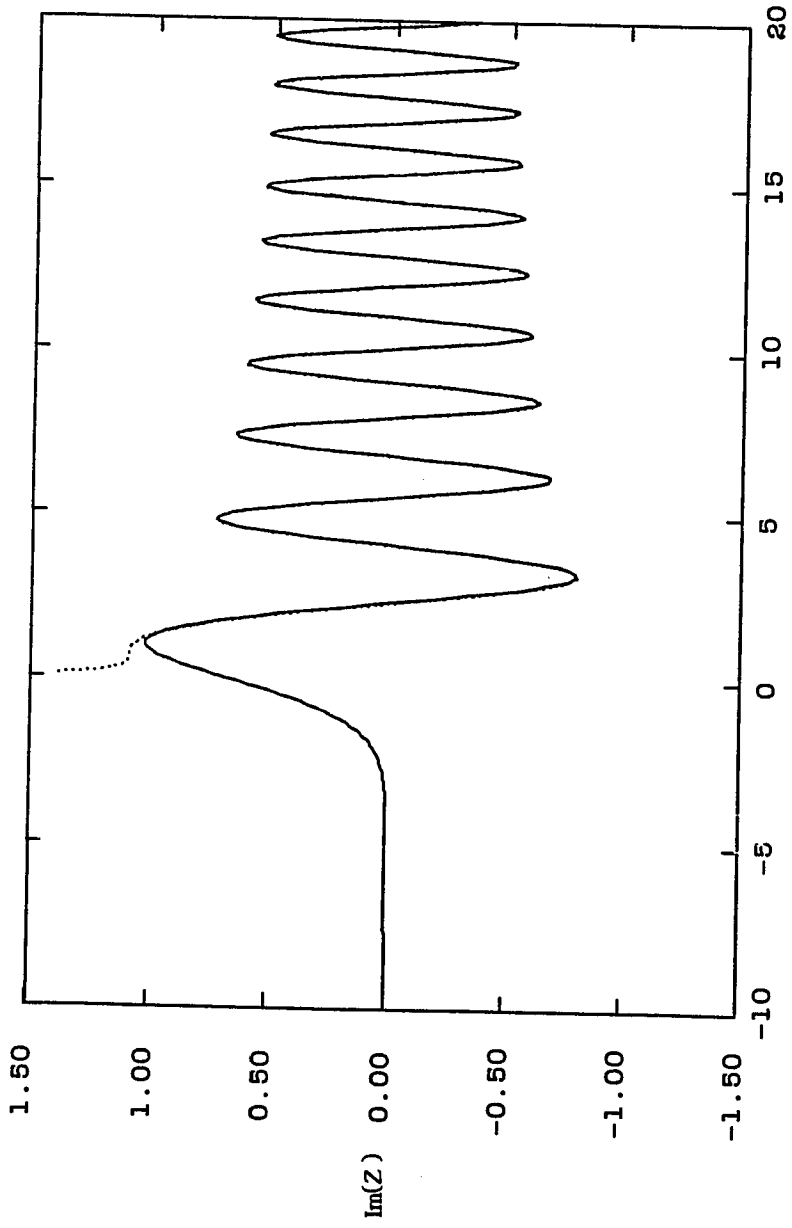

Figure 5.3

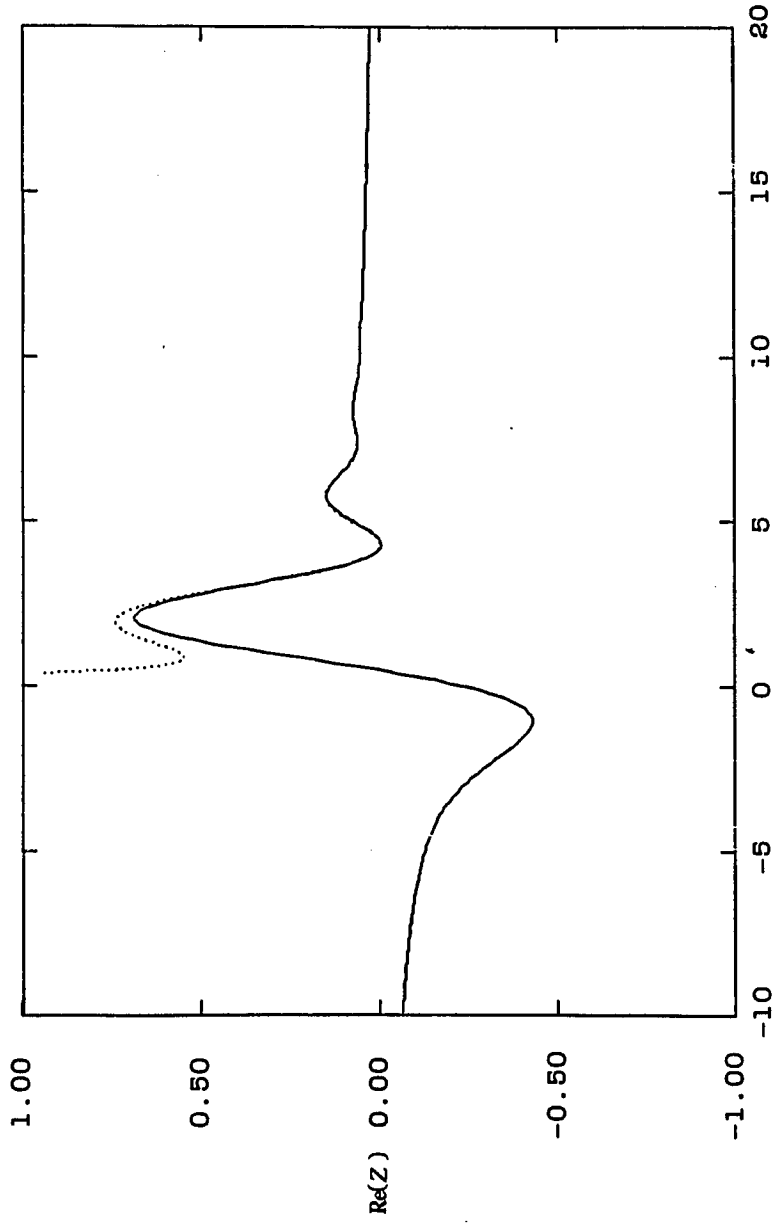

Figure 5.4

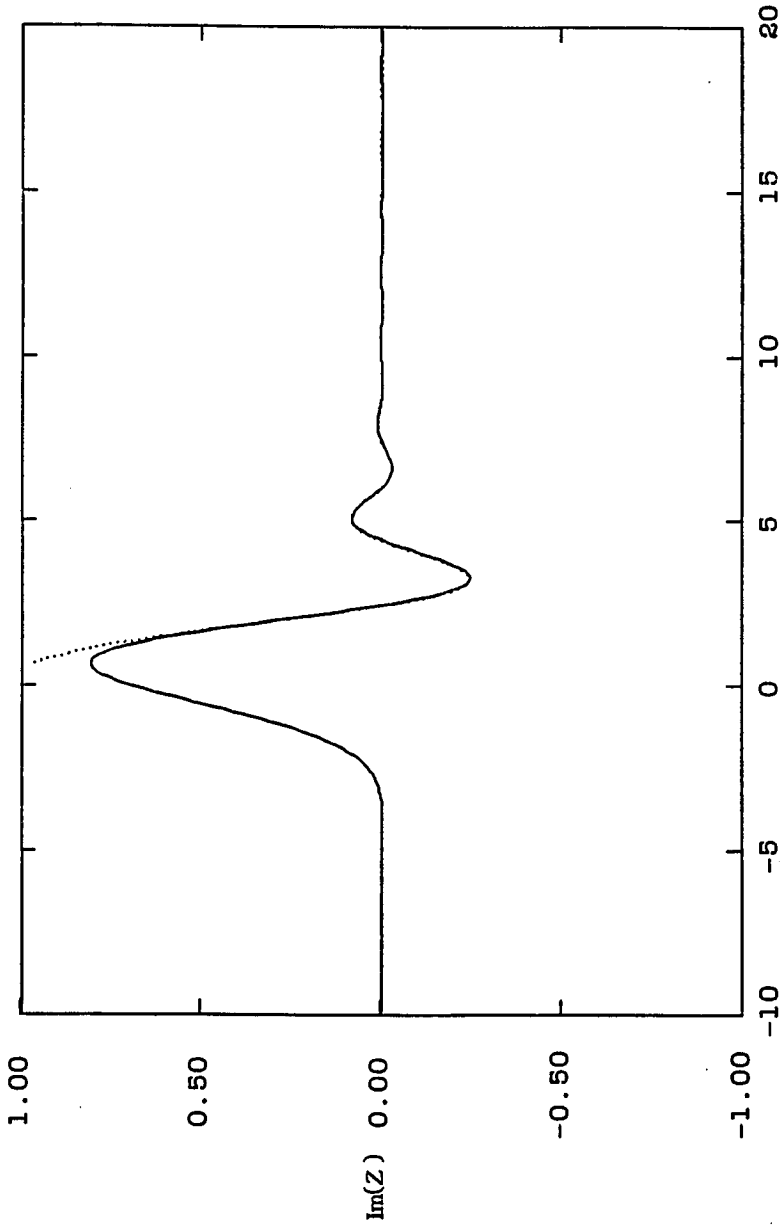

Figure 5.5

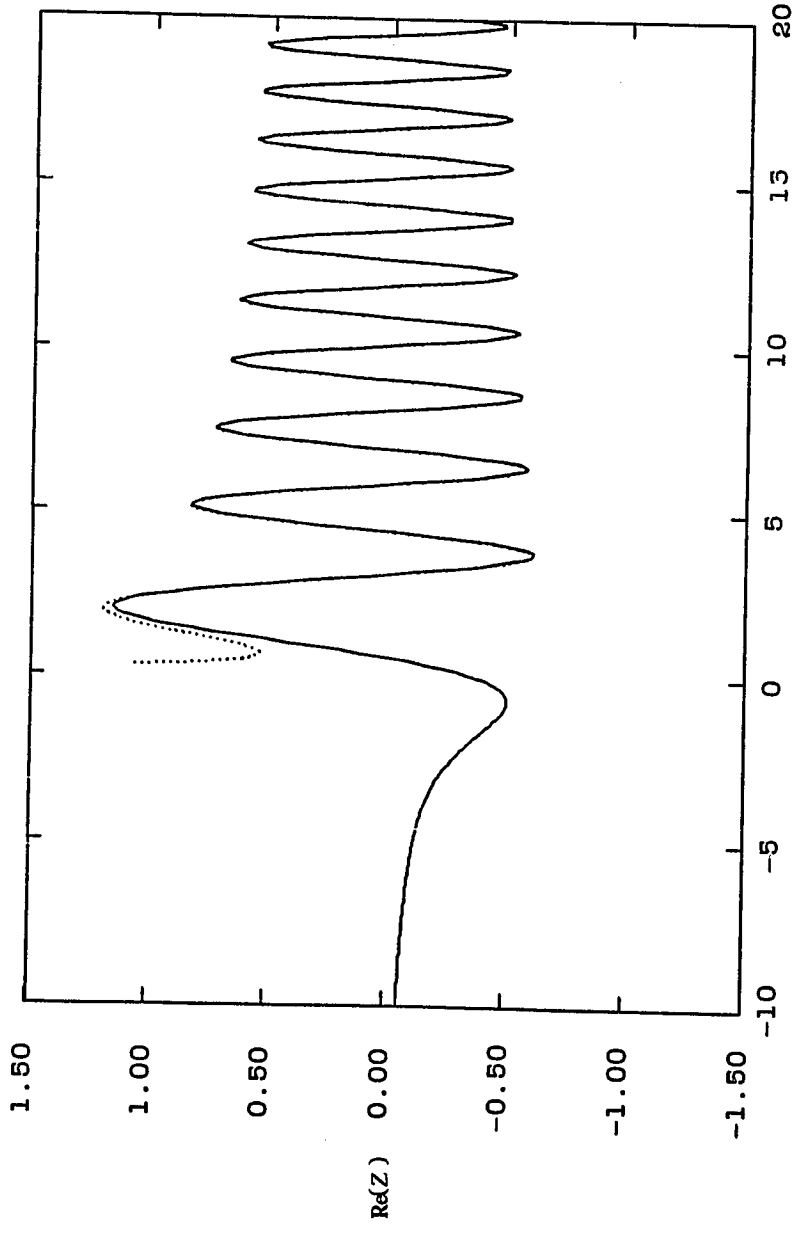

Figure 5.6

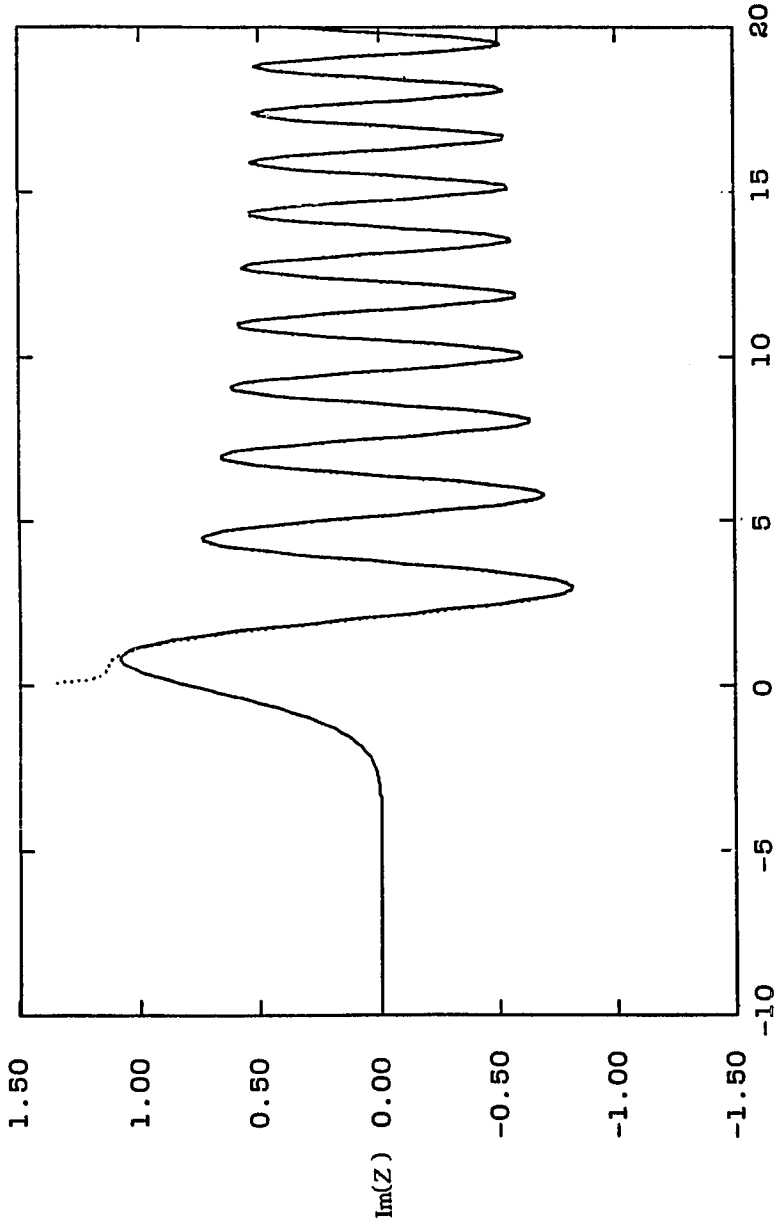

Figure 5.7

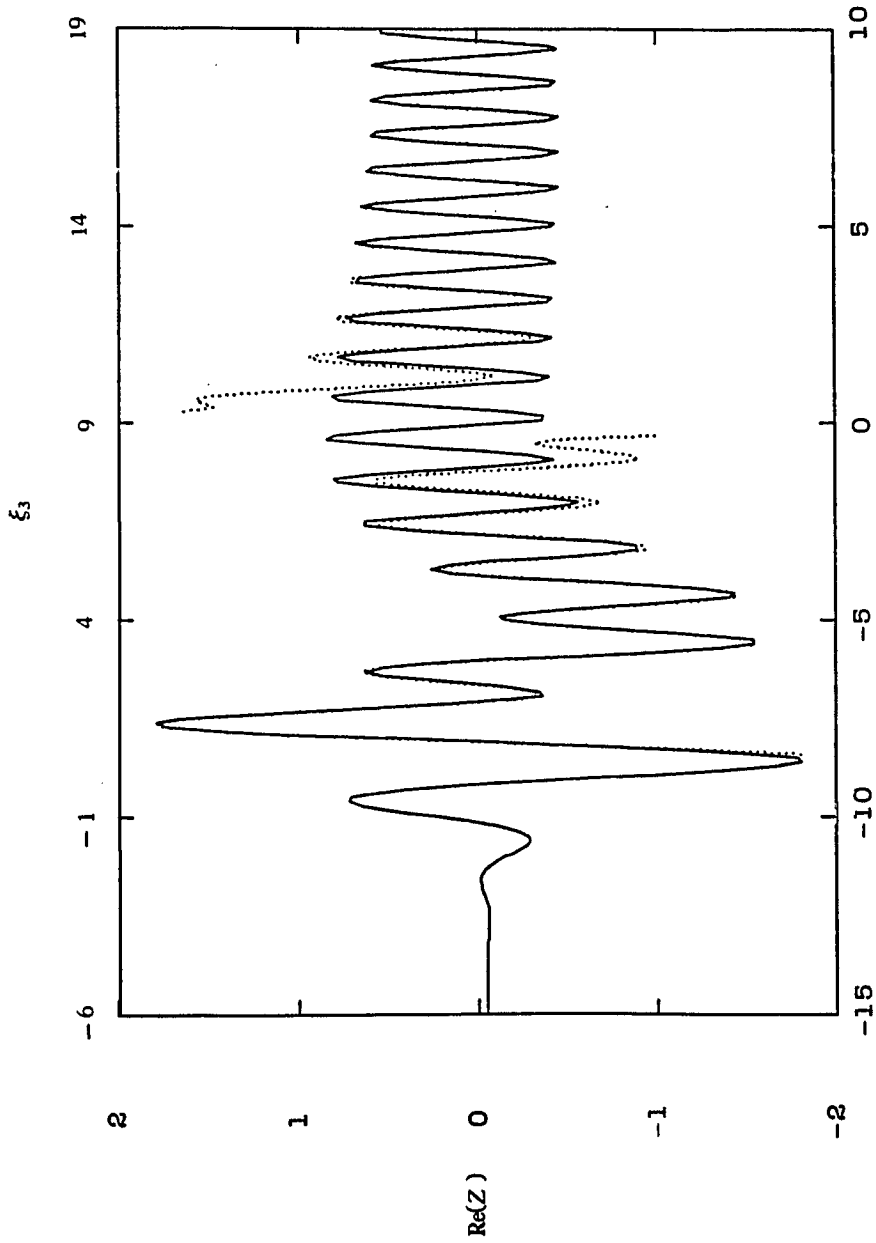

Figure 5.8

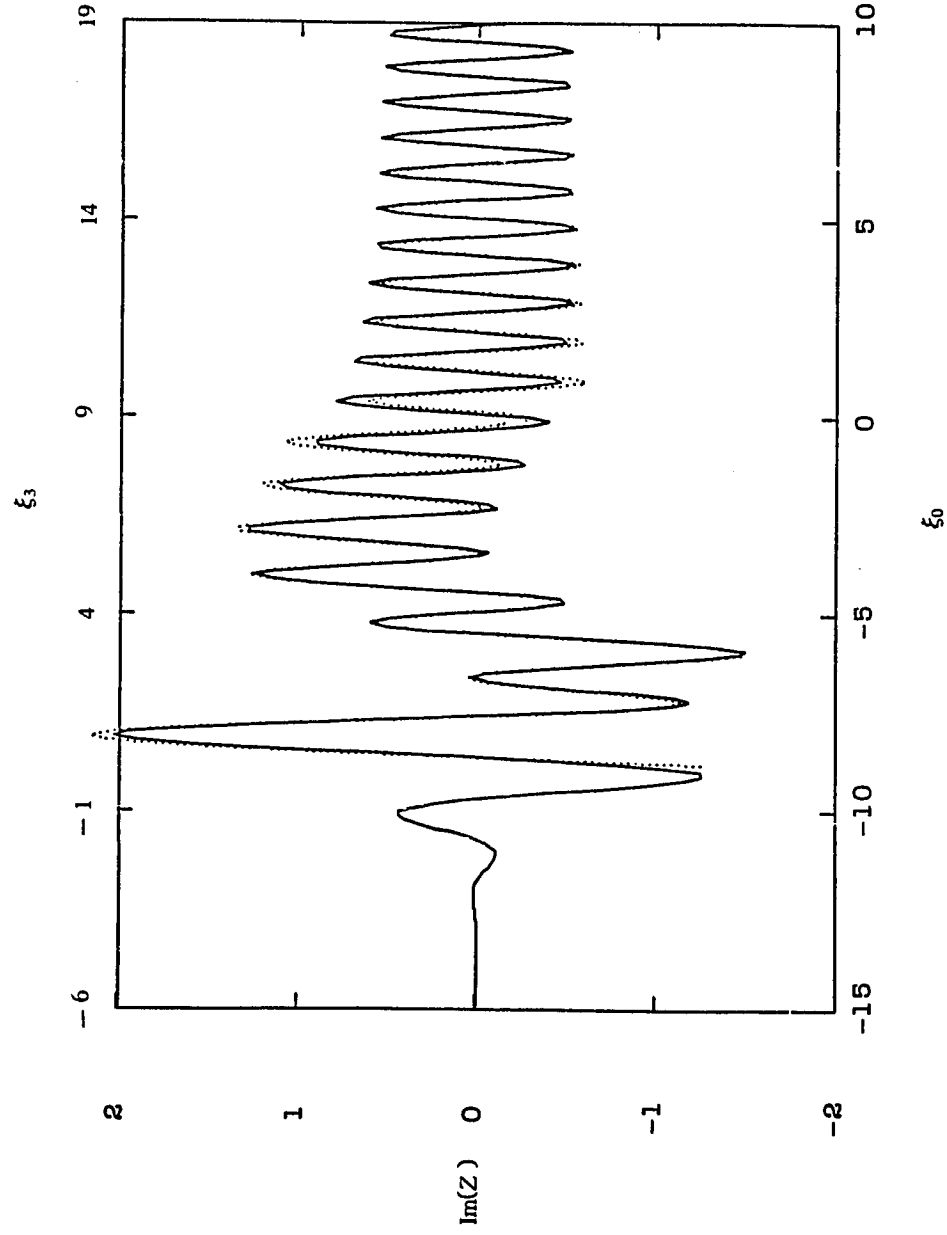

Figure 5.9

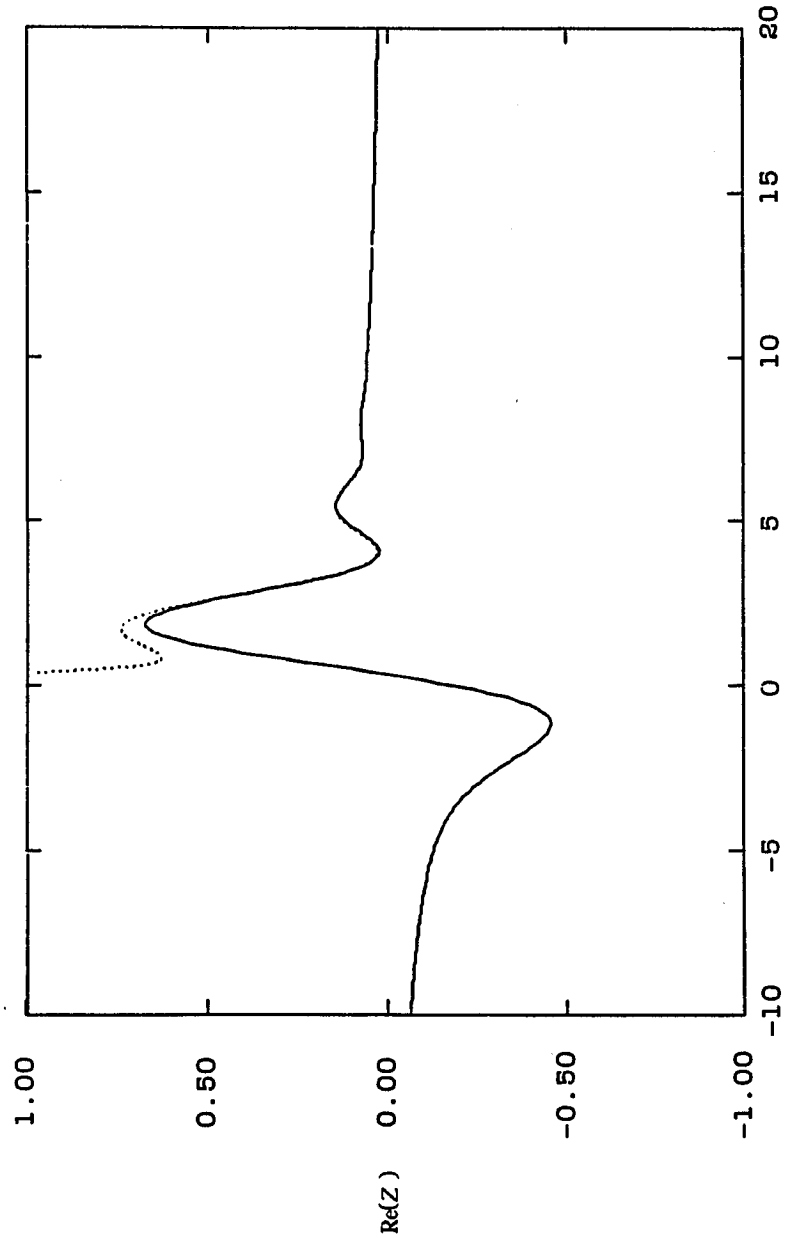

Figure 5.10

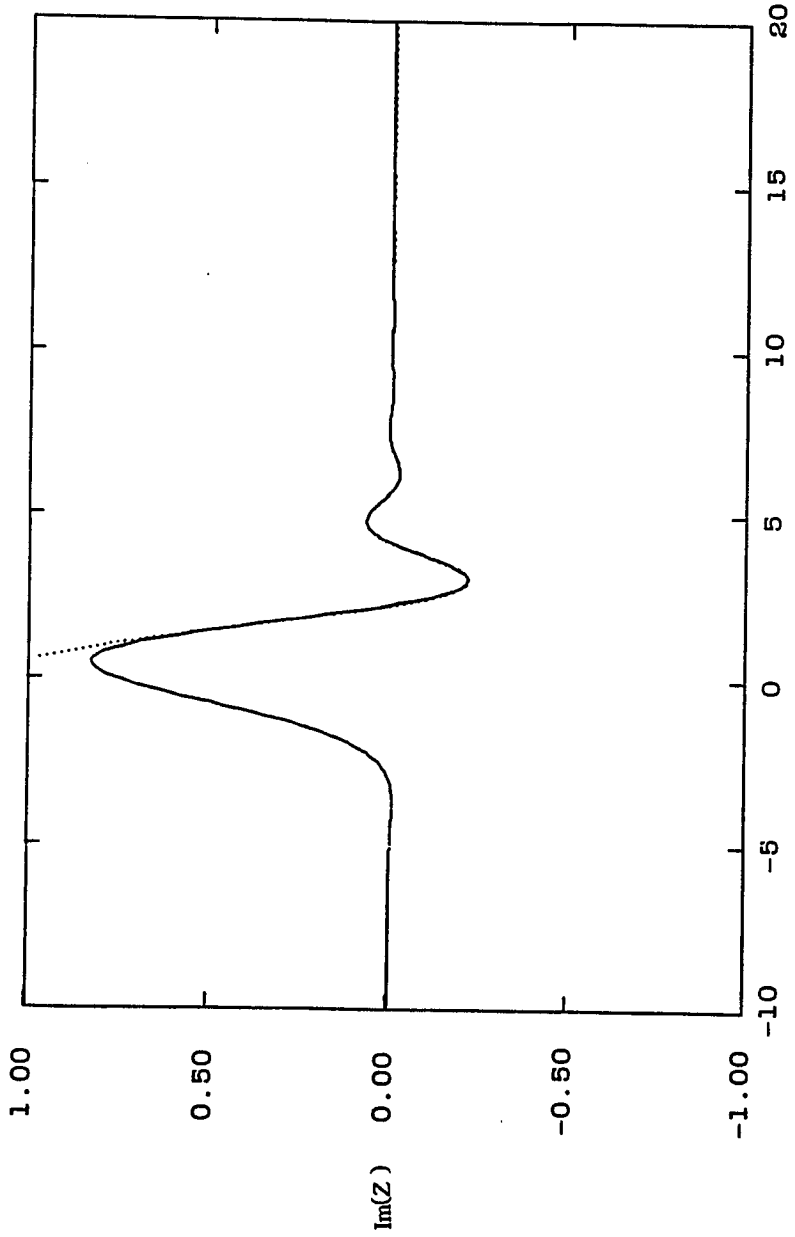

Figure 5.11

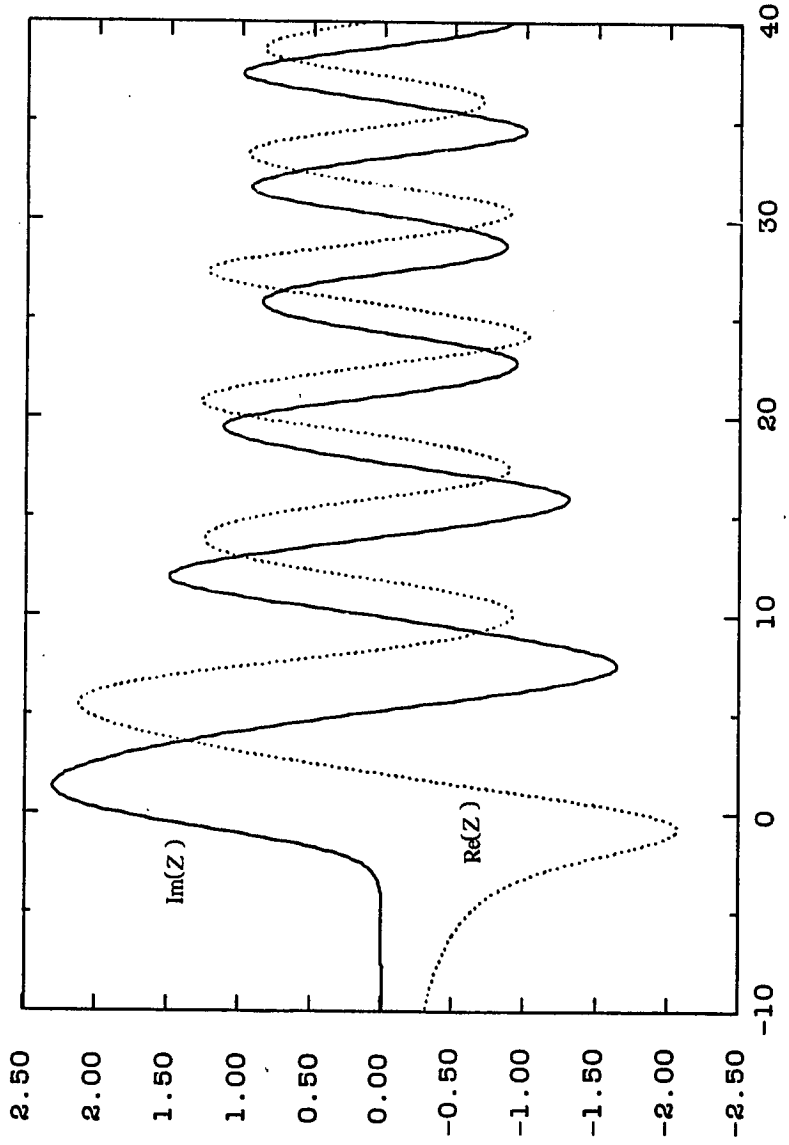

Figure 6.1

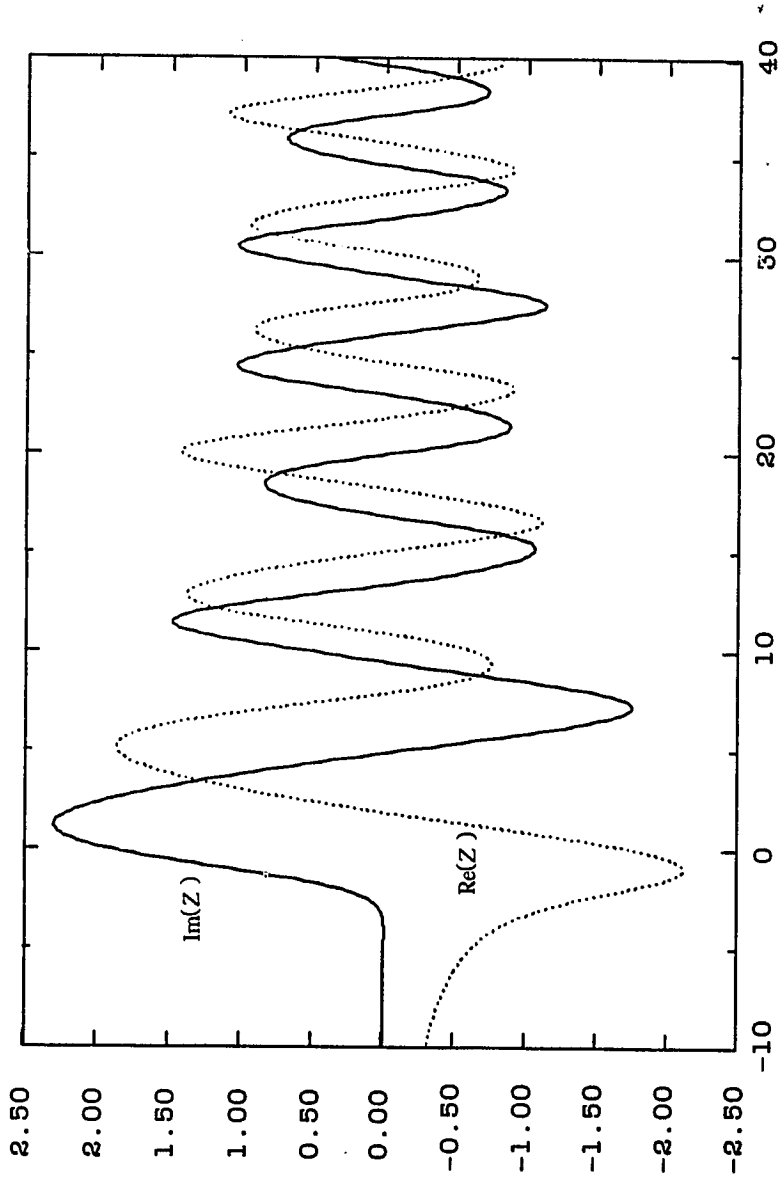

Figure 6.2

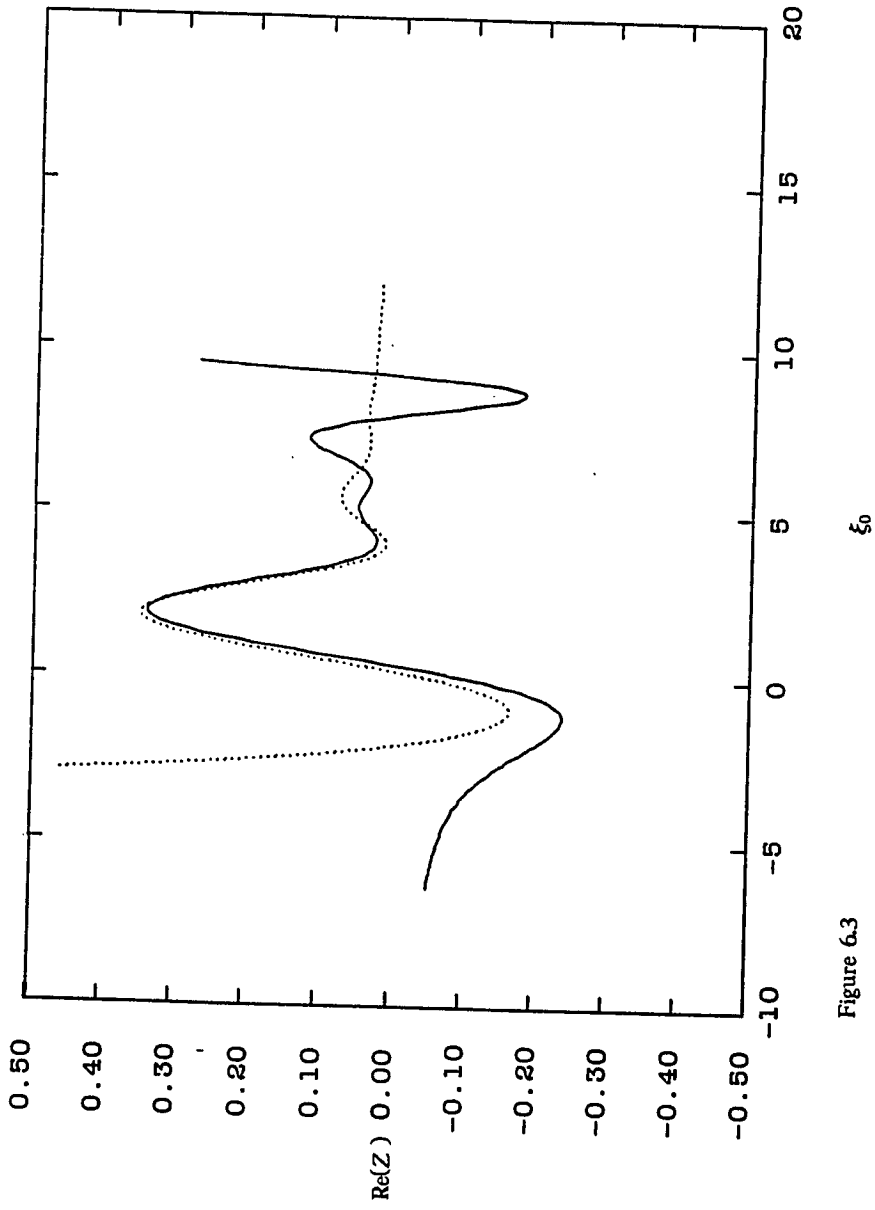

Figure 6.3

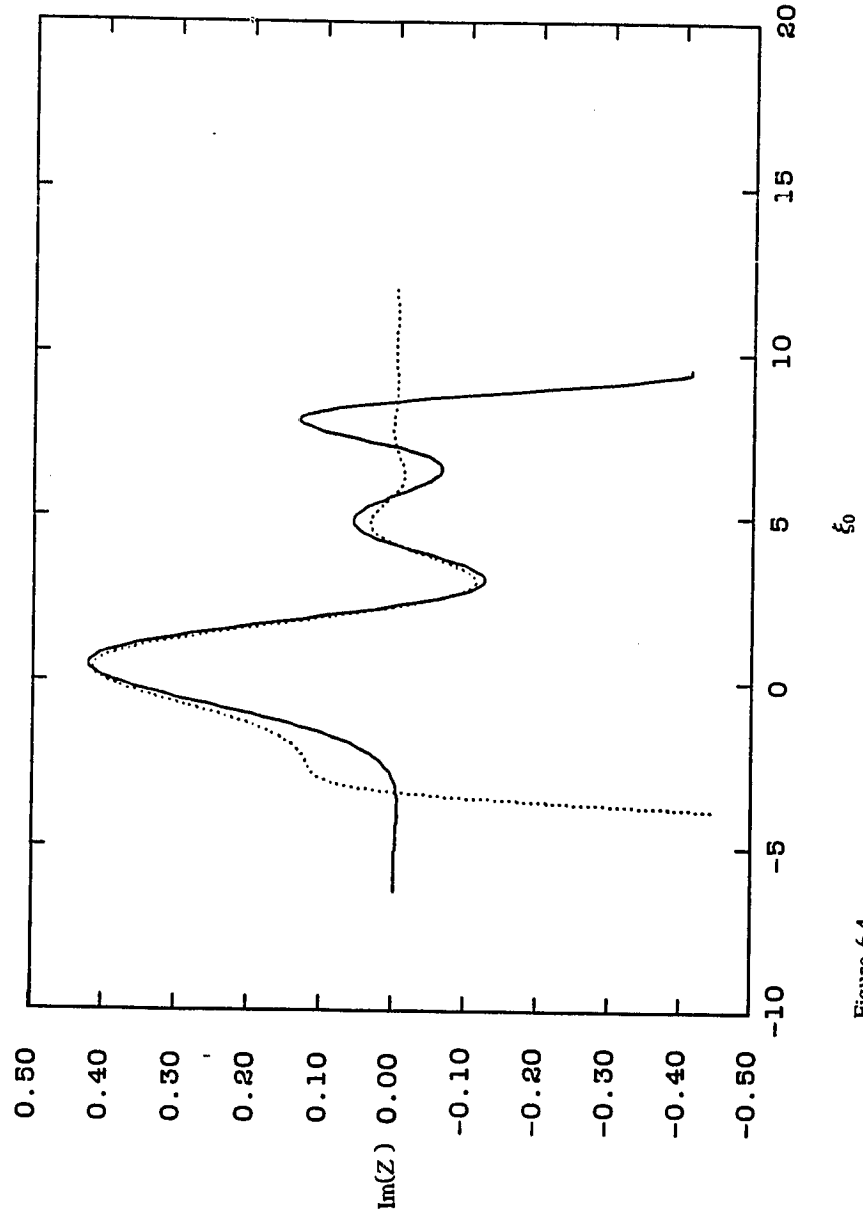

Figure 6.4

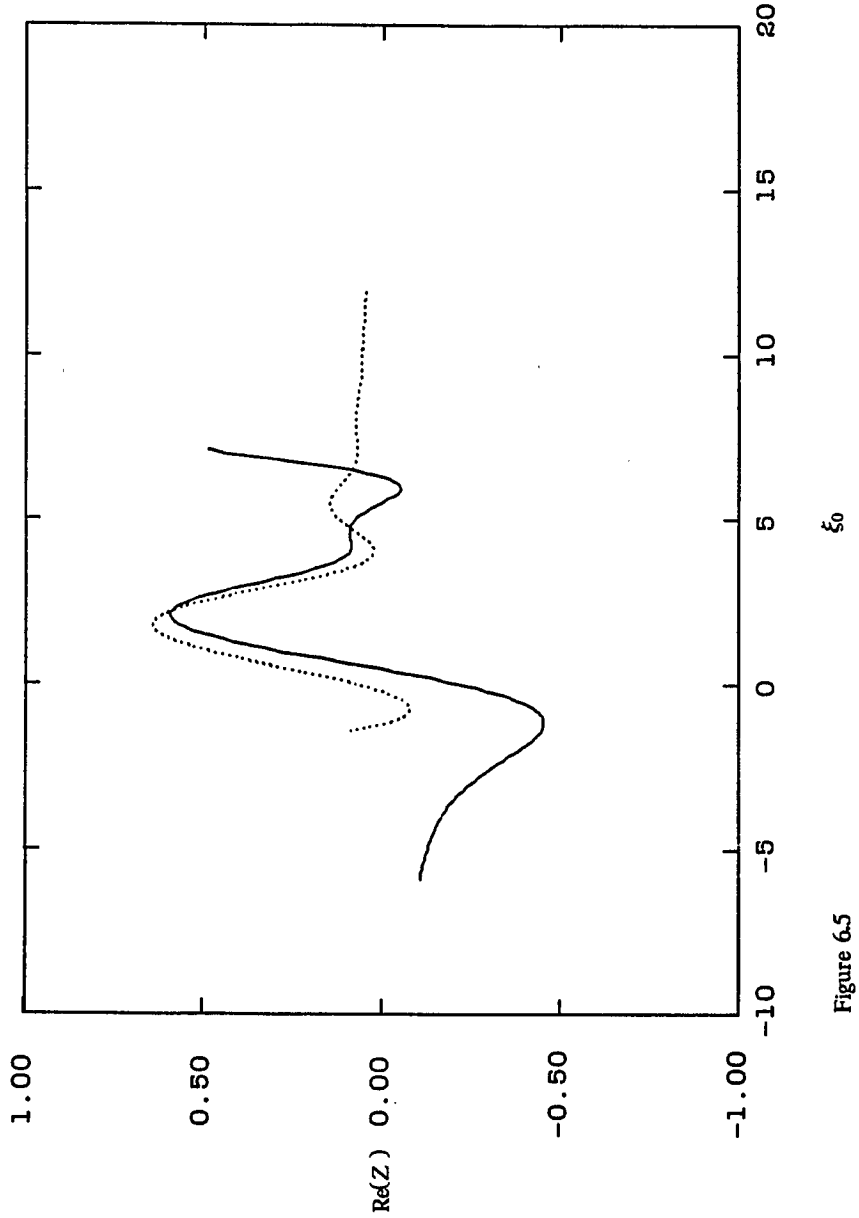

Figure 6.5

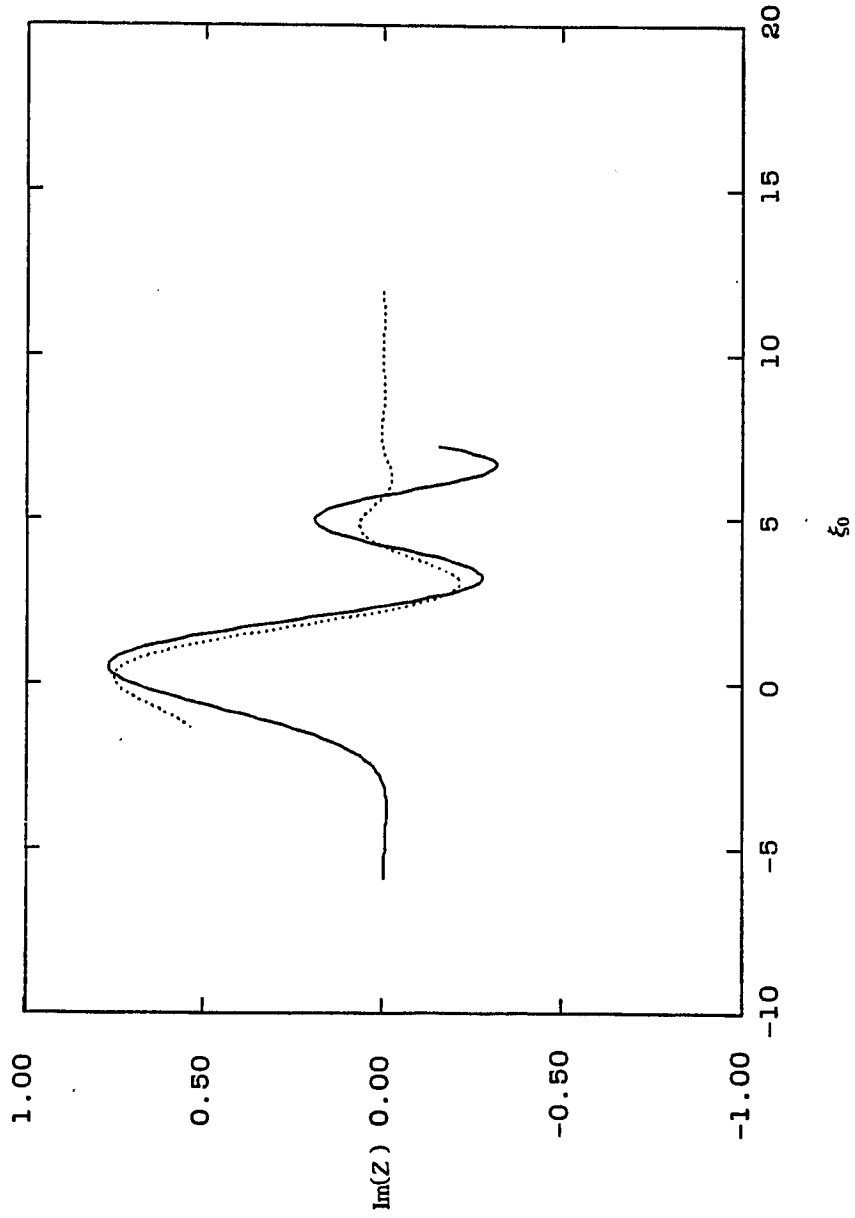

Figure 6.6

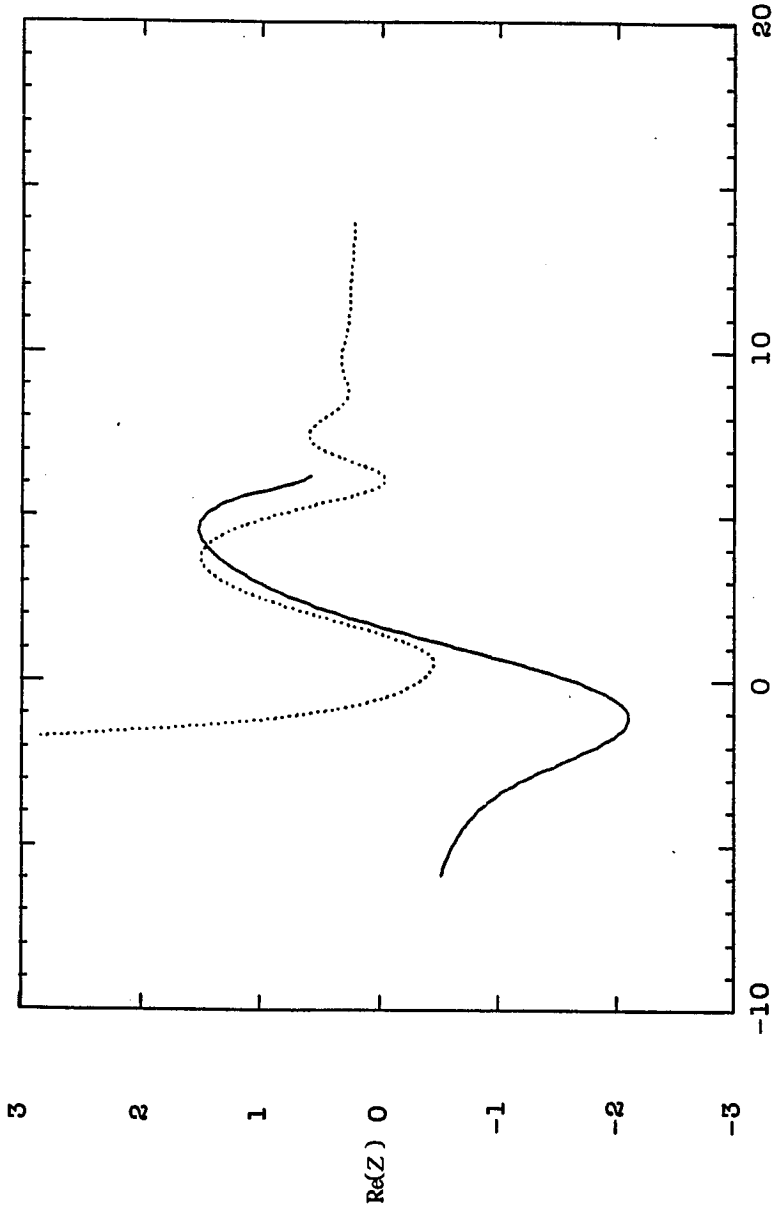

Figure 6.7

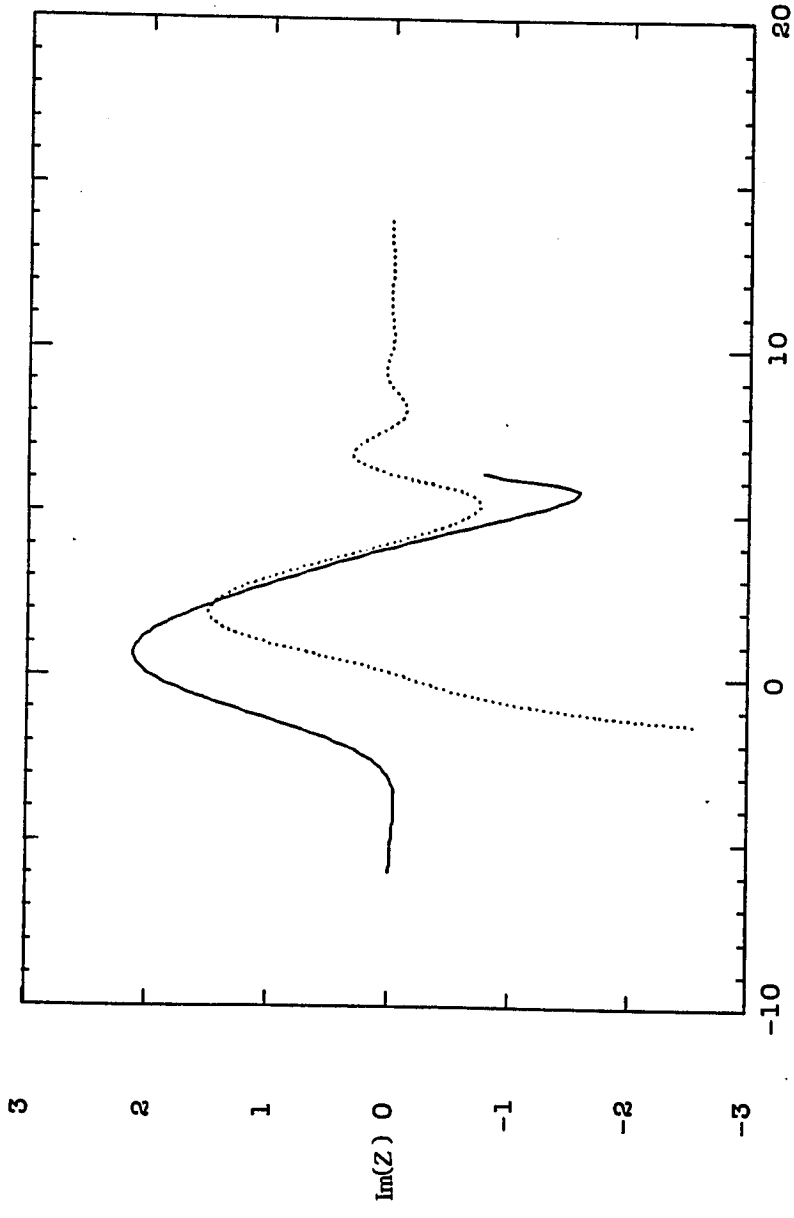

Figure 6.8

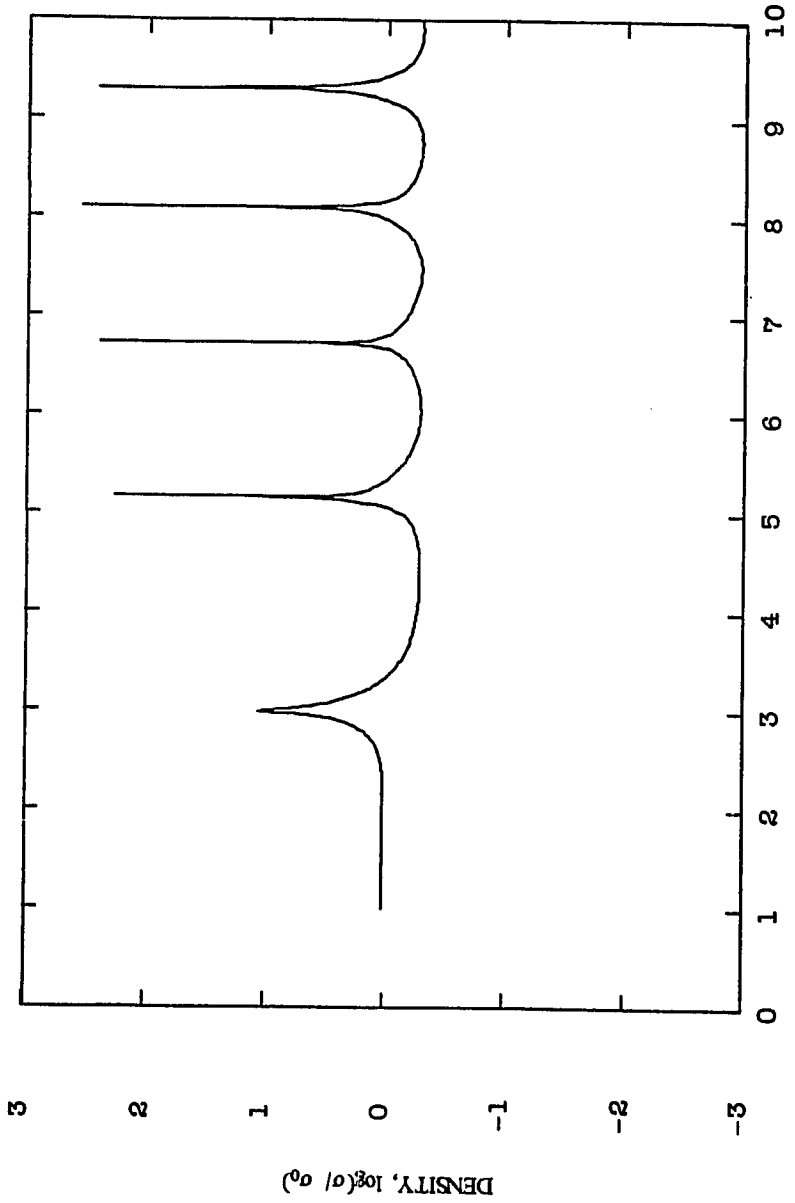

Figure 6.9

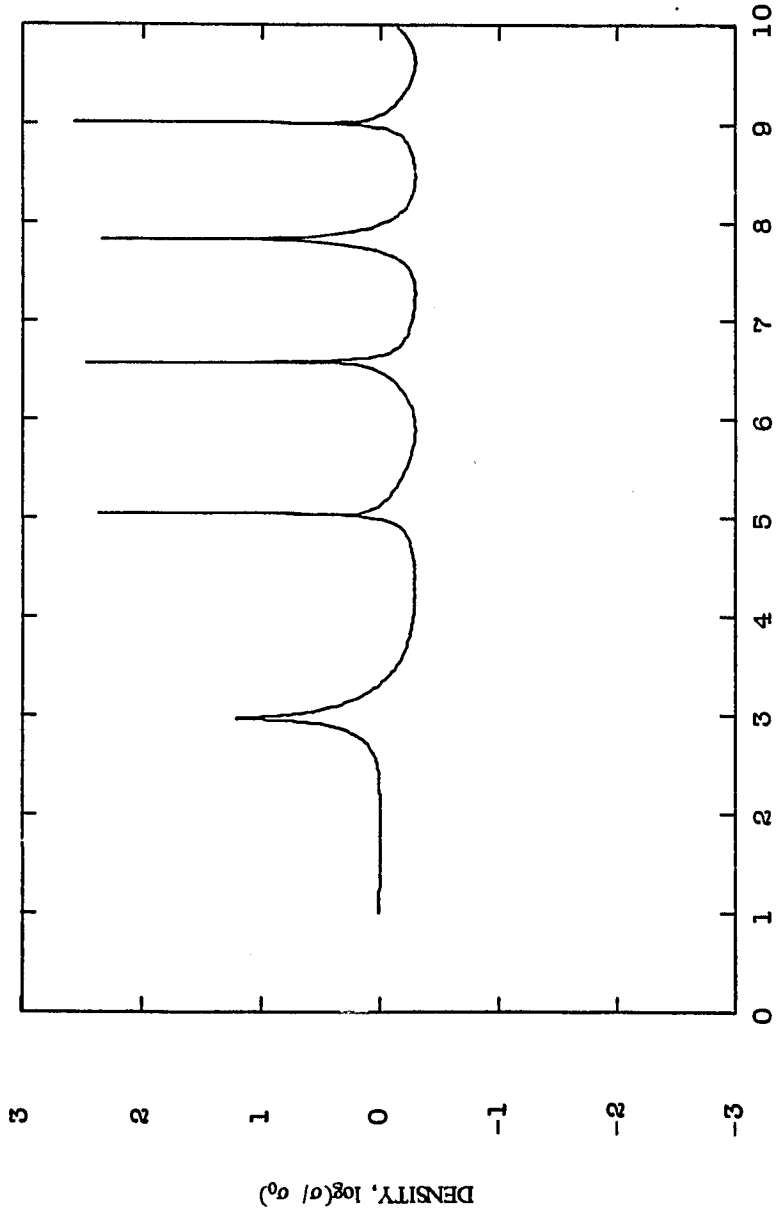

Figure 6.10

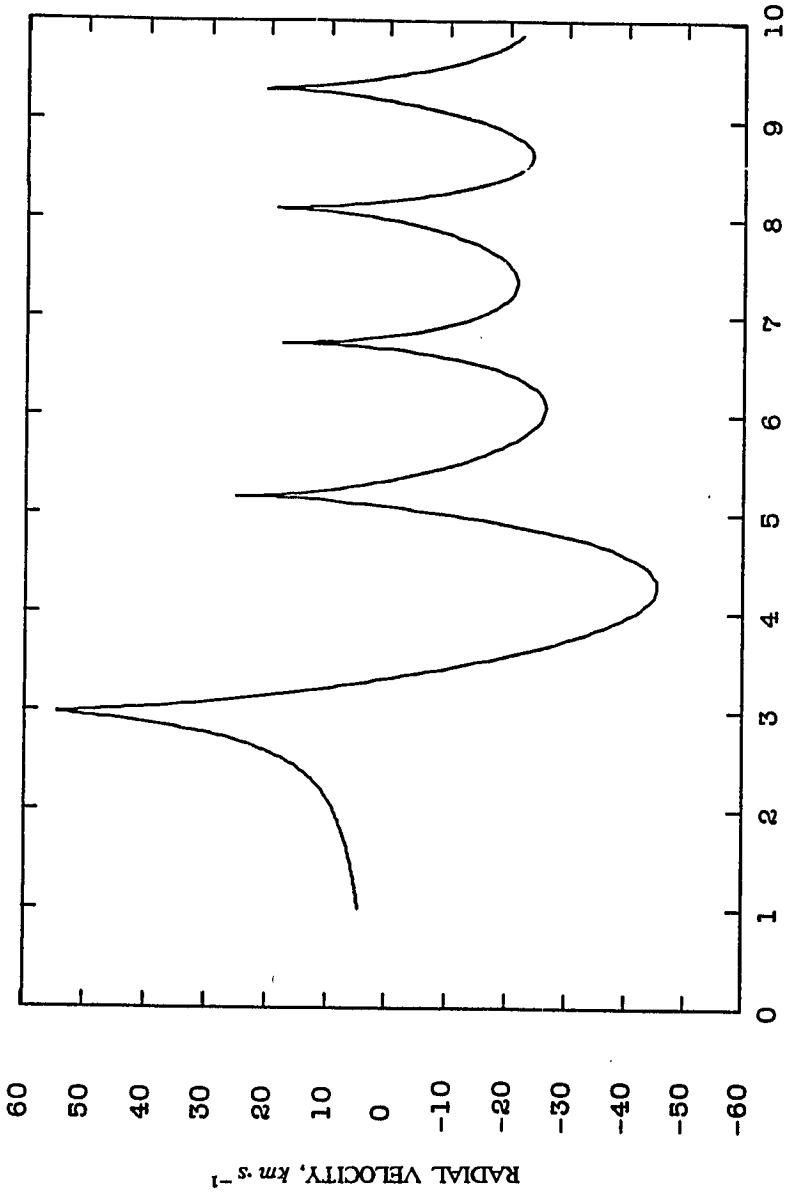

Figure 6.11

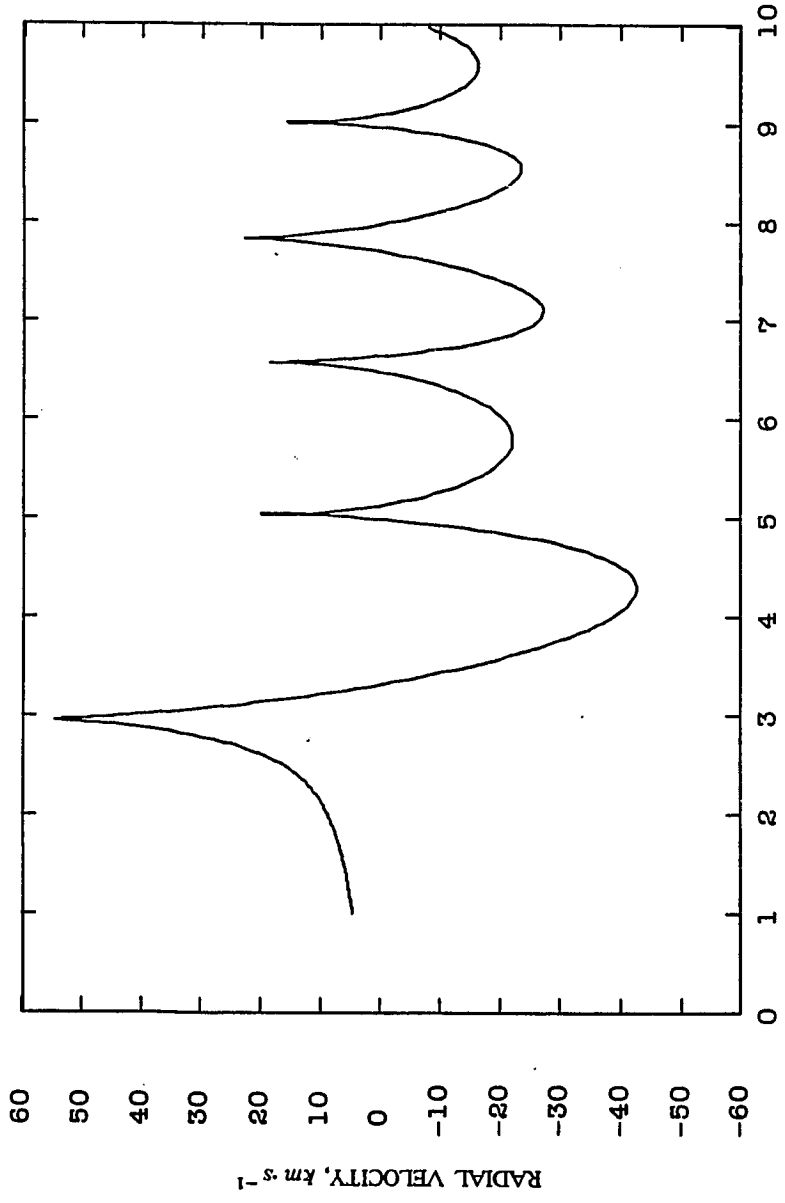

Figure 6.12

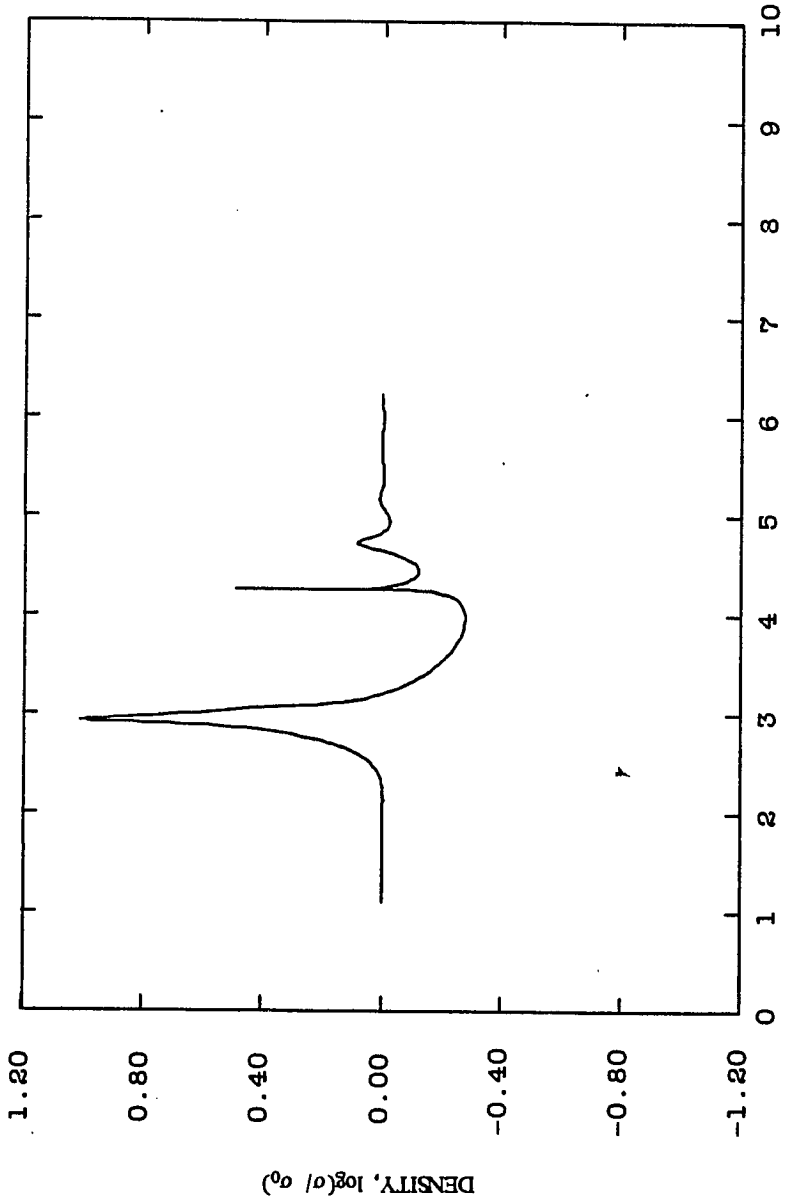

Figure 6.13

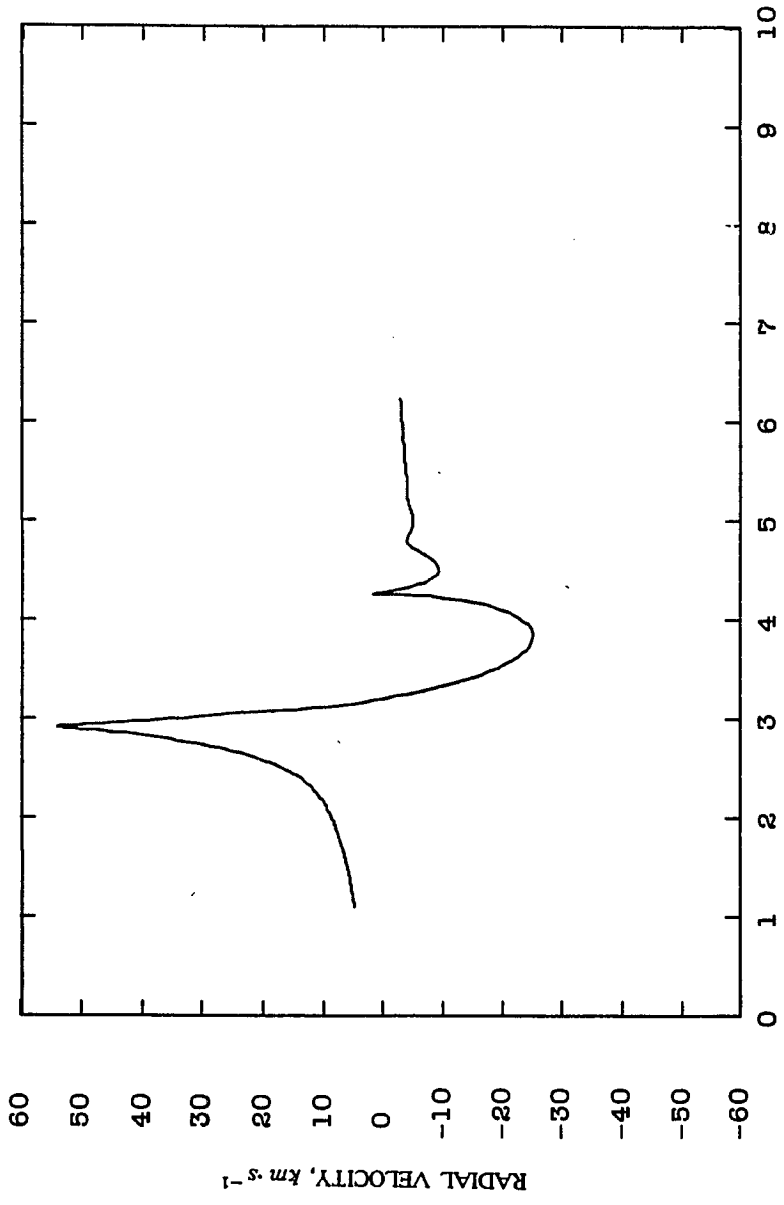

Figure 6.14

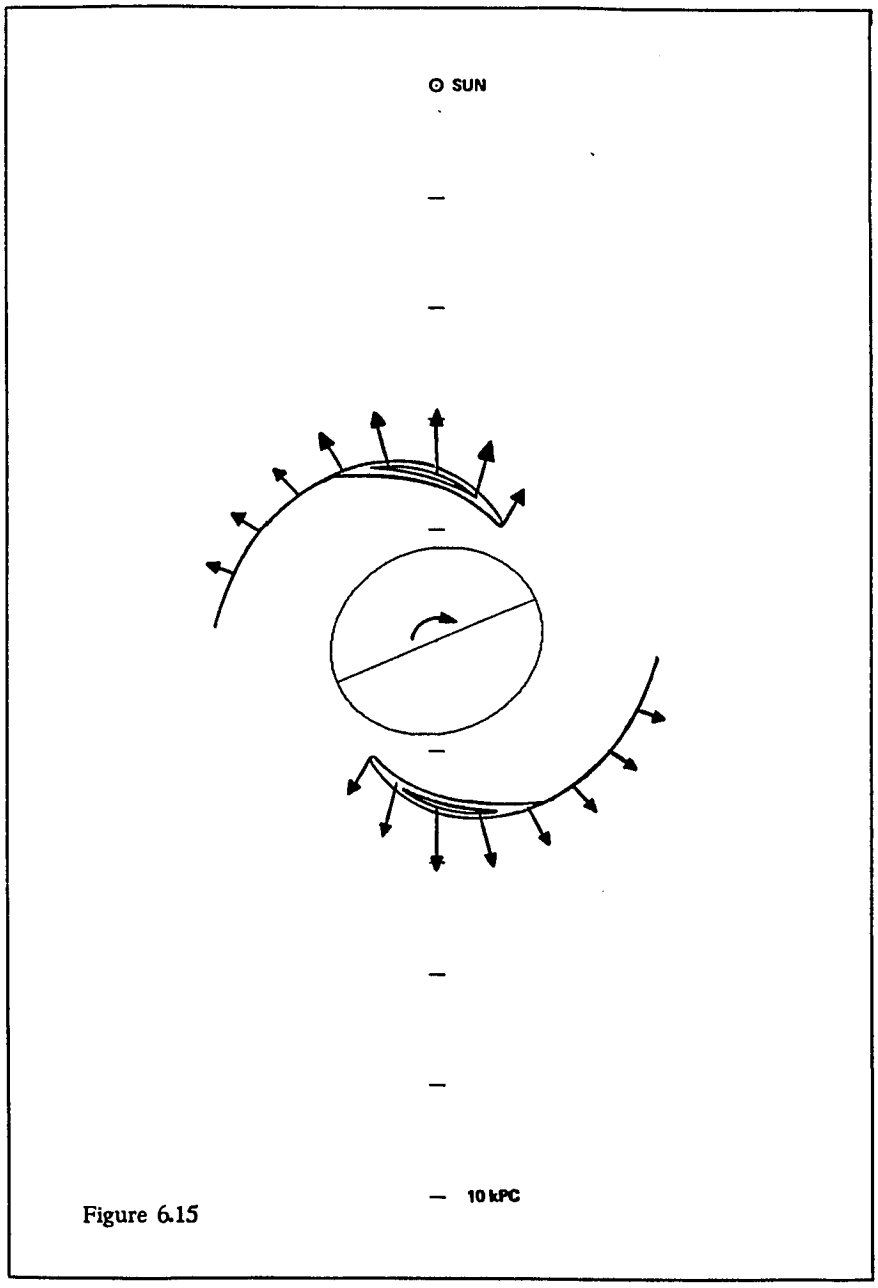

Figure 6.15

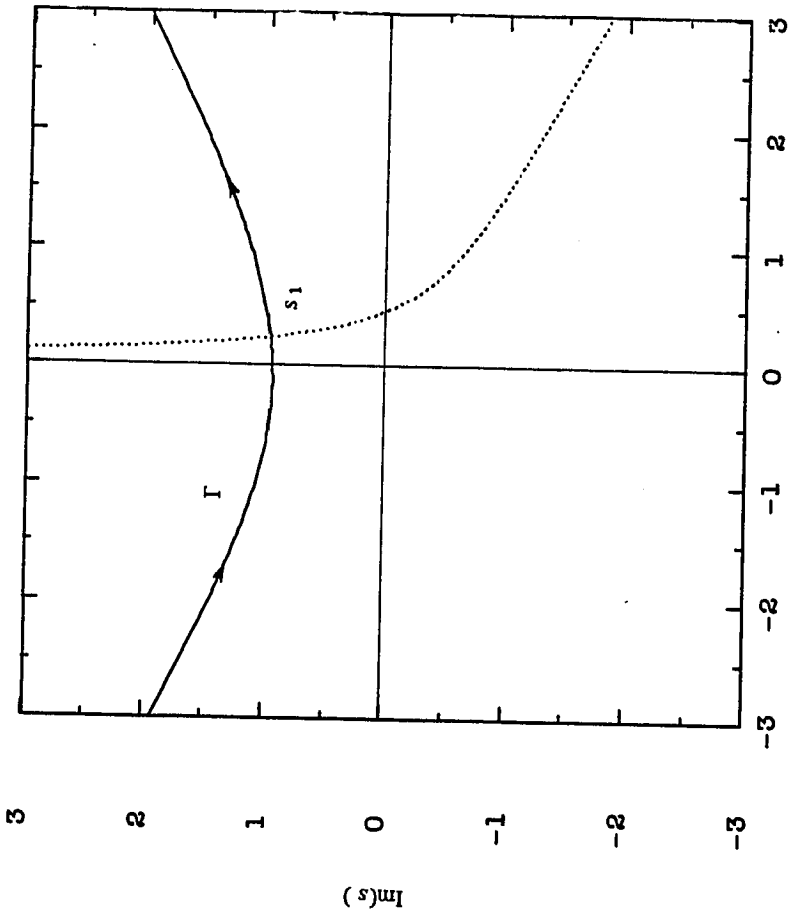

Figure B1

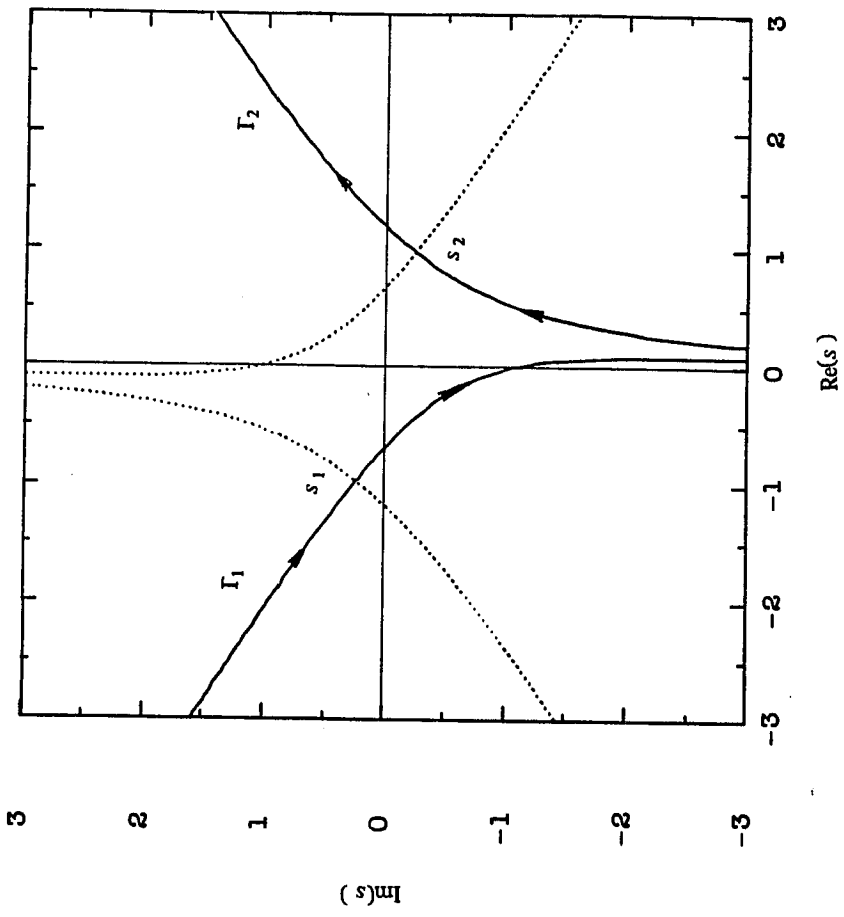

Figure B2

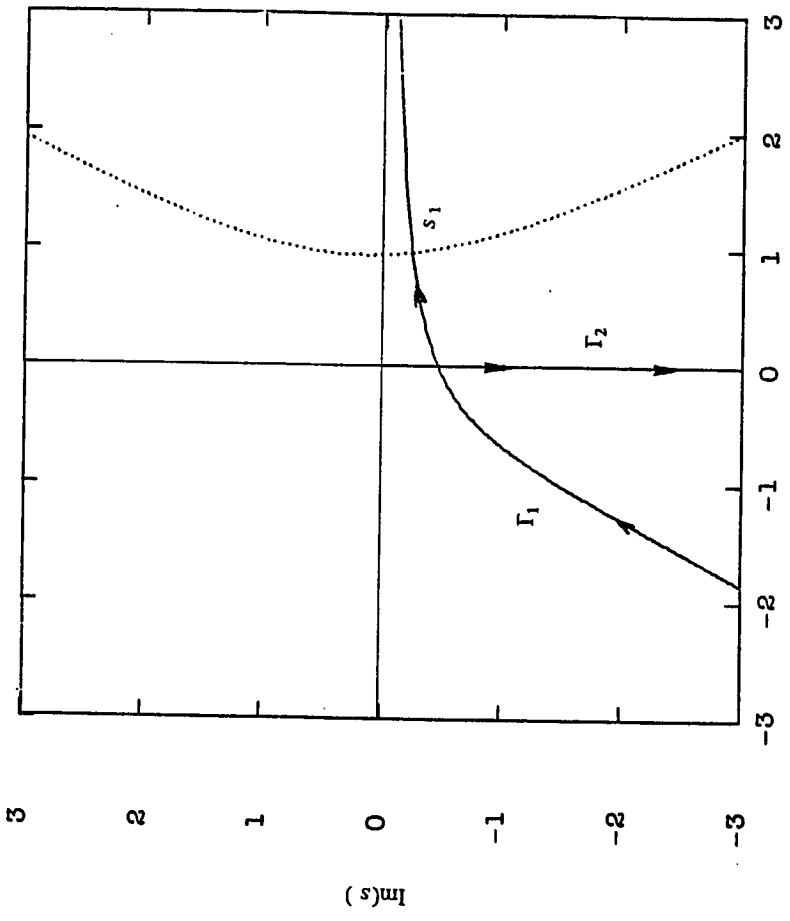

Figure B3

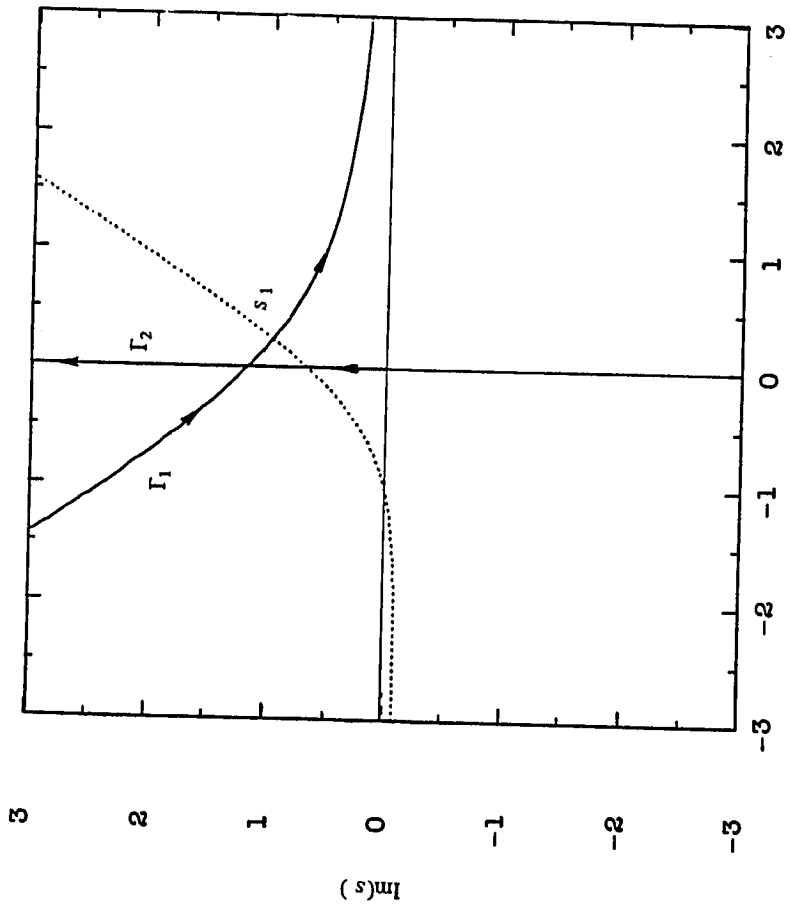

Figure B4

REFERENCES

[1] Abramowitz, M, and Stegun, I. A. (eds.) 1965, *Handbook of fiat hematical Functions* (New York: Dover Publications).

[2] Bertin, G., Lin, C. C., and Lowe, S. A. 1984, in *Proc. of a Course and Workshop on Plasma and Astrophysics*, Varenna, Italy, 28 Aug - 7 Sept, 1984, ESA SP-207, 115-120.

[3] Borderies, N, Goldreich, P., and Tremaine, S. 1982, *Nature*, 299, 209.

[4] ———. 1983a, *A. J.*, 88, 226.

[5] ———. 1983b, *Icarus*, 55, 124.

[6] ———. 1984, in *Planetary Rings*, ed. R. Greenberg and A. Brahic (Tucson: University of Arizona Press), p. 713.

[7] Cassen, P., and Summers A. L. 1983, *Icarus*, 53, 26.

[8] Cuzzi, J. N, Lissauer, J. J., and Shu, F. H. 1981, *Nature*, 292, 703.

[9] Feldman, S. I., and Lin, C. C. 1973, *Stud. Appl. fia th.*, 52, 1.

[10] Goldreich, P., and Tremaine, S. 1978a, *Icarus*, 34, 227.

[11] ———. 1978b, *Icarus*, 34, 240.

[12] ———. 1979, *Ap. J.*, 233, 857.

[13] ———. 1982, *Ann. Rev. Astr. Ap.*, 20, 249.

[14] Gradshteyn, I. S., and Ryzhik, I. M. 1980, *Tables of Integrals, Series, and Products* (New York: Academic).

[15] Landau, L. D., and Lifshitz, E. M. 1959, *Fluid fiecha nics* (Reading, Mass.: Addison-Wesley).

[16] Lin, C. C., and Bertin, G. 1985, in *IAU Symposium 106, The fiilky Way System*, ed. H. van Woerden, W. B. Burton, and R. J. Allen (Dordrecht: Reidel), P. 513.

[17] Lin, C. C., and Lau, Y. Y. 1975, *SIAfi J. Appl. fiat h.*, 29, 352.

[18] ———. 1979, *Stud. Appl. fiat h.*, 60, 97.

[19] Lin, C. C., and Shu, F. H. 1964, *Ap. J.*,140, 646.

[20] ———. 1966, *Proc. Nat. Acad. Sci.*, 55, 229.

[21] Lin, C. C., and Thurstans, R. P. 1984, in *Proc. of a Course and Workshop on Plasma and Astrophysics*, Varenna, Italy, 28 Aug - 7 Sept, 1984, ESA SP-207, 121-130.

[22] Lissauer, J. J., and Cuzzi, J. N. 1982, *Ap. J.*, 87, 1051.

[23] Porco, C. C., and Goldreich, P. 1987, *A. J.*, 93, 724.

[24] ———, 730.

[25] Sanders, R. H., and Prendergast, K. H. 1974, *Ap. J.*, 188, 489.

[26] Shu, F. H. 1984, in *Planetary Rings*, ed. R. Greenberg and A. Brahic (Tucson: University of Arizona Press), P. 513.

[27] Shu, F. H., Cuzzi, J. N., and Lissauer, J. J. 1983, *Icarus*, 53, 185.

[28] Shu, F. H., Dones, L., Lissauer, J. J., Yuan, C., and Cuzzi, J. N. 1985, *Ap. J.*, 299, 542 (**Shu et al.**).

[29] Shu, F. H., and Stewart, G. L. 1985, *Icarus*, 62, 360 (**SS**).

[30] Shu, F. H., Yuan, C., and Lissauer, J. J. 1985, *Ap. J.*, 291, 356 (**SYL**).

[31] Toomre, A. 1963, *Ap. J.*, 138, 385.

[32] Toomre, A. 1964, *Ap. J.*, 139, 1217.

[33] Toomre, A. 1969, *Ap. J.*, 158, 899.

[34] van der Kruit, P. C. 1971, *Astr. Ap.*, 13, 405.

[35] Yuan, C., 1984b, *Ap. J.*, 281, 600.